The Role of Glo3 in COPI regulation

By

Boyang (Betty) Xie

Dissertation

Submitted to the Faculty of the

Graduate School of Vanderbilt University

In partial fulfillment of the requirements

For the degree of

DOCTOR OF PHILOSOPHY

In

Biological Sciences

December 18, 2021

Nashville, Tennessee

ACKNOWLEDGEMENTS

I have received a great deal of support and help throughout the years hailing from across the ocean, working towards my Ph.D., and finally writing this thesis. Many thanks to all the friends, colleagues, and family members who supported me along the way.

First, I would like to express my deepest appreciation to my advisor, Dr. Lauren Jackson, for taking me in as a member in the lab, and for being a great mentor in both science and life. You've always been available to discuss science and ideas with me, always encouraged me to believe in myself and grow beyond limits. Thanks you for supporting me along the journey, and helping me become a real scientist and a stronger woman.

I would also like to extend my deepest gratitude to my committee: Dr. Borden Lacy, Dr. Jared Nordman, Dr. Yi Ren, and my chair Dr. Todd Graham, for providing all the constructive advice and being such a supportive committee throughout the years, especially Todd, deepest thanks for being a great chair, collaborator, and mentor to me.

Thanks to all the collaborators (especially members in the Graham lab) and colleagues, the Department of Biological Sciences and the Center for Structural Biology, for providing a great wealth of expertise and resources to assist my projects and my personal growth. Special thanks to Dr. Joel Harp for teaching me crystallography and always being so nice to help me with a million questions I had. I feel most grateful being in such a collaborative and supportive environment to make friends, communicate ideas, and vent the graduate school stress.

I feel very fortunate to have started my graduate school journey in the Jackson lab. They are my colleagues and family, I can't imagine a better group of people to have spent the years with. Many thanks to Amy for being the best lab manager, "lab mom", and a great research partner. Natalie and John, thank you so much for always helping out, troubleshooting with me, and being my colleagues and friends, as well as my inspiration and support. Thanks Mintu for being such an inspirational and knowledgeable

colleague. Meredith and Tara, thank you so much for all the great mentorship, friendship, and continued support. Allie, thanks you for being such a caring friend and I always loved your pizzelles. Thanks to Rodger for being a very friendly annex mate. And I would like to thank all the amazing undergraduate students I have worked with, especially Chris Jung, who helped in all my projects.

I'm also extremely grateful to all the precious friendship by my side. Past years have seen some of the biggest struggles in my life, but I know I've got their support every time I doubted myself. Thanks to the Girls Gang and the Mendel's Peas - Natalie, Nicole, Nikki, Adam, John, and Jessie - for every trivia, game night, and happy gathering night I spent with you. Special thanks to Natalie, I couldn't have gone so far without you and Georgie. Also thanks to my Chinese friends in Nashville. Yan, Pumpki, and Ling, you are my girls family and biggest support in Nashville, I loved every meal, outing, trip, and gathering with you. Chao, Susu, Yue, Kathy, Adam, Simeng, Bobo, Yongtai, thanks for being my Nashville Fa-Mi-Ly and supporting me in my life. Thanks Steven Zhou and Yetz for being my best game buddies. Thanks to friends in the BioSci department - Juan, Stephen, Cait, Michelle, Stephanie, Kevin, Kate, and Dylan - for helping me blend in a brand new environment. And many thanks to my lifelong friend Ruby and my cousin Yueyue.

Finally, I want to knowledge my family - I feel extremely lucky to have grown up in a loving and supportive family. My parents' pursuit of exploring the unknown have instilled a strong curiosity and a love of learning in me. I'm grateful that they never set up limits on what I could pursue, regardless of any social and culture norms. I know they would believe in me and support me forever. Thanks dad for always being wise and helping me find myself when lost in decisions, and thanks mom for being the first role model of strong woman to me. I love you both forever!

ACKNOWLEDGEMENT OF FUNDING

This work was supported by NIGMS R35GM119525 to Lauren Jackson and funding from the Pew Charitable Trusts to Lauren Jackson. Chapter II was supported in part by NIH R01GM118452 to Todd Graham.

PUBLICATIONS

The work in Chapter II is currently under review. The work in Chapter III appears in *Advances in Biological Regulation, 79, 100781*. Reuse is permitted (Xie et al., 2021).

Additional publications are as follows:

Kendall AK, **Xie B**, Xu P, Wang J, Burcham R, Frazier MN, Binshtein E, Wei H, Graham TR, Nakagawa T, Jackson LP. Mammalian Retromer Is an Adaptable Scaffold for Cargo Sorting from Endosomes. *Structure*. 2020 Apr 7;28(4):393-405.e4. doi: 10.1016/j.str.2020.01.009. Epub 2020 Feb 5. PMID: 32027819; PMCID: PMC7145723.

Xie B, Guillem C, Jung C, Kendall AK, Best J, Graham TR, and Jackson LP. (2021). An interaction between β'-COP and its ArfGAP, Glo3, is required to maintain post-Golgi cargo recycling. (*In revision*)

Chen K, Guo Q, Cui Y, Kendall AK, Sacharz J, Hill TA, Hall RJ, Norwood SJ, Leneva N, **Xie B**, Yang Z, Ghai R, Suga H, Fairlie D, Stroud DA, Jackson LP, Teasdale RD, Passioura T, Collins BM. (2020). *De novo* macrocyclic

peptides for inhibiting, stabilising and probing the function of the Retromer endosomal trafficking complex. (*In revision; available on bioRxiv*)

Date SS, Xu P, Hepowit H, Diab N, Best J, **Xie B**, Jackson LP, MacGurn JA, Graham TR. Ubiquitination regulates COPI-dependent retrieval of Golgi SNAREs. (*In preparation*)

TABLE OF CONTENTS

Page

LIST OF TABLES

LIST OF FIGURES

LIST OF ABBREVIATIONS

AP	adaptor protein
AP1	adaptor protein complex 1
AP2	adaptor protein complex 2
AP3	adaptor protein complex 3
AP4	adaptor protein complex 4
AP5	adaptor protein complex 5
APS	Advanced Photon Source
BoCCS	binding of coatomer, cargo, and SNAREs
COG	Conserved oligomeric Golgi
COPI	coat protein complex I
COPII	coat protein complex II
Cryo-EM	cryogenic electron microscopy
Cryo-ET	cryogenic electron tomography
EE	early endosome
ER	endoplasmic reticulum
GAP	GTPase activating protein
GEF	guanine exchange factor
GFP	green fluorescent protein
GGAs	Golgi-localized, γ-ear containing, ADP ribosylation factor binding family
GRM	Glo3 regulatory motif
HRP	horseradish peroxidase
IP	immunoprecipitation

ITC	isothermal titration calorimetry
PDB	Protein Data Bank
PIP	phosphatidylinositol phosphate
RMSD	root mean square deviation
SNARE	soluble N-ethylmaleimide-sensitive factor attachment protein receptor
TRAPPII	The trafficking protein particle II
TGN	trans-Golgi network
Ub	ubiquitin
VPS	vacuolar protein sorting associated protein

CHAPTER I

INTRODUCTION

Despite a large flux of material, each cellular compartment maintains a distinctive membrane composition and diverse environment. This is especially important for highly structured eukaryotic cells. Complicated intracellular trafficking pathways have evolved in eukaryotic cells to ensure the proper trafficking throughout the cell and control the size and composition of the membrane-bound compartments. This process is mediated by transport vesicles and tubules through rounds of vesicle or tubule budding and fusion reactions, or through contact sites between membranes. Vesicle trafficking flows along various highly organized and directional routes, and these routes can be broadly classified into two types: the secretory pathway and endocytic pathways (Figure 1-1). This thesis will focus on trafficking mediated by coated vesicles.

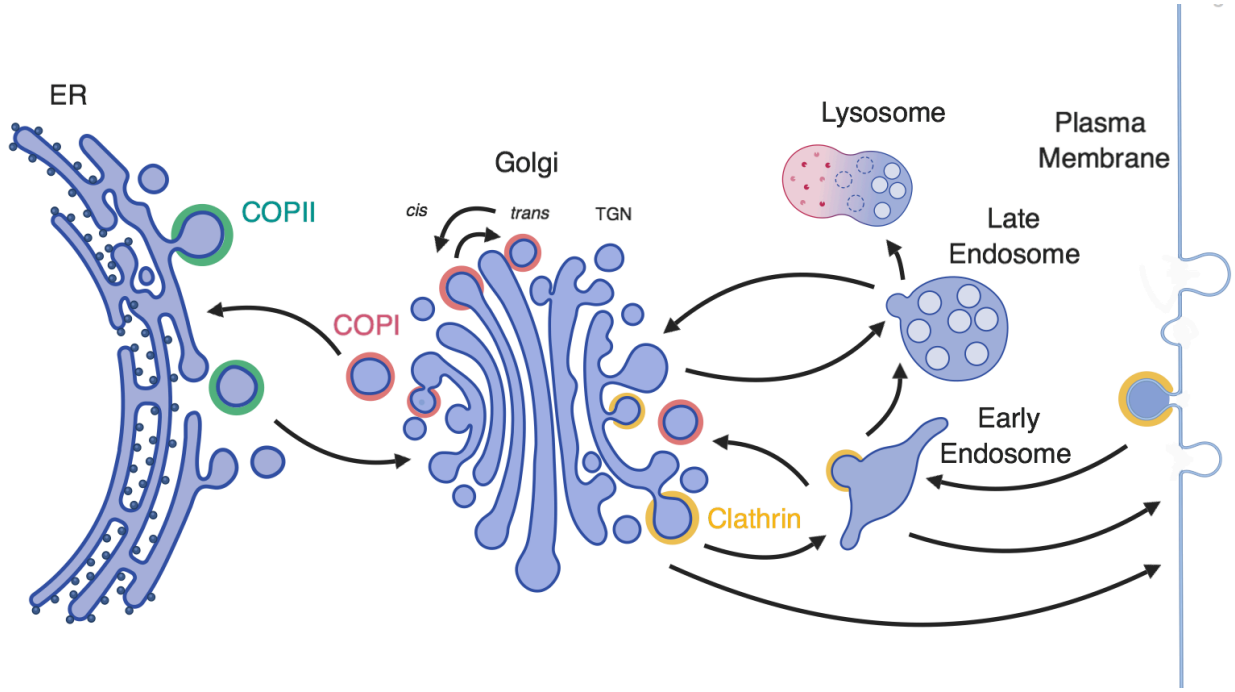

Figure 1-1. Eukaryotic intracellular membrane trafficking pathways. COPI-coated vesicles are colored in red, COPII-coated vesicles are colored in green, and clathrin coated vesicles are colored in yellow. COPI mediates transport between the Golgi stacks,

from the Golgi to the ER, and from the early endosomes to the tans-Golgi network. COPII vesicles transport newly synthesized proteins from the ER to the Golgi complex. And the clathrin coat can combine with various adaptors to function in various endocytic and recycling pathways. Created with BioRender.

Introduction to membrane trafficking

The early secretory pathway

The early secretory pathway mediates the protein flux outward from the endoplasmic reticulum (ER) toward the Golgi. The proteins are then sorted to the appropriate destinations of different cellular compartment or the plasma membrane (PM). In this pathway, newly synthesized proteins from the ribosome are translocated into the ER, where they continue to fold while early post-translational modifications take place in the lumen of the ER. Once ready, the proteins are then packaged and delivered to the early Golgi apparatus to receive further modifications. Escaped ER residents and other cycling trafficking machineries are retrieved back to the ER through retrograde vesicles. In metazoa, newly synthesized proteins first arrive at the ERGIC (ER-Golgi Intermediate Compartment) before cargoes are further delivered to the *cis*-Golgi. Within the Golgi complex, the Golgi cisternae are anterograde carriers themselves as they gradually mature into medial and *trans*-compartments, while resident Golgi proteins (such as glycosylation and other processing machineries) are constantly retrieved to earlier compartments by retrograde trafficking. (Barlowe and Miller, 2013; Bonifacino and Glick, 2004; Dunlop et al., 2017)

The endocytic pathway

The endocytic pathway controls the cellular process of internalizing macromolecules and surface proteins. It controls the protein and lipid composition of the plasma membrane, conducts communication with surrounding cells and the environment, as well as regulating the intracellular compartments. There are clathrin-mediated endocytosis (CME) and clathrin-independent pathways (caveolae uptake). After internalization, proteins are sorted by a series of endosomes at different maturation stages to different fates: being recycled back to the plasma membrane, delivered to lysosomes for degradation, or transported across the cell in polarized cells. Clathrin-mediated endocytosis is the most studied endocytic

mechanism. As a key component in the vesicular trafficking, it transports a wide range of cargo molecules through clathrin-coated pits (CCPs) and clathrin-coated vesicles (CCVs). (Reviewed in Elkin et al., 2016; Reider and Wendland, 2011; Wideman et al., 2014)

Vesicle coats

Vesicles are small, enclosed compartments that are separated from the cytosol by lipid membranes, and are generally classified by the types of protein coats around them. Eukaryotic cells contain a variety of different coated vesicles, and each type of vesicle carries out a specific step or a series of related steps in the trafficking pathway (Reviewed in Dell'Angelica and Bonifacino, 2019; Evans and Owen, 2002).

Among the spherical vesicular coats, COPI-coated vesicles bud from the Golgi apparatus and play an important role in retrograde cellular transport by mediating the trafficking between the Golgi compartments, from the Golgi back to the ER, and from the early endosome back to the *trans*-Golgi network (TGN) (Figure 2-2) (Cosson and Letourneur, 1994; Popoff et al., 2011; Xu et al., 2017; Yang et al., 2011). COPII vesicles transport newly synthesized proteins from the ER to the Golgi complex (Barlowe et al., 1994). The clathrin polymeric coat combines with various adaptor complexes to function in the endocytic and recycling pathways by mediating budding from the TGN, endosomal compartments, and plasma membrane (Robinson, 2004, 2015; Robinson and Bonifacino, 2001). AP-1 associates with clathrin to mediate transport from the TGN to the early endosome, and from the early or recycling endosomes back to the TGN (Hirst et al., 2013). AP-1 is also involved in polarized sorting in neurons and epithelial cells (Bremser et al., 1999; Farías et al., 2012; Fölsch et al., 2001; Gravotta et al., 2019). AP-2 also interacts with clathrin and transport cargoes from the plasma membrane to the endosome. In contrast, AP-3, AP-4, and AP-5 are not essential for viability in animals. AP-3 utilizes clathrin during its function from the early endosome to the lysosome (Peden et al., 2004; R et al., 1998). While some functions of AP-3 use clathrin (Dell'Angelica et al., 1998; Peden et al., 2002, 2004; SA et al., 2013; Theos et al., 2005), some other

functions of AP-3 do not (Peden et al., 2002; SA et al., 2013). Less is known about the exact roles of AP-4 and AP-5. AP-4 has been implicated to be important in the central nervous system and exports specific cargoes out of the TGN to the preautophagosomal structures (Davies et al., 2018; Ivankovic et al., 2019; Matsuda et al., 2008; Mattera et al., 2017; Pace et al., 2018). AP-5 has been discovered to play a role in lysosome maintenance by retrieving cargoes form the lysosomes back to the TGN (Hirst et al., 2011, 2018). (Reviewed in Bonifacino and Glick, 2004; Dell'angelica and Bonifacino, 2019; Robinson, 2015)

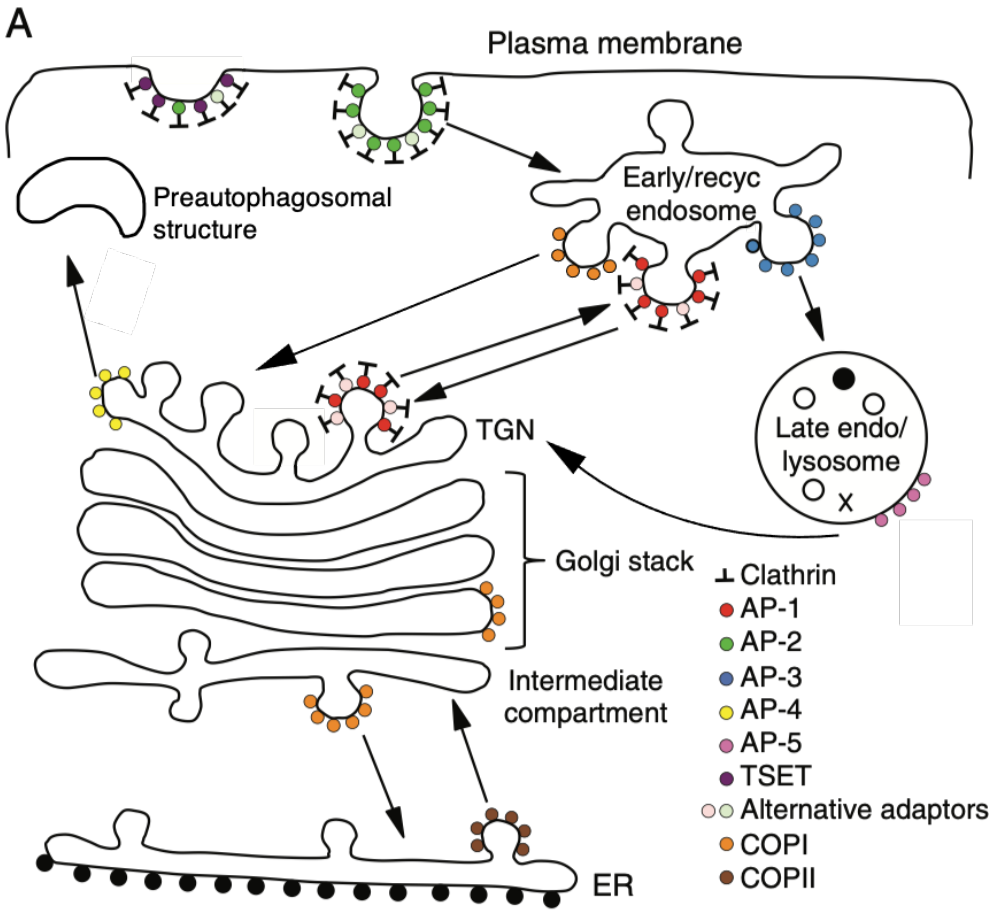

Figure 1-2. Diagram of a cell showing the APs, clathrin, COPI, COPII, alternative adaptors, and other complexes. TSET-mediated endocytosis does not happen in animals, while yeast, C. elegans, and flies lack AP-4 and AP-5. Adapted from Robinson, 2015.

The coats can appear in two forms: spherical vesicular coats, as appeared in COPI-, COPII-, and clathrin-coated vesicles; and tubular coats, such as the retromer complex. A clathrin coated vesicle

consists of three layers: an inner layer that consists of the membrane and the cargoes, a middle layer made up of adaptor and accessory proteins, and a coat scaffold outer layer (Figure 1-3) (Reviewed in Evans and Owen, 2002b; Robinson, 2015). In contrast to clathrin and COPII, for which adapter and cage form discrete layers and are recruited sequentially, the entire COPI (coat protein complex I) coat is highly interconnected and is recruited *en bloc* (Bykov et al., 2017; Dodonova et al., 2015; Hara-Kuge et al., 1994).

The basic machinery of membrane trafficking at the protein family level is conserved across the span of eukaryotic diversity (Dacks and Robinson, 2017; Wideman et al., 2014). The scaffold of different outer coat complexes share similar structural motifs, which suggest they have arisen from a common ancestor via ancient gene duplications (Dacks and Field, 2007; reviewed in Devos et al., 2004). The COPI B-subcomplex, COPII, and clathrin outer coats all contain N-terminal β-propeller and C-terminal α-solenoid domains and were thought to form lattices or cages to stabilize and drive membrane curvature during vesicle formation (Dodonova et al., 2015; Fotin et al., 2004; Stagg et al., 2008) (Figure 1-3). However, despite the similarities, the coats have evolved differently in terms of their architectures. In the clathrin cage, trimers of clathrin heavy chains form triskelion assembly units that center on the vertices of the cage (Lee and Goldberg, 2010). While the long α-solenoid domains curve outward and join the neighboring α-solenoid domains, the β-propeller domains project inwards to interact with the adaptor protein complexes (Collins et al., 2002; Fotin et al., 2004; Ter Haar et al., 2000; Heldwein et al., 2004). Unlike clathrin, the COPII outer coat assembly unit comprises of two copies of Sec13/31 that form a α-solenoid dimer rod capped by two β-propeller domains at each end (Hutchings et al., 2018; Stagg et al., 2008). To assemble, four α-solenoid dimer rods converge to form the vertex and the cage geometry varies depending on the size (Stagg et al., 2008). The COPI cage has an intermediate design between COPII and clathrin: while COPI B-subcomplex has vertex interactions involving the axial ends of β-propeller domains like the COPII cage, it resembles clathrin in the arrangement where three curved α-solenoid domains

radiating from a common center (Dodonova et al., 2015; Lee and Goldberg, 2010). (Reviewed in Noble and Stagg, 2015; Dell'angelica and Bonifacino, 2019)

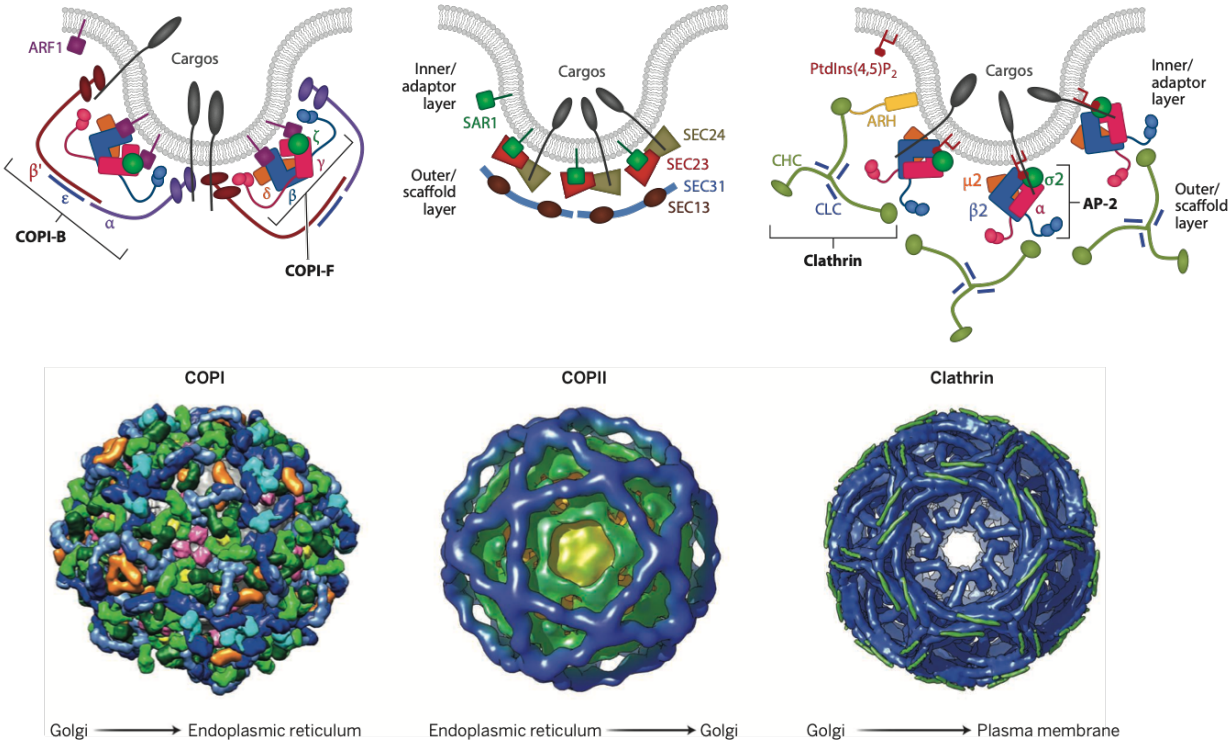

Figure 1-2. Schematics of COPI, COPII, and AP2-associated clathrin coats (top panel); and EM models of different assemblies of the COPI, COPII, and clathrin coats (bottom panel). The AP2-clathrin and COPII have distinct layers of adaptors and outer coats, and cargo recognition is primarily mediated by the adaptors. COPI F- and B-subcomplexes are not layered and are both in close proximity to the membrane, cargo recognition mainly happens through the B-subcomplex. The PDB accession codes for these models are: COPI (EMD-2985, EMD-2986, EMD-2987, EMD-2988, EMD-2989), COPII (EMD-1511), clathrin (1XI4). Adapted from Noble and Stagg, 2015; Dell'Angelica and Bonifacino, 2019.

The adaptor complexes

Adaptors serve to link the outer coat scaffold to the vesicle membrane and cargoes. The two most common adaptor families are the heterotetrameric adaptor-containing coat family and the monomeric Golgi-localized, γ-ear containing, ADP ribosylation factor binding family (GGAs) (Robinson, 2004, 2015; Robinson and Bonifacino, 2001). Often considered a more ancestral coat, COPII has a two-subunit Sec23/24 cargo adaptor that has a direct role in membrane shaping (Figure 1-3) (Barlowe et al., 1994; Zanetti et al., 2013). The adaptor complexes of COPI and clathrin share more similarities and both belong

to the heterotetrametric adaptor protein family, or APs (Figure 1-4). Originally named as “assembly polypeptides”, the family consists of seven structurally and evolutionarily related members: AP-1, AP-2, AP-3, AP-4, AP-5, the F-subcomplex of COPI, and TSET (Reviewed in Hirst et al., 2013; Robinson, 2015; Robinson and Bonifacino, 2001). Among the family members, APs-1-3 associate with clathrin coats in various trafficking pathways, and COPI F-subcomplex associates with the outer-coat-like COPI B-subcomplex (Reviewed in Dell’angelica and Bonifacino, 2019). The APs serve as adaptors during vesicle formation, where they interact with cargoes (though in COPI it’s mainly the B-subcomplex that binds cargoes), accessory proteins, and scaffolds. Structurally, the APs are all heterotrimers that each has two large (~100 kDa), one medium (~50 kDa), and one small subunits (~20 kDa) (Robinson, 2004; Robinson and Bonifacino, 2001). The two large subunits fall into two families: the β family and the “EGADZ” (ε/γ/α/δ/ζ) (Dacks and Robinson, 2017). Both of the large subunits of the APs have a N-terminal α-solenoid trunk domain (also called the heat-repeat domains) and a C-terminal appendage domains, connected by a flexible linker known as a “hinge”. The medium-sized subunits contain a longin domain followed by a “μ homology domain” (MHD), and the small σ subunits consist of a single longin domain. (Collins et al., 2002; Reviewed in Dacks and Robinson, 2017)

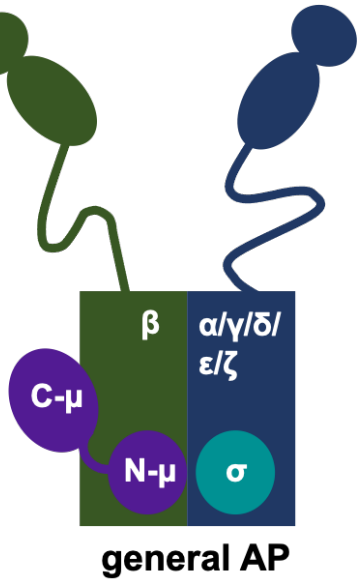

Figure 1-3. The schematic of a general AP complex. The "core complex" includes two large subunits, one medium subunit, and one small subunit. Note that the AP-5 ζ subunit lacks the appendage domain.

SNAREs and accessory proteins

SNAREs (soluble N-ethylmaleimide-sensitive factor attachment protein receptor) are another important component of vesicles. SNAREs are localized to vesicles (v-SNAREs) and target membranes (t-SNAREs) and form a complex that bridges and fuses the membranes (Söllner et al., 1993) (Figure 1-5). The SNARE complex is composed of three or four SNARE proteins, and at least two of them must be anchored in the vesicle and target membranes through the C-terminal transmembrane domains. The SNARE motifs in SNAREs that mediate folding and binding to each other to form a parallel four-helix bundle during vesicle fusion (Hayashi et al., 1994; Sutton et al., 1998). Four classes of SNARE motifs are distinguished (R-SNARE, Qa-SNARE, Qb-SNARE, and Qc-SNARE motifs) and the four-helix bundle is composed of one member from each of the four classes (Kloepper et al., 2007). R-SNAREs usually corresponds to the v-SNAREs, and the Q-SNAREs usually corresponds to the t-SNAREs (Parlati et al., 2000). The core of the bundle consists of hydrophobic residues packed into 15 layers. Inside the hydrophobic core, the "0" layer located in the center of the bundle has one arginine residue from R-SNARE and three glutamine residues

from Q-SNAREs to make hydrogen bonds (Sutton et al., 1998). After being transported with vesicles as part of the mechanism, SNAREs often need to be retrieved and therefore act as cargoes to COPI. (Reviewed in Südhof and Rothman, 2009; Yoon and Munson, 2018)

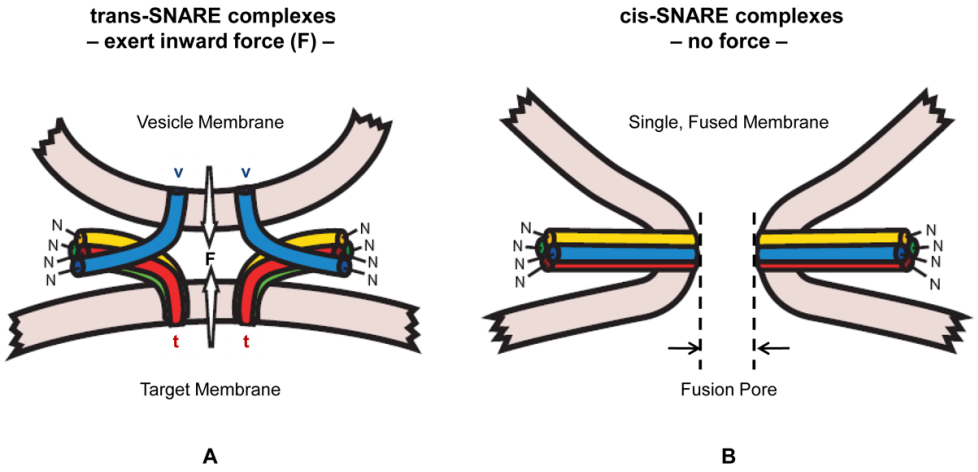

Figure 1-4. The schematics of trans-SNARE and cis-SNARE complexes. The trans-SNARE complex is formed by three helices anchored in one membrane (t-SNAREs or Q-SNARE) and another helix anchored in the other membrane. The SNAREs act as a zipper during the assembly process, which progresses from the membrane-distal N-terminus to the membrane-proximal C-terminus, generating an inward force that pulls the membrane to come together and fuse. After fusion is finished, the SNAREs are in a low energy *cis*-SNARE status. Südhof and Rothman, 2013.

Vesicles also require various types of accessory proteins. In clathrin coated vesicles, the accessory proteins are recruited by the appendage domains. For example, Eps15 and amphiphysin bind AP-2 α and β subunits, respectively, and function in early stage vesicle formation and maturation (Owen et al., 2000; Schmid et al., 2006). Accessory proteins may also interact with lipids and other proteins to assist in cargo sorting, vesicle scission, uncoating, and regulate the process to ensure all steps occur in correct order and locations (Bhave et al., 2020; McMahon and Boucrot, 2011).

Vesicle formation

Vesicle formation must follow a set of precisely organized sequential interactions to ensure all necessary components, including cargoes and SNAREs, are correctly packed into the newly formed vesicle. Taking the clathrin coated vesicles as an example, this happens when cytoplasmic coat protein complexes

assemble on a membrane surface, where they capture cargo proteins and polymerize into cages to deform the plasma membrane or an organelle membrane into a bud, then the vesicles are released by scission from the membrane. After leaving the membrane, the vesicle is soon uncoated and continues to be transported along the cytoskeleton to the target membrane, where the vesicle is recognized by tethers and Rabs. The final docking and fusion of the vesicle is mediated by pairing of v-SNARE on the vesicle and t-SNARE on the target membrane. (Figure 1-6) (Reviewed in Bonifacino and Glick, 2004; Kirchhausen et al., 2014)

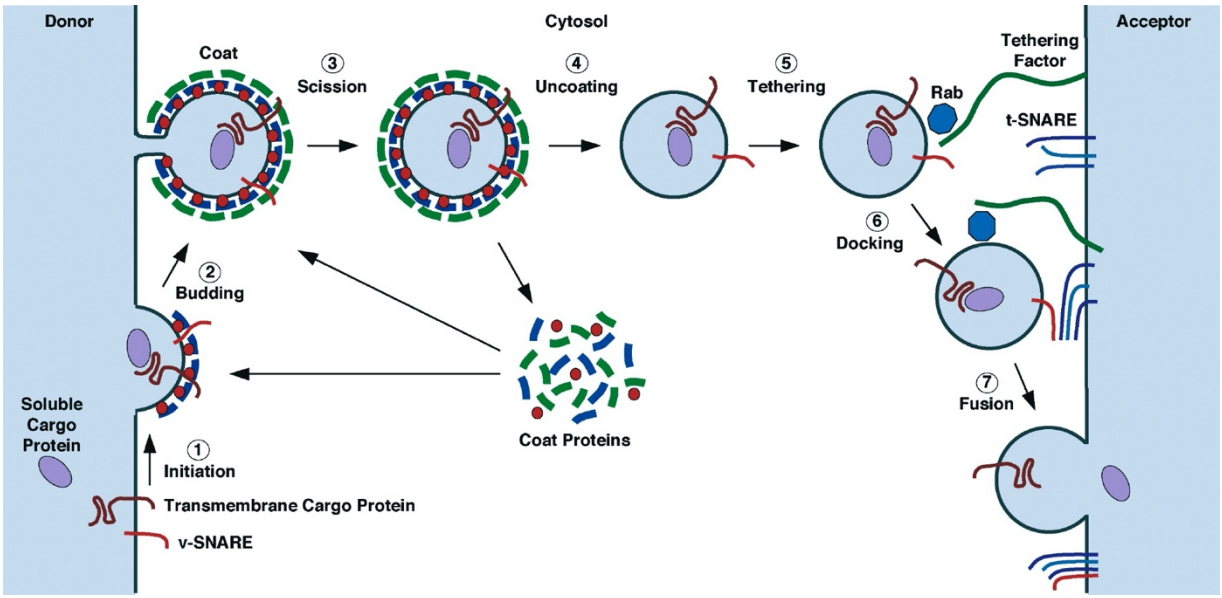

Figure 1-5. The steps of vesicle formation, uncoating, and fusion with target membrane. (1) Initiation. When cargo is present, the coat components are recruited to the site of emergence via a membrane-associated GTPase or specific phosphoinositides. (2) Budding. The coat components of the vesicle polymerizes into a cage-like structure, driving the membrane curvature and cargo concentration. (3) Scission. The vesicle is severed from the donor membrane through the actions from the coat or with accessory proteins. (4) Uncoating. The coat disassembles after vesicle budding and cytosolic coat proteins are recycled for further use. (5) Tethering. The uncoated vesicle arrives at the acceptor membrane and becomes tethered through Rab GTPase and tethering factors. (6)Docking. The SNAREs form a four-helix *trans*-SNARE complex. (7) Fusion. The *trans*-SNARE complex pulls the vesicle and acceptor membranes together and promotes membrane fusion. The SNAREs are then recycled. Bonifacino and Glick, 2004.

A common mechanism between COPI-, COPII-, and clathrin-coated vesicles is that small GTPases are required for membrane recruitment during vesicle trafficking. COPI, AP-1, AP-3, AP-4, and the GGAs are recruited by Arf1, an Arf (ADP ribosylation factor) family GTPase (Barlowe et al., 1994; Ooi et al., 1998; Serafini et al., 1991; Wang et al., 2003) whereas COPII requires another Arf family GTPase member, Sar1

(Secretion associated Ras related GTPase 1). The exception is AP-2, because AP-2 binds directly to PtdIns(4,5)P_2 and other accessory proteins (Collins et al., 2002; Jackson et al., 2010). (Reviewed in Donaldson and Jackson, 2011; Robinson, 2015)

The Arf family of small GTPases have been found to play important roles as "molecular switches" to regulate membrane trafficking. GTP binding activates Arf GTPases, whereas hydrolysis of GTP to GDP returns Arf GTPases to an inactive conformation. Thus, Arf family GTPase activity is dependent on a cycle of GTP binding and hydrolysis, which in turn recruits and regulates coat function (Figure 1-7). The regulation of Arf GTPases is achieved by corresponding ArfGEFs (Guanine Nucleotide Exchange Factors) and ArfGAPs (GTPase-Activating Proteins), which catalyze GTP binding and hydrolysis, respectively (Chardin et al., 1996; E et al., 1995; Peyroche et al., 1996). The Arf family of GTPases are distinct from other families of small regulatory GTPases in possessing an amphipathic N-terminal helix (N0 helix) (Antonny et al., 1997). Upon recruitment to the membrane, the N-terminal amphipathic helix in the Arf family GTPase inserts into the membrane, and this step is a prerequisite for Arf activation by ArfGEFs (Antonny et al., 1997; Peyroche et al., 1996). After that, recruitment of coat components and membrane curvature is facilitated. Like other small GTPases, Arf family members contain the canonical nucleotide-sensitive switch I and switch II loops (Amor et al., 1994). However, they also have a unique interswitch region that connects the switches I & II and acts as an allosteric push button between the active and inactive states (Pasqualato et al., 2002). The interswitch conformational rearrangement is coupled to the N-terminal amphipathic helix, allowing communication between nucleotide binding and membrane association (Amor et al., 1994) (Figure 1-7). (Reviewed in Donaldson and Jackson, 2011; Goldberg, 1998; Jackson and Bouvet, 2014)

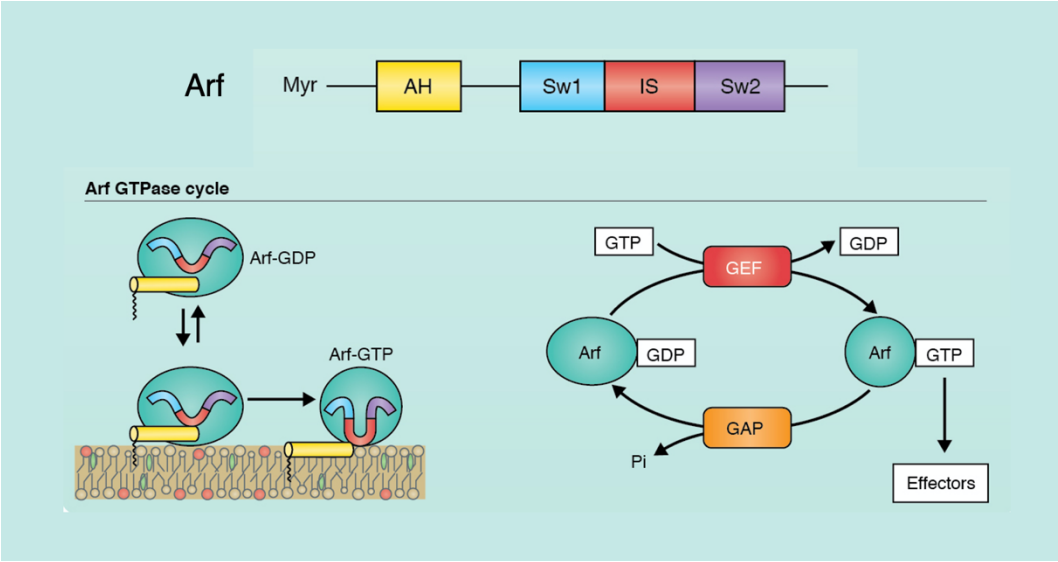

Figure 1-6. The schematics of Arf sequence and Arf GTPase cycle. AH: Amphipathic Helix; Sw1: Switch I; IS: Interswitch; Sw2: Switch II. Upon membrane recruitment, the N-terminal amphipathic helix insets into the membrane, which couples the rearrangement of the interswitch region that connects Switches I & II. Such conformational change is a prerequisite for activation by ArfGEF. Adapted from Jackson and Bouvet, 2014.

In addition to the GTPase regulations, AP complexes have been found to undergo conformational rearrangements during vesicle formation, and these different states may enable spatiotemporal control of AP activity (Figure 1-8) (Ghosh and Kornfeld, 2003; Matsui and Kirchhausen, 2002; Rapoport et al., 1997). In AP-2, the first crystal structure obtained was in a soluble cytosolic state that has inactive, or "closed" conformation, where only a single membrane binding pocket in α is exposed (Collins et al., 2002; Gaidarov and Keen, 1999). In this "closed" conformation, other cargo, membrane, and clathrin binding sites are masked (Kelly et al., 2014). When AP-2 is bound to synthetic cargo peptides, a different crystal structure reveals that high concentrations of cargo are able to induce a "partially open" conformational change in AP-2 (Kelly et al., 2008). The σ2 dileucine binding site is now exposed and occupied by cargo and therefore displacing the N-terminus of β2 and inducing a 20° flexion of α helical solenoids. The active, or "open" form of AP-2 was obtained through co-crystallizing AP-2 with a tyrosine motif peptide (Jackson et al., 2010). In this conformation, the μ2 C-terminus is dislodged and rotated out from the center of the AP-2 complex, and all cargo- and membrane-binding site are now co-planar. Such conformational change

from “closed” to “open” is considered the allosteric activation of APs. Similarly, AP-1 also has a cytosolic “closed” conformation and an active “open” conformation (Heldwein et al., 2004; Ren et al., 2013). However, AP-1 also seems to have a “hyper-open” form when viral proteins are engaged (Jia et al., 2014).

Membrane binding may stimulate conformational change of soluble APs, when they are localized to the site of emergence through the phospholipid-binding site exposed in the closed conformation (Figure 1-8). For AP-2, presence of cargo in PIP2-containing membrane cooperatively stimulates AP-2 to bind clathrin in a hierarchical progression (Kadlecova et al., 2017; Kelly et al., 2008, 2014). Other accessory proteins, such as the Eps15 and FCHo1/2, were also discovered to act in the allosteric activation of AP-2 (Benmerah et al., 1995; Iannolo et al., 1997; Ma et al., 2016). In contrast, AP-1 needs membrane-associated, GTP-bound Arf1 for its allosteric activation (Le Borgne et al., 1996; Seaman et al., 1996; Stamnes and Rothman, 1993; Traub et al., 1993). Each Arf1 engages with AP-1 via two interfaces at the same time: the C-terminal β1 subunit in one copy of AP-1 and the central region of γ subunit in another copy of AP-1. The interface with β1 subunit buries the switch I & II regions of Arf1 that are important to interact with effectors upon GTP binding (Kumawat et al., 2017). Phosphorylation also plays a stimulatory or stabilization effect on the active open AP conformations, and there are multiple phosphorylated sites on APs (Reviewed in Beacham et al., 2019).

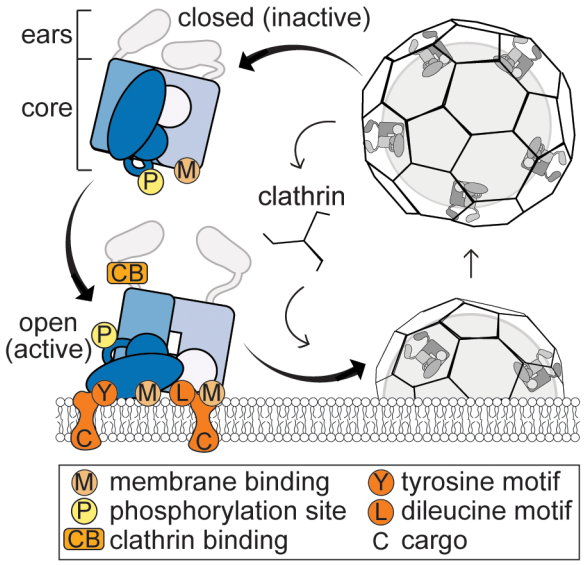

Figure 1-7. The cycle of AP conformational changes. APs change from cytosolic "closed" conformation to membrane-associated "open" conformation during vesicle formation. Upon conformational change, the membrane, cargo, and clathrin binding sites are exposed. Adapted from Beacham, Partlow, and Hollopeter, 2019.

Introduction to COPI coated vesicles

The COPI coat

In the COPI system, the adaptor and outer coat components are combined in a cytoplasmic heteroheptameric complex (α/β/β'/γ/δ/ε/ζ) that is recruited *en bloc* onto the Golgi membrane (Hara-Kuge et al., 1994), which is distinct from the stepwise accretion of clathrin and COPII (Figure 1-9) (Hutchings et al., 2018; Kovtun et al., 2020; Noble et al., 2012). COPI can be biochemically divided into two subcomplexes (Schledzewski et al., 1999a; Yu et al., 2012). The outer cage-like B-subcomplex (α-/β'-/ε-COP subunits) is similar to clathrin, as both α-COP and β'-COP contain the N-terminal β-propeller and C-terminal α-solenoid domains found in clathrin (Lee and Goldberg, 2010; Lowe and Kreis, 1996; Pavel et al., 1998). The β-propeller domains are also known as the WD-repeat domains, which have about 40 amino acids terminating in tryptophan (W) and glutamic acid (D). The adaptor-like F-subcomplex (β-/γ-/δ-/ζ-COP subunits) and APs evolved from a common ancestor and share both structural and functional similarities: the two large subunits of β-COP and γ-COP contain the α-solenoid trunk domains and β-appendage

domains connected by the hinges; the medium-sized δ-COP consists of a longin domain and a μ-homology domain; and a small ζ-COP subunit that only contains a longin domain (Dacks and Robinson, 2017). The domains tend to occur in pairs due to gene duplications during the evolution from the early ancestral coat complex (Dacks and Robinson, 2017). All the subunits of COPI co-ordinate to form the highly-intertwined architecture of COPI (Dodonova et al., 2015, 2017). The ε-COP is the only non-essential subunit and it emerged last during evolution (Duden et al., 1998) (Figure 1-9).

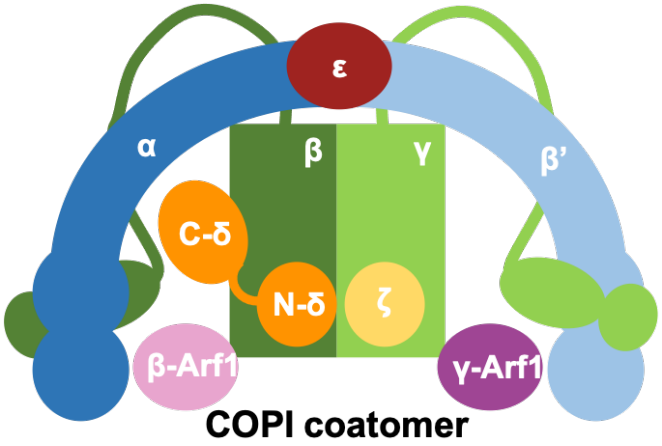

Figure 1-8. The schematic of COPI coatomer. The B-subcomplex is composed of α-/β'-/ε-COP subunits, and F-subcomplex consists of β-/γ-/δ-/ζ-COP subunits. Arf1 appears in two niches in COPI, *i.e.* two different molecules of Arf1 bind β-COP and γ-COP respectively: β-Arf1 and γ-Arf1.

In contrast to the distinct layers of adaptors and outer cage structures in COPII and clathrin coated vesicles, COPI coatomer forms clusters of flexibly linked units (Faini et al., 2012) (Figure 1-10). The symmetric basic unit of the COPI coat is called the COPI triad and is composed of three heptamers (Figure 1-10). The triads are linked by flexible domains forming dimeric or trimeric interactions depending on the positions in the coat (Dodonova et al., 2015), and the corresponding linkages are grouped into types I – IV (Dodonova et al., 2017). This combination of two-fold and three-fold symmetries contributes to the assembly of a curved lattice. (FIGURE 1-10) By altering the angles between the adjacent triads, the COPI coat is able to adapt to form vesicles of varying sizes and degrees of curvature (Faini et al., 2012).

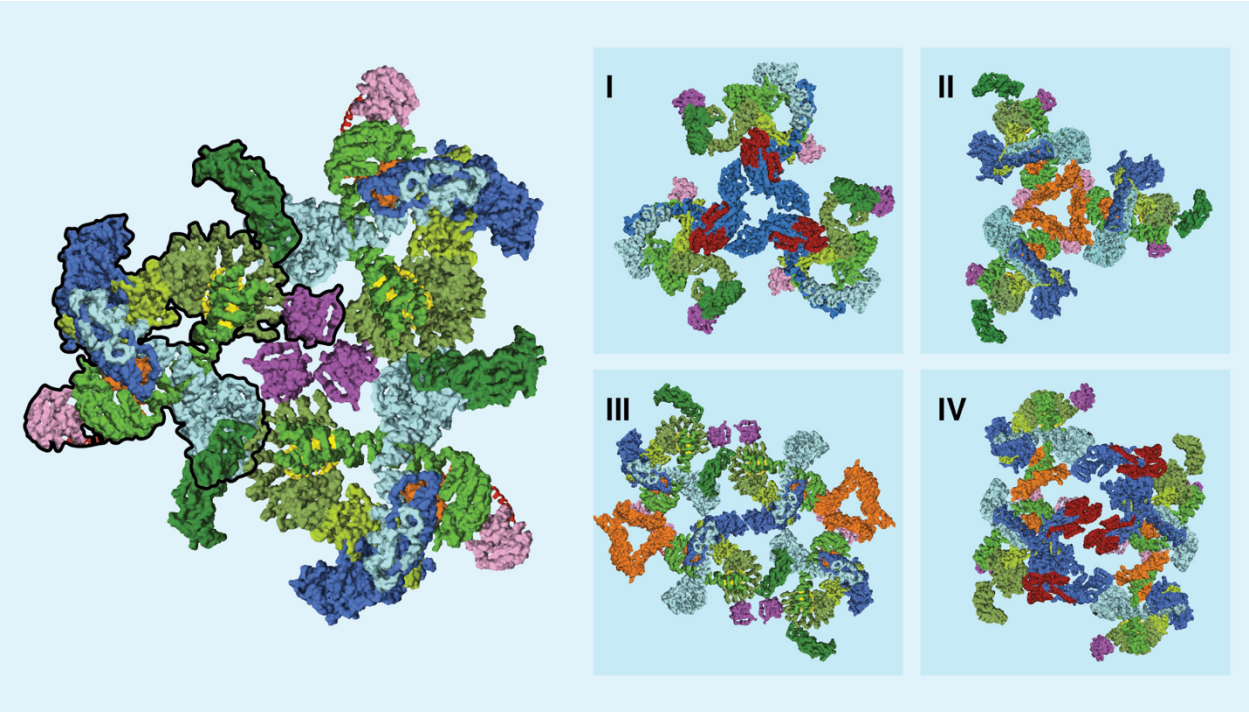

Figure 1-9. The COPI triad and linkages. Three COPI heptameric coatomers form the symmetric triad. Triads are basic units of the COPI coat and are connected by flexible domains forming four types of dimeric or homotrimeric linkage patterns in the coat. The flexible C-termini of α-COP and ε-COP mediate the central contacts in linkage type I and IV, and μHD of δ-COP mediates the central contacts in linkage type II. Combinations of such two-fold and three-fold symmetries facilitates the assembly of curved lattices. Color coded as in Figure 1-11. Adapted from Arakel and Schwappach, 2018.

COPI formation

Biogenesis of COPI is controlled by the monomeric GTP-binding protein Arf1 (Figure 1-11). During early stages of vesicle formation, Arf1(GDP) comes to the site of vesicle emergence and undergoes guanine nucleotide exchange mediated by an ArfGEF called GBF1 (Gea1/2 in yeast), which is catalyzed by the conserved Sec7 domain (Jackson, 2014; Mossessova et al., 1998; Peyroche et al., 1996). Upon nucleotide exchange, a myristoylated amphipathic helix at the amino terminus of Arf1 becomes exposed and stably anchors Arf1(GTP) to the membrane lipid bilayer (Antonny et al., 1997; Franco et al., 1996; Liu et al., 2009). Together with the presence of a membrane protein, such as a SNARE protein or a cargo receptor, Arf1(GTP) subsequently recruits coatomer proteins to the site *en bloc* (Hara-Kuge et al., 1994), which differs from the successive recruitment of AP-1/2 and clathrin coated vesicles or COPII. At the same time, GBF1 interacts with the γ-COP appendage domain, spatially restricting the COPI coatomer in the

vicinity of activated Arf1 (Deng et al., 2009). Protein cargo is then packaged, and a COPI-coated vesicle buds off (Figure 1-11). Before vesicle fusion with a target membrane, the protein coat is shed. Coat dissociation is thought to be mediated by hydrolysis of Arf(GTP), which is stimulated by an ArfGAP (Tanigawa et al., 1993). Apart from coat dissociation, the importance of GTPase hydrolysis has also been implicated in the COPI cargo-sorting process. Early *in vitro* reconstitution experiments using purified Golgi complex showed disabling the GTP hydrolysis on Arf1 resulted in less cargo being packed in to COPI vesicles (Lanoix et al., 2001a; Lee et al., 2005; Nickel et al., 1998; Pepperkok et al., 2000).

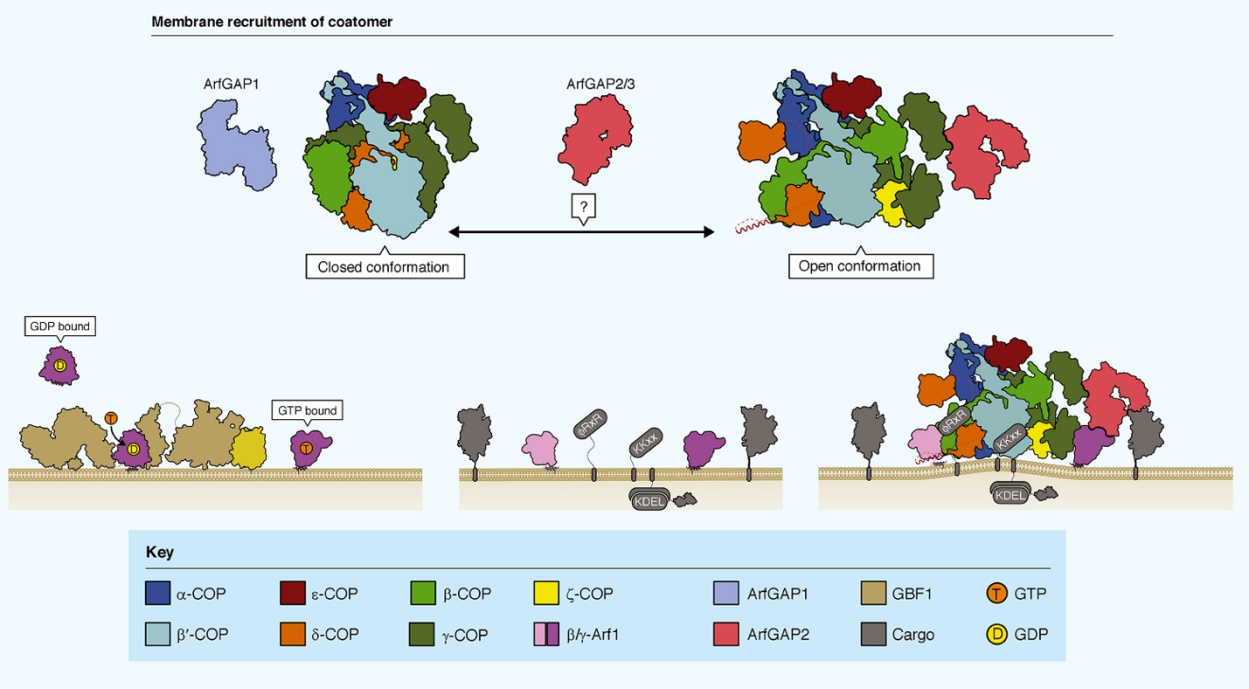

Figure 1-10. COPI formation. Arf1 undergoes a conformational change upon membrane-associated and is activated by the ArfGEF. Activated Arf1 then help recruits the COPI coatomer and ArfGAP2/3. Adapted from Arakel and Schwappach, 2018.

In COPI, two different molecules of Arf1 have been proposed to bind β-COP and γ-COP respectively; we will call these β-Arf1 and γ-Arf1. In a COPI triad, γ-Arf1 occupies the center of the triad and β-Arf1 locates at the periphery where the membrane surface is more exposed (Arakel et al., 2019a; Dodonova et al., 2017). Structural and protein interaction evidence suggest that each Arf1 niche preferentially recruits one of two ArfGAP types known to affect COPI (Arakel et al., 2019a; Dodonova et

al., 2017) (Figure 1-11; Figure 1-12). Binding of these Arf1 molecules happen on almost equivalent surfaces and the interactions are GTP-dependent (Dodonova et al., 2017; Yu et al., 2012). Binding of Arf1 to β-COP and γ-COP then facilitates the membrane association of the cytosolic heteroheptameric COPI coatomer, and confines COPI orientation relative to the membrane (Yu et al., 2012). More recently, through yeast experiments and EM tomography data, a helix in δ-COP has also been identified to interact with activated Arf1 in the Switch I region, interswitch and C-terminal helix (Arakel et al., 2016). This surface is located on Arf1 in a region accessible when Arf1 is in the GTP-bound status and the N-terminal amphipathic helix is inserted into the membrane (Goldberg, 1998; Liu et al., 2009; Pasqualato et al., 2002). The surface is occupied by the N-terminal amphipathic helix when Arf1 is in the GDP-bound status (PDB: 1HUR) (Amor et al., 1994). This interaction further stabilizes Arf1 in the active state and in turn, GTP hydrolysis by Arf1 can directly modulate the conformation of δ-COP and thus other binding partners (Arakel et al., 2016; Dodonova et al., 2017). Together, previous studies have suggested that GTP hydrolysis is coupled to COPI cargo packaging through a conformational change in COPI.

Both AP-1 and AP-2 show they go through a large conformational change from a closed cytoplasmic form to an open membrane-associated form, when the adaptor complex is recruited to the membrane. Such conformational changes couple membrane recruitment to cargo sorting by unmasking the cargo-binding sites in the adaptor complex (Collins et al., 2002; Jackson et al., 2010; Kelly et al., 2008, 2014). In contrast, COPI appears to present a “hyper-open” conformation compared to AP-2 when it becomes membrane-associated (Dodonova et al., 2015). Multiple lines of evidence suggest that COPI coatomer undergoes a conformational change upon membrane recruitment. However, we still don’t know in what steps Arf1(GTP) hydrolysis and cargo recognition are carried out. Previous studies believed binding of p24 family proteins, a highly conserved family of type I transmembrane proteins that are abundant in early secretory pathway, can induce a conformational change in COPI (Aguilera-Romero et al., 2008; Langer et al., 2008; Reinhard et al., 1999). Early cryo-EM data of yeast COPI suggested high

flexibility in the coatomer (Yip and Walz, 2011). However, another study using recombinant human COPI failed to observe any significant differences between cytosolic coatomer and membrane-associated coatomer (Wang et al., 2016).

ArfGAPs in COPI mediated trafficking

ArfGAPs play critical roles in COPI coated vesicles because Arf1 has very low intrinsic GTPase activity (Luo et al., 2009a; Weimer et al., 2008). There are 31 genes discovered in human to encode proteins that contain ArfGAP domains. ArfGAPs are multidomain proteins that can be divided into ten subtypes based on phylogenetic analysis and shared domain structure (Inoue and Randazzo, 2007; Kahn et al., 2008; Randazzo and Hirsch, 2004; Spang et al., 2010). Since the discovery of ArfGAPs (Cukierman et al., 1995), it has been established that in the GAP domain, a catalytic arginine, or "arginine finger" is important in stimulating the GTP hydrolysis by Arf GTPases (Ahmadian et al., 1997; Cherfils and Zeghouf, 2013; Scheffzek et al., 1998). During this process, the arginine finger is inserted into the nucleotide-binding site of Arf GTPases to stabilize the transition state of the reaction, with the help from a conserved glutamine in the switch II region of the GTPase (Cherfils and Zeghouf, 2013; Ismail et al., 2010).

Apart from the canonical roles in GTP hydrolysis, ArfGAPs also operate as cargo adaptors and carry out important interplay between GTP hydrolysis, cargo sorting, and vesicle formations (Aguilera-Romero et al., 2008; Aoe et al., 1997; Bigay et al., 2005; Lee et al., 2005; Nie and Randazzo, 2006; Park et al., 2015; Robinson et al., 2006; Schindler et al., 2009; Spang et al., 2010). Most data suggest the cycle of GTP binding to Arf1 and GTP hydrolysis is linked to both coat association with and dissociation from the membranes. Therefore, ArfGAPs are needed to trigger coat dissociation but their activity needs to be delayed until the vesicle is budded off. In addition to this, multiple studies showed that ArfGAPs are also needed during cargo packaging and coat formation, since inhibition of GTP hydrolysis results in deficient sorting and accumulation of COPI on the membrane (Lanoix et al., 2001b; Nickel et al., 1998; Presley et al., 2002; Tanigawa et al., 1993).

The yeast counterparts of mammalian ArfGAP1 and ArfGAP2/3 are Gcs1 and Glo3, respectively. Gcs1 and Glo3 regulate COPI transport and they have been previously shown to have overlapping functions and interact with COPI coatomers *in vitro* (Poon et al., 1999; Weimer et al., 2008; Yang et al., 2002). COPI in turn facilitates the ArfGAP-dependent GTP hydrolysis of Arf1 (Ahmadian et al., 1997; Dodonova et al., 2017; Goldberg, 1999, 2000a; Luo et al., 2009b, 2009a). In EM tomography data obtained from *in vitro* reconstituted COPI coated vesicles, ArfGAP2/3 was positioned near γ-Arf1 that was bound to γ-COP, while β-Arf1 in complex with β-COP did not seem to recruit ArfGAP2/3 (Dodonova et al., 2017). Therefore, the authors proposed Arf1 exists in two distinct environments within the COPI coat architecture and such spatial separation has functional implications. This is further supported by protein interaction data by Arakel and colleagues (Arakel et al., 2019a).

ArfGAP1, or Gcs1 in yeast, is recruited to membrane in a coatomer-independent manner, and contains the ArfGAP lipid-packing sensor (ALPS) motif that forms amphipathic helix on curved membrane, coupling GTP hydrolysis to driving membrane curvature (Bigay et al., 2003, 2005; Mesmin et al., 2007; Kliouchnikov et al., 2009; Schindler et al., 2009; Weimer et al., 2008). There's controversy about whether ArfGAP1 interacts with COPI. Some studies suggest ArfGAP interacts with the δL motif in δ-COP with low affinity and helps orient ArfGAP1 in the assembled coat and stabilize the molecule in the vicinity of β-Arf1 (Cosson et al., 1998; Rawet et al., 2010; Spang et al., 2010; Suckling et al., 2015; Weimer et al., 2008). While other studies failed to replicate this result (Arakel et al., 2019a).

In contrast, ArfGAP2/3, or Glo3 in yeast, does not have a ALPS motif and is recruited to membranes in a coatomer-dependent manner. Glo3 has multiple interaction site in its BoCCS (Binding of Coatomer, Cargo, SNAREs) region that interact with COPI (Frigerio et al., 2007; Lewis et al., 2004; Schindler et al., 2009; Watson et al., 2004) (Figure 1-12). It also has a C-terminal GRM (Glo3 Regulatory Motif) region that communicates between the GAP and BoCCS through a highly conserved tandem repeat ISSxxxFG sequence (Schindler et al., 2009; Yahara et al., 2006). The GAP domains of ArfGAP2/3 have lower intrinsic

GAP activity (Kliouchnikov et al., 2009; Luo et al., 2009b; Weimer et al., 2008). The strong association of ArfGAP2/3 to cytosolic COPI coatomer may indicate it is co-recruited to the membrane with coatomer (Arakel et al., 2019a; Eugster et al., 2000; Lewis et al., 2004; Watson et al., 2004) and may play more important roles in coatomer polymerization and Golgi integrity (Kartberg et al., 2010).

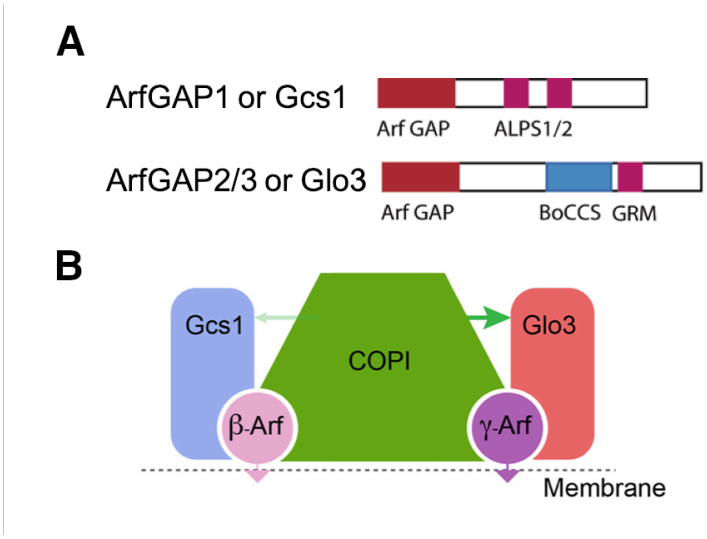

Figure 1-11. The schematics of ArfGAP1 and ArfGAP2/3, and their proposed distinct niches in COPI. (A) The schematics of ArfGAP sequences. ArfGAP1 or Gcs1 consists of a N-terminal GAP domain, and C-terminal ALPS (ArfGAP Lipid-Packing Sensor) motifs. ArfGAP2/3, or Glo3 contains a N-terminal GAP domain, an internal BoCCS (Binding of Coatomer, Cargo, SNAREs) region, and a C-terminal GRM (Glo3 Regulatory Motif) region. (B) The schematic of the heptameric COPI coatomer in complex with two Arf1 molecules (β-Arf1 and γ-Arf1) and two yeast ArfGAPs (Glo3 and Gcs1). The thickness of the arrows indicates the different affinities between the COPI coat and the two ArfGAPs. Structural and protein interaction data suggest Glo3 preferentially binds γ-Arf1 and Gcs1 preferentially binds β-Arf1. Adapted from Spang, Shiba, and Randazzo, 2010; Arakel et al. 2019.

As an integral part of the COPI vesicle, the Glo3 interactions with COPI coat proteins, SNAREs and cargoes are vital for its functions. The GAP domain, BoCCS region, and regulatory GRM region communicate with each other, linking the stimulation of GTP hydrolysis with vesicle formation (Schindler et al., 2009). The BoCCS region is unstructured, but was found to be essential for coatomer association and its function in yeast (Schindler et al., 2009). Previous studies have shown neither Glo3 nor Gcs1 are essential in yeast but combined deletion of both is inviable for yeast (Frigerio et al., 2007; Poon et al., 1999). More recently, Arakel *et al.* used catalytically "dead" versions (R54K in Gcs1 and R59K in Glo3) of Glo3 and Gcs1 and obtained remarkably distinct phenotypes (Arakel et al., 2019b, 2019a; Lewis et al.,

2004; Yanagisawa et al., 2002). Mutation of the arginine fingers to lysines in the GAP domains resulted in drastically impaired GAP activity of both Glo3 and Gcs1, however, cells harboring the Gcs1 GAP-dead mutant were viable, while Glo3 GAP-dead mutant was lethal. In addition, such lethality of Glo3 GAP-dead mutation can be reversed by disabling either the GRM or BoCCS regions (Arakel et al., 2019a). These data suggest Glo3 needs both a functional GAP domain and a functional BoCCS region. And together with the proposed distinct locations of Glo3 and Gcs1 in COPI, the GAP action in β-Arf1 and γ-Arf1 seems functionally distinct.

Altogether, it is currently unclear why COPI utilizes two ArfGAPS. Previous studies have suggested a common role of stimulating GTPase activity, as well as temporally and functionally separate roles for ArfGAP1 (or Gcs1) and ArfGAP2/3 (or Glo3): they are both involved in cargo packaging during nascent vesicle formations (Lanoix et al., 2001a; Rein et al., 2002; Schindler et al., 2009) but tend to carry out different steps in different stages.

COPI scission, uncoating, tethering

Arf1 plays an important role in the Scission of COPI coated vesicles. Scission of COPI from membrane depends on the ability of Arf1 to oligomerize (Beck et al., 2008, 2011), but vesicle release from the membrane is independent of GTP hydrolysis (Adolf et al., 2013). Furthermore, the presence of budding scars suggest the completion of COPI coat polymerization is not required in order to form a fully enclosed vesicle (Faini et al., 2012). Other auxiliary factors have also been implicated to regulate the process, including acyl-CoA, CtBP/BARS, PLD2, and DAG (diacyl-glycerol) (Fernández-Ulibarri et al., 2007; Ostermann et al., 1993; Yang et al., 2005, 2008).

The uncoating process of the COPI coat starts after vesicle scission and needs to be removed before vesicle fusion with the acceptor membrane (Bykov et al., 2017). However, partial coat components may remain and is needed for docking, since α-COP was discovered to interact with Dsl1, a tethering factor (Travis et al., 2019). GTP hydrolysis is required in the coat removal process, though the exact mechanism

and timing are unclear. Previous studies disabling the GTP hydrolysis resulted in failure to release COPI from the membrane (Presley et al., 2002; Tanigawa et al., 1993). Earlier studies investigating the half-lives of COPI coat and Arf1 support a model where the polymerized COPI coat remains on the vesicle after GTP hydrolysis and Arf1 dissociation (Liu et al., 2005; Presley et al., 2002; Yang et al., 2002). However, more recent evidence found coat dissociation happens gradually soon after vesicle release and the stoichiometry of COPI coat and Arf1 remain unaltered in different stages of the disassembly process, suggesting the dissociation of COPI coat and Arf1 is likely linked and synchronized (Bykov et al., 2017). It is currently not exactly known which of two ArfGAPs facilitates the coat removal process and in what step once the membrane curvature threshold is surpassed. Given the distinct niches of Gcs1 and Glo3 in COPI, it could be regulated by Glo3 at the center of the COPI coat triads or regulated by Gcs1 at the periphery of the triads, or both. Alternatively, they may function in different classes of COPI vesicles that are responsible for different pathways or cargoes.

The final stage of COPI trafficking is vesicle fusion with the target membrane mediated by vesicle tethers located on the target membranes. Tethers are large proteins or multiunit assemblies that recognize and bind vesicles. COPI employs a Dsl1 complex to bring in the incoming vesicles and coordinate SNAREs pairing [Andag and Schmitt, 2003]. Other proteins have also been identified to bind COPI during tethering, such as p115 (Uso1) (Guo et al., 2008; Ren et al., 2009), TRAPPII (the TRAfficking Protein Particle II) (Yamasaki et al., 2009), and the COG (Conserved Oligomeric Golgi) complex (Miller and Moultrie, 2013) [Miller, 2013]. Tethering is mediated by directly interacting with the COPI coat or factors like SNAREs and Rab GTPases (Cai et al., 2007).

COPI functions and cargoes

While the knowledge of molecular mechanisms is lacking, functions of COPI are fairly well understood. COPI is essential as a component of cellular transport. The best characterized function of

COPI system is the retrograde transport of escaped ER proteins and machinery proteins from the Golgi to the ER and trafficking within the Golgi stacks (Popoff et al., 2011; Yang et al., 2011). Another more recently recognized COPI function is the transport from early endosomes (EE) to the TGN (Aniento et al., 1996; Kawada et al., 2015; Schindler and Spang, 2007; Whitney et al., 1995; Xu et al., 2017). Apart from these, COPI-dependent retrograde transport is also recognized to play important roles in maintaining correct steady-state distribution of proteins within the Golgi stack and ER quality control, lipid droplet homeostasis, mRNA transport, breaking down of the nuclear envelope, viral replication, and pathogen entry (Beller et al., 2008; Bi et al., 2007; Cureton et al., 2012; Guo et al., 2008; Liu et al., 2003; Misselwitz et al., 2011; Park et al., 2018; Sicari et al., 2020; Soni et al., 2009; Thiam et al., 2013; Trautwein et al., 2004; Wilfling et al., 2014; Zabezhinsky et al., 2016).

The dilysine motif

Currently, a variety of COPI cargoes have been identified. COPI cargoes include proteins that are directly recognized by the COPI coat and proteins that are recognized by COPI through receptors. Six out of the seven subunits of COPI coatomer are membrane proximal, suggesting that different subunits of COPI may be able to engage in cargo recognition. Cargo recognition process in COPI is largely mediated by cargo motifs on the cytoplasmic domains of the cargo proteins. The first and the best characterized cytosolic sorting signal was the dilysine motif at the carboxyl terminus of type I transmembrane proteins, which was identified and defined in adenoviral E3 protein using yeast and mammalian reporter-based assays (Jackson et al., 1990a; Nilsson et al., 1989). Previous studies have revealed that the C-terminal dilysine motifs is recognized by the β'-COP and α-COP propeller domains that are positioned adjacent to the membrane, in which lysines are strictly required at the -3 and -4 (KKxx) or -3 and -5 (KxKxx) positions relative to the C-terminus (Cosson and Letourneur, 1994; Gaynor et al., 1994; Jackson et al., 1990a). More recent studies provided high-resolution crystal structures that reveal the mechanism of how dilysine motifs bind on the top surface of the N-terminal propeller domains of α-COP and β'-COP. In this model,

the acidic C-terminus in the dilysine motif (K(x)KxxCOO-) binds directly to the basic patch in the propeller domains, and the carbonyl groups at the -2, -3, and -4 positions act as a molecular ruler to orient the motif on the propeller domain surface through hydrogen bonding with two arginine residues (Jackson et al., 2012; Ma and Goldberg, 2013). Lysines at both -3 and -4 (KKxx) or -3 and -5 (KxKxx) positions are tolerated since each lysine residue interacts preferentially with an acidic patch in the propeller domain. Examples of dilysine cargoes include components of N-linked oligosaccharyltransferase complexes in the ER, glycoprotein protein receptors that cycle between the ER and Golgi, and some viral glycoproteins that hijack the transport pathway during entry to the cells.

The aromatic cargo motifs

Another earlier identified type of coatomer binding signal is based on aromatic residues found in some members of the p24 membrane protein family, where a $FFxxBBX_n$ ($n \geq 2$; B is a basic amino acid) is present on the cytosolic tails (Béthune et al., 2006). The p24 family protein members may contain dilysine or diphenylalanine motifs. They have been observed in COPI coated vesicles and are considered to facilitate coatomer and Arf1 recruitment during COPI formation and luminal cargo sorting (Aguilera-Romero et al., 2008; Bonnon et al., 2010; Bremser et al., 1999; Fiedler et al., 1996; Sohn et al., 1996). In the diphenylalanine motif, the two phenylalanine residues are responsible for recognition of p24 family members by two separate sites on the γ-COP trunk and appendage domains, as well as p24 dimerization (Gommel et al., 2001; Spang, 2013). Other aromatic sorting motifs include a "δL" motif that is recognized by δ-COP for retrieval to ER (Cosson et al., 1998), and a FxxxFxxxFxxLL motif in the Dopamine1 receptor that mediates interaction with γ-COP (Adolf et al., 2013; Bermak et al., 2002).

The arginine-based cargo motifs

Arginine-based motifs are related to the important role of COPI in assembly-dependent quality control of protein channels and receptors retained in ER. The arginine-based signal motif, (Φ/Ψ/R)RxR (where Φ/Ψ stands for an aromatic or bulky hydrophobic residue) is located on the cytoplasmic domains

of subunits formed in multimeric complexes such as cell surface receptors and ion channels (Zerangue et al., 1999, 2001). These motifs were first identified in the invariant chain of the major histocompatibility complex class II, and unlike the dilysine motifs, they are not confined to the carboxyl termini and may appear in multiple copies along the cytoplasmic domains (Shikano and Li, 2003). The arginine-based motif is exposed to COPI and therefore induce retrograde transport when the heteromultimeric proteins are not fully assembled, while correct assembly and post-translational modifications mask the arginine-based sorting motif (Arakel et al., 2014; Kilisch et al., 2016; Schwappach et al., 2000; Yuan et al., 2003). The motif is found to be recognized collectively by highly conserved stretches in the β-COP and δ-COP subunits through studies in yeast (Michelsen et al., 2007). Another type of arginine-based cargo motif, ΦKRxLxKR, presents in a subset of glycosyltransferases and mediate their retrieval from more distal parts of the Golgi to the *cis*-Golgi through recognition by δ- and ζ-COP subunits (Liu et al., 2018).

The KDEL and HDEL cargoes and receptors

Another kind of interaction between membrane proteins and COPI has also been demonstrated in sorting of resident soluble chaperones in the lumen of the ER. This interaction depends on a C-terminal tetra-peptide signal: HDEL (His-Asp-Glu-Leu) in yeast and KDEL (Lys-Asp-Glu-Leu) in mammalian cells (Lewis and Pelham, 1992; Munro and Pelham, 1987; Pelham, 1991; Semenza et al., 1990). Recognition is mediated by an ER protein retention receptor known as HDEL or KDEL-receptors, which recognize the Golgi-luminal proteins destined for ER retrieval through the HDEL or KDEL signals. The receptors interact with COPI coatomer via a KKxSxxx signal in the cytosolic tail, this requires serine phosphorylation (Cabrera et al., 2003). The dissociation of ligand from HDEL/KDEL receptors is probably dependent on the pH difference between ER and Golgi, where higher pH results in dissociation (Dominguez et al., 1998; Lee et al., 2005; Townsley et al., 1993; Wilson et al., 1993). A recent crystal structure of the KDEL receptor has confirmed the prediction and revealed the mechanism of the pH dependent conformational changes upon KDEL binding (Bräuer et al., 2019).

Ubiquitinated SNAREs as cargo

As mentioned in previous section, vesicles need v-SNAREs to fuse with target membranes bearing complementary t-SNAREs, therefore it is important to ensure that v-SNAREs recycle back to the donor membranes in order to sustain the vesicle transport pathways. COPI recognize multiple v-SNARE proteins, such as Snc1 and Bet1, though the molecular mechanism is not thoroughly understood (Martínez-Menárguez et al., 1999; Xu et al., 2017). The best characterized v-SNAREs recycling by COPI is Snc1. β'-COP recognizes Snc1 when Snc1 is linked with K63-polyubiquitin, and recycles Snc1 through the endocytic pathway to the TGN for reuse in exocytosis (Xu et al., 2017).

Other cargoes of COPI

Other cargoes get encapsulated into COPI through receptors. Many proteins are recognized by Rer1 through the transmembrane domains; and some Golgi-localized glycosyltransferases (Such as Mnn9 and Gnt) are packaged into COPI through recognition of a semiconserved cytoplasmic sorting motif of (F/L)-(L/V)-(S/T) by Vps74, a GOLPH3 family protein (Eckert et al., 2014; Ishii et al., 2016; Sato et al., 2001; Shibuya et al., 2015; Tu et al., 2008, 2012).

COPI related diseases

Giving its important role in the intracellular trafficking system and in maintaining the correct morphology and components of cellular compartments, mutations in COPI have been found to cause a range of diseases and disorders.

Immunological diseases

Several families with individuals that suffer from a rare form of autoimmune syndrome have been identified to bear various missense monoallelic mutations in the gene coding the residues 230-241 of the α-COP β-propeller domain. The syndrome is now referred to as COPA syndrome. COPA syndrome primarily affects the lungs (usually interstitial lung), joints (inflammatory arthritis), and occasionally kidneys, and its

disease mechanism involves autoimmunity and inflammation (Jensson et al., 2017; Noorelahi et al., 2017; Taveira-Dasilva et al., 2018; Volpi et al., 2018; Watkin et al., 2015). The syndrome has significantly varied age of onset in patients and has an inheritance pattern of being autosomal dominant with incomplete penetrance and variable expression (Taveira-Dasilva et al., 2018; Watkin et al., 2015). Since the mutations fall in the region involved in dilysine cargo recognition (Jackson et al., 2012; Ma and Goldberg, 2013), it is possible that the syndrome is caused by dysregulation of dilysine cargoes and related ER stress and altered autophagosomes (Watkin et al., 2015).

Developmental diseases

Another β-propeller domain related disorder in COPI is located in the β'-COP subunit. A rare missense mutation (R254C) in the β'-COP N-terminal propeller domain acts as a hypomorphic allele to cause primary microcephaly-19. Patients with the disease experience small brain sizes, reduced cortical area, insufficient weight gain with normal height, cortical blindness, and developmental delay. It may be caused by human brain being sensitive to reduced COPI function during development (DiStasio et al., 2017).

δ-COP (ARCN1) is also related to developmental disorders. Monoallelic loss-of-function mutations (including one frameshift) were found in patients with facial dysmorphisms, severe micrognathia, rhizomelic shortening, microcephalic dwarfism, and developmental delay (Izumi et al., 2016).

Cancer

COPI has also been discovered to be related to hepatocellular carcinoma (HCC). A recent study revealed that overexpression of COPB2, which encodes the β'-COP subunit of COPI, is a phenotype in HCC. Silencing the COPB2 inhibited the proliferation, migration, and invasion of HCC, and therefore is a novel prognostic biomarker and therapeutic target for HCC (Zhang et al., 2021).

Pathogen-related diseases

In addition, obligatory pathogens, such as viruses like the SARS-CoV-2, can hijack the secretory pathway for virion assembly and budding (Sicari et al., 2020). For example, COPI can bind the KxHxx motif in the cytosolic domain of the S protein in SARS-CoV-2, which is important in S protein accumulation in ERGIC and is crucial for assembly (McBride et al., 2007).

Other COPI-related diseases

Other COPI related disorders include brain malformations caused by mutations in the nucleotide-binding site of Arf1. And a mutation (D193N) in the KDEL receptor (a COPI cargo) causes dilated cardiomyopathy in mice (Ge et al., 2016; Manneville et al., 2008).

Research objectives

This research seeks to identify additional binding partners of β'-COP and characterize the molecular basis and functions of Glo3-mediated regulation in COPI through β'-COP. Chapter II details the work identifying Arf1 and its ArfGAP, Glo3, as direct binding partners of β'-COP. I used pulldown assays, ITC (Isothermal Titration Calorimetry), and structural approaches to identify the tripartite interactions, quantify the binding affinity between β'-COP and Glo3 BOCCS region, and map key residues on both Glo3 and β'-COP. It also features the implications of the β'-COP/Glo3 interaction in Glo3 engagement with the COPI coat, as well as cargo sorting *in vitro* and *in vivo* using budding yeast. Chapter III focuses on the structure of the Glo3 GAP domain followed by structural analysis and implications on its molecular niche in the COPI coat. Chapter IV features a discussion of this work and future directions for further investigating the Glo3-mediated COPI regulation. This work provides new insights in β'-COP as a molecular platform in COPI as well as the functional separation of ArfGAPs in COPI, it also opens new questions on how and why GTP hydrolysis is coupled to multiple activities in COPI through the ArfGAP.

CHAPTER II

AN INTERACTION BETWEEN β'-COP AND ITS ArfGAP, GLO3, IS REQUIRED TO MAINTAIN POST-GOLGI CARGO RECYCLING

Boyang Xie[1,2], Clara Guillem[1], Christian Jung[1], Amy K. Kendall[1,2], Jordan T. Best[1], Todd R. Graham[1], and Lauren P. Jackson[1,2,3]

[1]Department of Biological Sciences, Vanderbilt University, Nashville, TN, USA
[2]Center for Structural Biology, Vanderbilt University, Nashville, TN, USA
[3]Department of Biochemistry, Vanderbilt University, Nashville, TN, USA

[†]Correspondence to lauren.p.jackson@vanderbilt.edu

This article is under review with the same title.

Abstract

As an essential component of the cellular trafficking system, COPI plays important roles by retrieving protein cargoes at the Golgi and endosomes. The COPI budding and fusion cycle starts when a small GTPase, Arf1, is recruited to the membrane. ArfGAP proteins regulate the COPI coat, but the molecular details of COPI recognition by ArfGAP proteins are still unclear. Here, by utilizing various biochemical and biophysical approaches, we were able to identify Arf1 and the yeast ArfGAP, Glo3, as direct binding partners of β'-COP, and reveal how the β'-COP β-propeller domains directly engage Glo3. Through ITC (Isothermal Titration Calorimetry) experiments and systematic truncation, we quantified the interaction between β'-COP and Glo3, and determined the minimal β'-COP binding region in Glo3. Calorimetry data also demonstrate that both the β-propeller domains of β'-COP are required to bind Glo3 through electrostatic interactions. We further used a structure-directed mutagenesis approach and identified an acidic patch on the β'-COP C-terminal propeller domain (D437/D450) and two lysine patches in the Glo3 BoCCS (Binding of Coatomer, Cargo, and SNAREs) region that mediate the interaction between the two proteins. Point mutations in either β'-COP or Glo3 BoCCS region abrogate the interaction *in vitro*. When tested *in vivo*, the loss of β'-COP/Glo3 interaction caused aberrant Golgi morphology and Ste2 mis-sorting to the vacuole. Together, our data suggest the β'-COP/Glo3 interaction is important both for cargo recycling via the TGN and the endosomes, and for *cis*-Golgi-ER retrieval. β'-COP serves as a molecular platform in COPI to coordinate interaction with various protein partners during the process.

Introduction

The COPI coat is an essential component of the eukaryotic vesicular membrane trafficking system, and it is conserved from yeast to human (Arakel et al., 2018; Duden, 2003; Jackson, 2014). It has been established that COPI plays important roles, including the retrieval of ER (endoplasmic reticulum) resident proteins from the Golgi back to the ER; retrograde trafficking within the Golgi compartments; and

recycling cargoes from the early endosomes back to the TGN (Popoff et al., 2011; Xu et al., 2017; Yang et al., 2011). COPI has been implicated in maintaining protein and lipid homeostasis in different cellular compartments (Beller et al., 2008), protein quality control (Arakel et al., 2014; Kilisch et al., 2016; Schwappach et al., 2000; Yuan et al., 2003), pathogen entry (Guo et al., 2008; Misselwitz et al., 2011; Park et al., 2019), and viral replication (Cureton et al., 2012). Viral glycoproteins hijack established COPI motifs to circumvent host immunity (Goepfert et al., 1997; Pääbo et al., 1986). Most recently, it has been noted that SARS-COVID-2 virus hijack the host cell's trafficking pathways, including COPI, to assemble and release the viral coat (Sicari et al., 2020). Mutations and mis-regulations of COPI subunits have been linked to multiple hereditary and acquired diseases, including autoimmune arthritis (the COPA syndrome), microcephaly, and cancer (Bhandari et al., 2019; DiStasio et al., 2017; Izumi et al., 2016; Jensson et al., 2017; Noorelahi et al., 2017; Taveira-Dasilva et al., 2018; Volpi et al., 2018; Watkin et al., 2015; Zhang et al., 2021).

The COPI coatomer consists of seven subunits (α-/β-/β'-/γ-/δ-/ε-/ζ-COP subunits) that form the triad assembly units of the coat (Dodonova et al., 2015; Hara-Kuge et al., 1994) (Figure 1-9). During vesicle formation, the COPI heptamer is recruited *en bloc* onto the membrane following recruitment by the cargo and Arf1, a small GTPase (Hara-Kuge et al., 1994). The COPI heptamer can be conceptually divided into two subcomplexes. The F-subcomplex (β-/γ-/δ-/ε-/ζ-COP subunits) is structurally and functionally similar to the AP complexes in clathrin coated vesicles (Schledzewski et al., 1999b). The B-subcomplex (α-/β'-/ε-COP) is comparable to the clathrin cage, though they evolved separately (Dacks and Robinson, 2017; Yu et al., 2012). In contrast to the layered organizations of clathrin and COPII, the COPI subunits have multiple contact sites with each other and therefore the coat is highly interwoven (Dodonova et al., 2015; Kovtun et al., 2020; Noble et al., 2012). The COPI B-subcomplex subunits of α- and β'-COP contain β-propeller domains (also known as WD-repeat domains) that recognize the dilysine cargo motifs in the

transmembrane cargoes of COPI (Jackson et al., 2012; Ma and Goldberg, 2013). In addition, β'-COP also binds K63-linked ubiquitin chains (Xu et al., 2017).

Biogenesis of COPI is controlled by a small monomeric GTPase, Arf1, whose activity is dependent on a cycle of GTP binding and GTP hydrolysis (Figure 1-7). Binding of GTP activates Arf1, whereas hydrolysis of GTP returns Arf1 back to its inactive form. During COPI vesicle formation, Arf1(GDP) comes to the site of site of vesicle emergence. Upon membrane recruitment, a myristoylated and amphipathic helix at the N-terminus of Arf1 anchors to the membrane, triggering a conformational change in Arf1, and Arf1 undergoes guanine nucleotide exchange mediated by an ArfGEF (Antonny et al., 1997; Franco et al., 1996; Jackson, 2014; Liu et al., 2009; Mossessova et al., 1998; Peyroche et al., 1996). Arf1(GTP) subsequently recruits coatomer proteins, membrane curvature is driven, the cargo is packed together with SNAREs, and COPI buds off. ArfGAPs are critical regulators of COPI function that have been implicated in coat assembly, cargo/SNARE sorting, and coat disassembly, but their precise roles remain poorly understood (Lanoix et al., 2001a; Lee et al., 2005; Lewis et al., 2004; Nickel et al., 1998; Pepperkok et al., 2000; Reinhard et al., 2003; Robinson et al., 2006; Tanigawa et al., 1993). Two ArfGAP proteins, Glo3 and Gcs1 are essential pairs for COPI transport in yeast, and they have overlapping functions (Poon et al., 1999). Glo3 corresponds to the ArfGAP2/3 in mammalian cells and the counterpart of Gcs1 is ArfGAP1. Yeast tolerates the loss of either Glo3 or Gcs1, but the deletion of both ArfGAPs is lethal (Poon et al., 1999). The Glo3 GAP activity seems to be especially important: yeast strains harboring the GAP-dead version of Glo3 (R59K) have a dominant lethal phenotype even with the presence of functional Gcs1, but strains harboring only the GAP-dead version of Gcs1 (R54K) are viable (Arakel et al., 2019a).

It is currently unclear how ArfGAPs engage with the COPI coat and perform their functions in trafficking. In the classic model, ArfGAPs were thought to drive coat disassembly by stimulating GTP hydrolysis and Arf1 release from the membrane, therefore recycling the COPI coat for further use. However, more recent data have suggested that Glo3 also plays an important role in COPI assembly,

including cargo/SNARE engagement through its internal BoCCS (Binding of Coatomer, Cargo, SNAREs) region (Schindler et al., 2009). Both biochemical and genetic data suggest Glo3, not Gcs1, stably associates with the COPI coat (Arakel et al., 2019a), and the GAP domain of ArfGAP2/3 has been shown to localize near the B-subcomplex in cryo-electron tomography (cryo-ET) reconstructions *in vitro* (Dodonova et al., 2017). Despite multiple lines of evidence, it is still unclear where Glo3 interacts directly with COPI.

Previous work and data lead us to the hypothesis that the propeller domains in β'-COP are strong candidates for engaging different proteins regulators in the COPI coat (Jackson et al., 2012; Lemmon and Traub, 2012; Miele et al., 2004; Muenzner et al., 2017). In this chapter, we identified the ArfGAP, Glo3, and Arf1 as additional direct binding partners for the β'-COP propeller domains *in vitro.* We then characterized the β'-COP/Glo3 interaction by mapping the minimal binding regions and identifying the specific residues on both proteins, and we quantified the binding affinities using ITC. We tested structure-based mutations *in vitro* by disrupting the β'-COP/Glo3 interaction to see its effect on Glo3 engagement to COPI and dilysine cargo transport *in vitro*. We also tested different cargo sorting and Golgi morphology in budding yeast.

Results

β'-COP interacts with COPI components of Glo3 and Arf1 in vitro

β-propeller domains (WD-repeat domains) are known protein binding platforms. We sought to identify other direct binding partners for the β'-COP propeller domains beyond the well-established dilysine motif cargo (Jackson et al., 2012, 1990b; Letourneur et al., 1994; Ma and Goldberg, 2013; Townsley and Pelham, 1994). We used recombinant purified β'-COP double propeller domains (residues 1-604 with a C-terminal GST tag, or β'-COP-GST; Figure 2-2A) as bait in pulldown experiments to isolate potential binding partners from budding yeast cell lysates. Through mass spectrometry (Mass Spectrometry Research Center, Vanderbilt University), we identified both Glo3 and Arf1 as potential

binding partners for β'-COP (Table A2-1), with 100% probability and spectrum coverages of 14% and 22%, respectively (Figure 2-1; Table A2-1). Our data agrees with the previous yeast two-hybrid data that shows Glo3 associating with β'-COP and γ-COP in COPI (Poon et al., 1999).

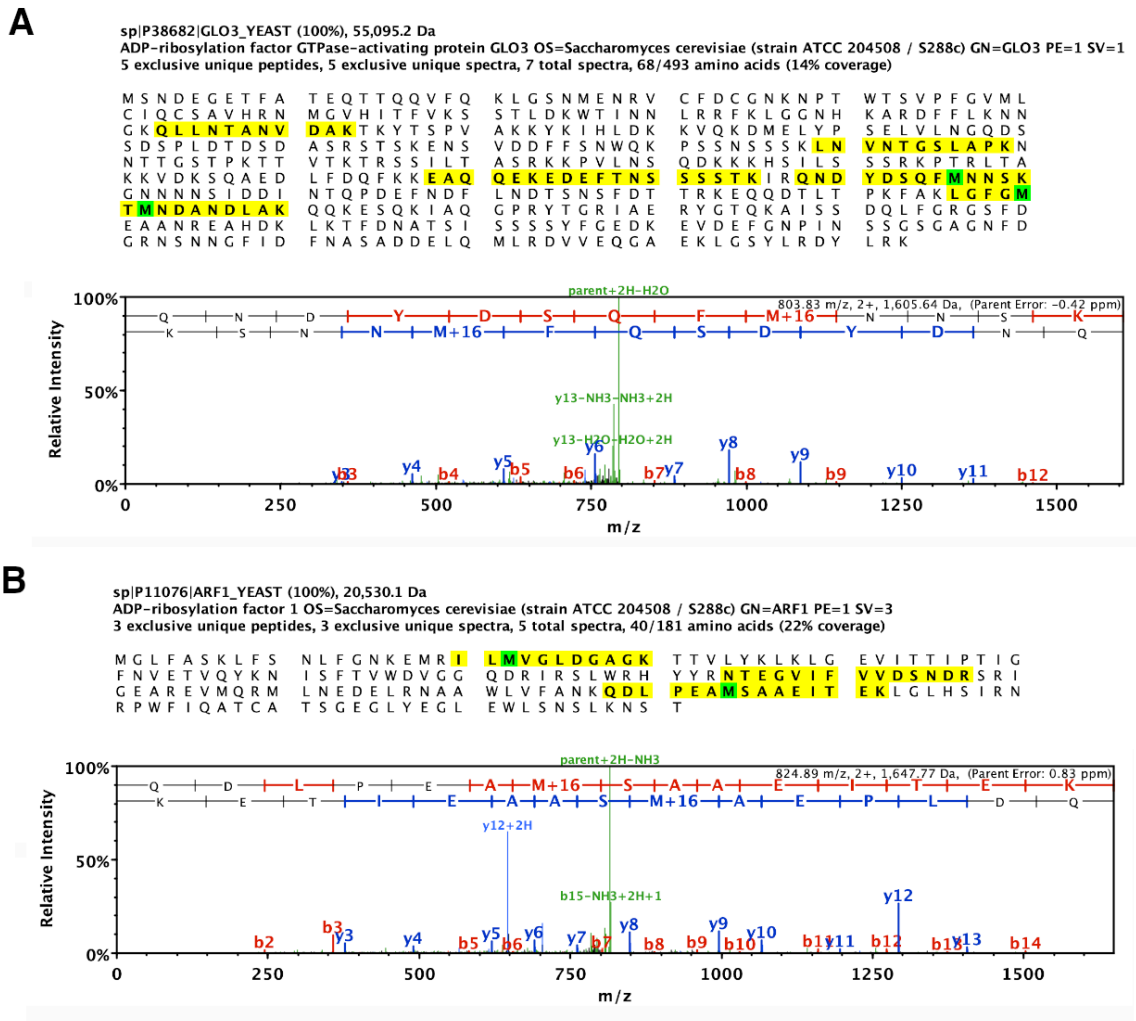

Figure 2-1. Mass spectrometry (MS) identifies Glo3 and Arf1 as binding partners for β'-COP. Amino acids matched to a spectrum are labeled in yellow, amino acids with a post-translational modification are marked in green. Representative MS spectra the mass spectrometer generated are shown in the panels below each protein sequence. B-ion series (fragment peaks that appear to extend from the N-terminus) are colored in red and y-ion series (fragment peaks that appear to extend from the C-terminus) are colored in blue. The amino acid sequence is shown across the top of each panel and the parent ion mass is listed. (A) β'-COP pulls down Glo3 from the yeast lysate. Glo3 has a MS spectrum coverage of 14% and a probability of 100%. (B) β'-COP pulls down Arf1 from the yeast lysate. Arf1 has a MS spectrum coverage of 22% and a probability of 100%.

We next undertook biochemical pulldown experiments to ascertain whether β'-COP, Glo3, and Arf1 directly bind each other *in vitro* (Figure 2-2). To test this, we used recombinantly purified β'-COP

double propeller, full length Glo3, and GTP-locked (Q71L) or GDP-locked (T31N) Arf1 (Figure 2-2A). In initial experiments, His-tagged β'-COP and N-terminally GST-tagged Arf1 constructs were used and no direct binding between β'-COP and Arf1 was observed. We then utilized GST-tagged β'-COP and C-terminal His-tagged Arf1 constructs, and our experiment showed for the first time that β'-COP double propeller (β'-604-GST) interacts directly with both Glo3 and Arf1 in either nucleotide-bound state, suggesting the bulky N-terminal GST tag in Arf1 might have blocked its interaction with β'-COP (Figure 2-2B; Figure 2-3).

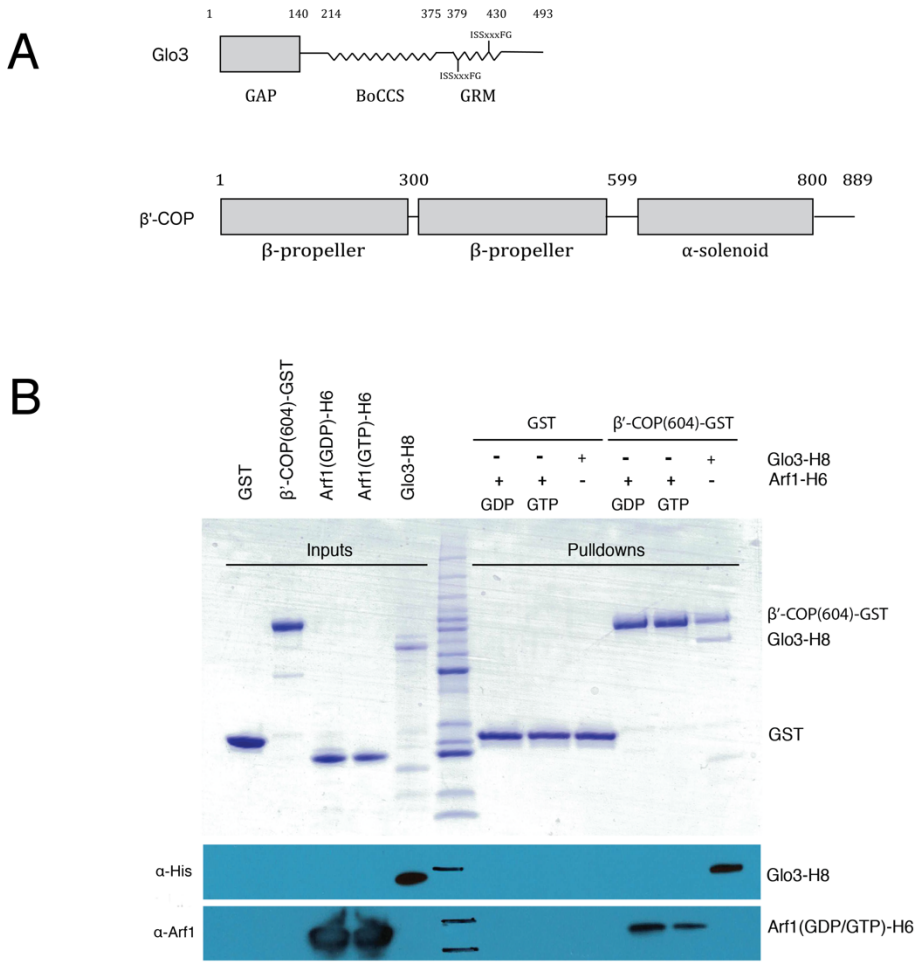

Figure 2-2. β'-COP propeller domains directly bind Glo3 and Arf1 in vitro. (A) schematics of yeast Glo3 and β'-COP proteins. Glo3 consists of a GAP domain (residues 1-140), an internal BoCCS region (residues 214-375), and a C-terminal GRM region (residues 375-493). β'-COP contains two β-propeller (also known as WD-repeat) domains followed by an α-solenoid. The N-terminal propeller domain recognizes dilysine motifs in transmembrane cargo proteins and the α-solenoid interacts with α-COP. (B) The GST-pulldown experiments used C-terminal GST-tagged β'-COP double propeller domains (residues 1-604) as bait and either full-length Arf1-H6 or full-length Glo3-H8 as prey. We tested both GDP-locked (T31N) and GTP-locked (Q71L) Arf1. The results show β'-COP interacts directly with both versions of Arf1 and with Glo3 in vitro. The top panel shows the Coomassie-stained SDS-PAGE

gel and the bottom two panels show the western blots against the Glo3 His8 tag (α-His; Abcam NB100-63173) or against yeast Arf1 (α-Arf1, from the Graham lab, Vanderbilt University).

The β'-COP/Glo3 interaction can be visualized with Coomassie staining, suggesting the binding affinity (K_d) falls within the low micromolar range, while the β'-COP/Arf1 interactions appear to be weaker in affinity. A three-way pulldown suggests β'-COP, Glo3, and Arf1 interact with each other simultaneously *in vitro* (Figure 2-3). When excess (five-fold molar) Arf1 is present, the β'-COP/Glo3 complex does not appear to favor either nucleotide-bound Arf1. These data are further supported by the *in vitro* cryo-ET reconstruction of the COPI coat on membrane, where β'-COP and Arf1 are adjacent to each other in the structure.

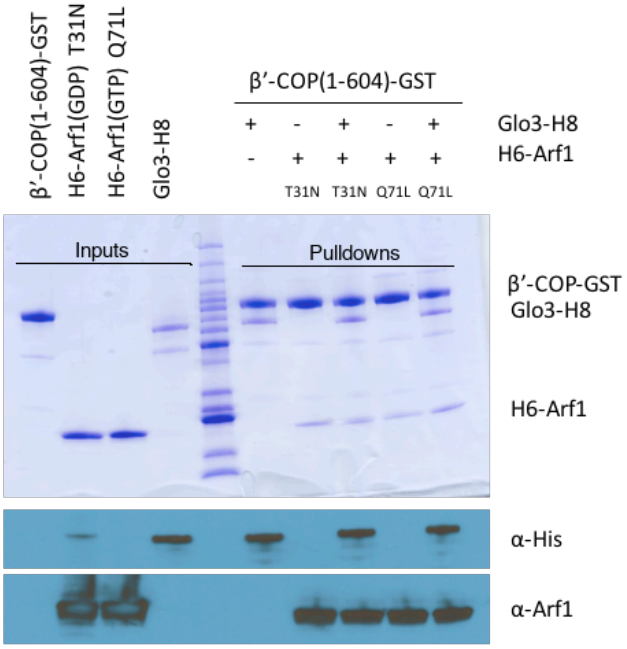

Figure 2-3. β'-COP, Arf1, and Glo3 form a ternary complex in vitro. Pulldown experiments used C-terminal GST-tagged β'-COP double propeller domains (residues 1-604) as bait and either full-length Arf1-H6 or full-length Glo3-H8 as prey. We tested β'-COP binding to both nucleotide-bound forms of Arf1: GDP-locked (T31N) and GTP-locked (Q71L). β'-COP pulls down both Arf1 and Glo3 simultaneously. β'-COP alone does not appear to show a preference for either nucleotide-bound version of Arf1; it pulls down GDP-locked and GTP-locked Arf1 equally well when excessive Arf1 is added (at 5:1 molar ratio).

After confirming the direct interactions, we then investigated which part of Glo3 directly interacts with β'-COP propeller domains. Glo3 consists of a N-terminal GAP domain, an unstructured internal BoCCS

region and a C-terminal GRM region (Glo3 Regulatory Motif) (Figure 2-2A). We purified GST-tagged recombinant proteins encompassing each of the Glo3 components and conducted pulldown experiments with His-tagged β'-COP double propeller (Figure 2-4). The data shows only the Glo3 BoCCS region can pulldown β'-COP propeller domains. The Glo3 BoCCS region has previously been shown to engage COPI coat and SNAREs in cell lysates, but the COPI subunit responsible for associating with Glo3 was previously unknown.

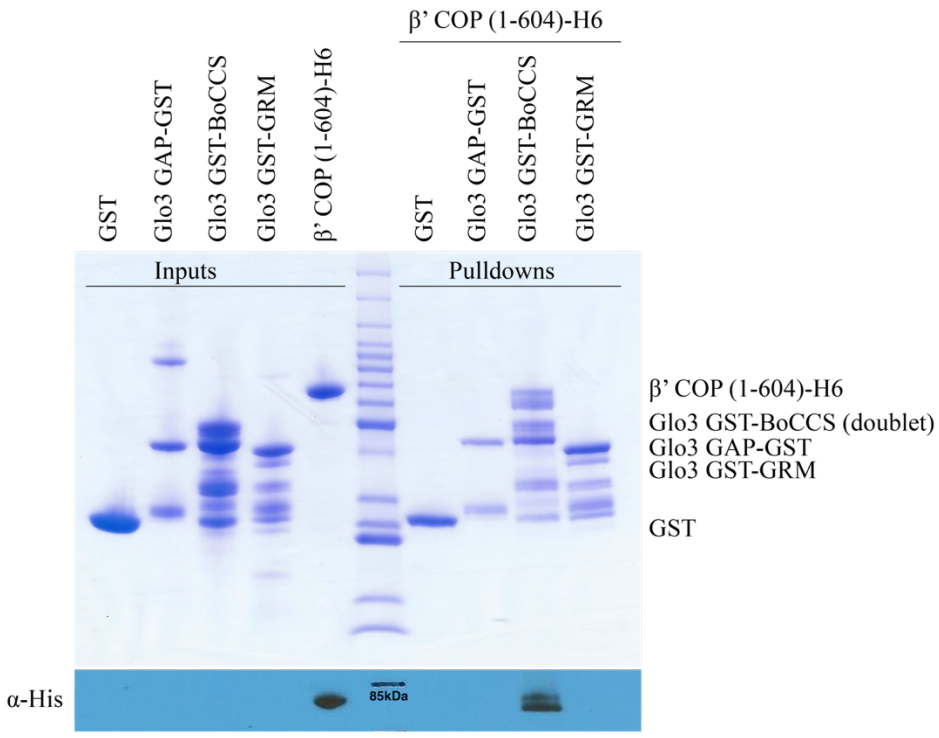

Figure 2-4. β'-COP propeller domains directly binds the Glo3 BOCCS region *in vitro*. Recombinantly purified GST-tagged Glo3 fragments (GAP-GST, residues 1-150; GST-BoCCS, residues 208-383; or GST-GRM, residues 350-493) were used as baits and β'-COP was used as prey to determine which part of Glo3 binds β'-COP. The result show only the GST-BoCCS fragment exhibited direct affinity with β'-COP. Both the purified BoCCS and GRM fragments are unstable in solution, most likely due to the long regions predicted to be unstructured. Mass spectrometry data (not shown) confirms the doublet binds in the GST-BoCCS input lane corresponds to the Glo3 BoCCS region. Figure was generated by Christian Jung.

Glo3 BoCCS binds both β'-COP propellers with low micromolar affinity

Our biochemical data suggested the interaction between β'-COP and Glo3 lies in the low micromolar range and therefore is within the detection limit of ITC. We thus quantified the β'-COP/Glo3 interaction using ITC. To ascertain the minimal binding region for structural studies, we further mapped the binding region within Glo3 using purified recombinant protein fragments in ITC (Figure 2-5A; Figure 2-6; Table A2-2). All affinity tags on the recombinant proteins were cleaved before running the ITC experiments. The pulldown experiments indicated that β'-COP only binds BoCCS region (residues 208-375) in Glo3 directly (Figure 2-4). In our initial ITC runs, the interaction between β'-COP and Glo3 BoCCS region appear to have a low micromolar K_D and 1:1 stoichiometry (Figure 2-6A). We generated and purified a series of Glo3 BoCCS constructs truncated at either N- or C-terminal ends and quantified their interaction with the untagged β'-COP double propeller domain by ITC (Figure 2-5A; Figure 2-6B). Full length and longer purified Glo3 fragments appear to be unstable over time, but the short Glo3 BoCCS region fragments used in the ITC experiments exhibited high purity and stability and therefore was suitable to be used in further structural analysis (Figure 2-4; Figure 2-6C).

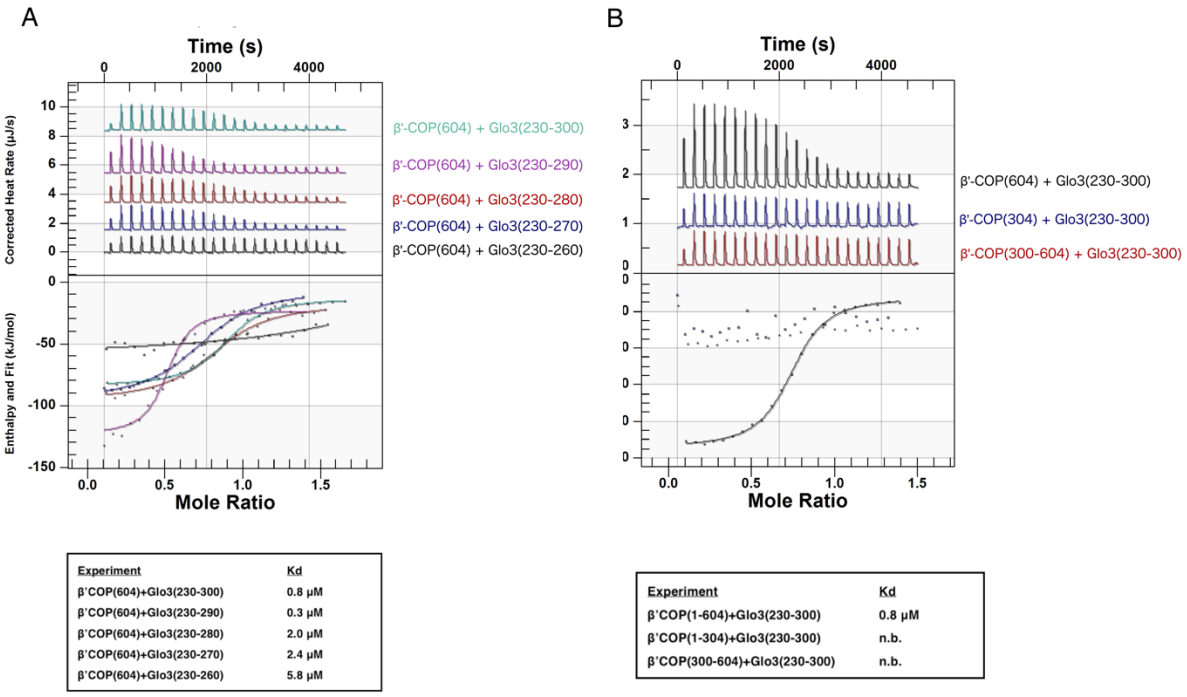

Figure 2-5. Residues within the Glo3 BoCCS region directly bind both β'-COP propeller domains with low micromolar affinity. (A) Purified recombinant proteins (untagged β'-COP residues 1-604 and Glo3 fragments as labelled) were used in ITC (isothermal titration calorimetry) experiments to quantify binding affinities; representative traces are shown. β'-COP binds Glo3 fragments located within the BoCCS region. All fragments exhibit low micromolar K_D values (0.8-6 µM) and 1:1 stoichiometry, but the highest affinity interaction occurs between β'-COP 1-604 and Glo3 residues 230-290. Truncating residues from the C-terminus gradually lowers the binding affinity with β'-COP. (B) Representative ITC experiments between untagged Glo3 BoCCS fragment (residues 230-300) and N-terminal β'-COP propeller domain (residues 1-304), C-terminal β'-COP propeller domain (residues 300-604), or both β'-COP propellers (residues 1-604). Each propeller domain on its own exhibit trace that is insufficient to be measured by calorimetry (marked "n.b." for no binding when K_D < 300 µM), comparing to the low micromolar binding affinity when both propeller domains are present. These data suggest both propellers are required to bind Glo3.

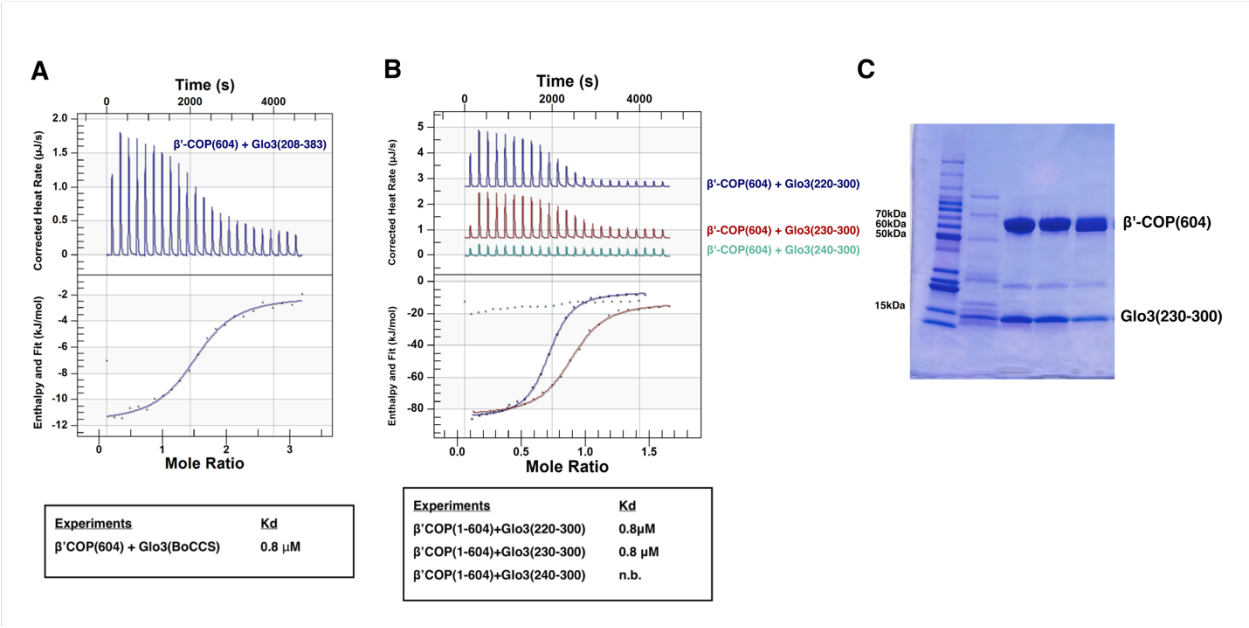

Figure 2-6. The Glo3 BoCCS region interacts directly with β'-COP. (A) ITC experiment with full BoCCS Glo3 fragment (residues 208-383) shows a low micromolar K_D. (B) ITC experiments to ascertain minimum Glo3 fragment required for binding β'-COP. Glo3 N-terminal residues 230-240 are required for measurable binding in calorimetry, while removing residues 220-230 exhibits no measurable effect on binding affinity. "n.b." denotes no measurable binding in the calorimeter (K_D > 300µM). (C) Representative SDS-PAGE gel of the β'-COP (residues 1-604) and Glo3 (residues 230-300) complex across the gel filtration peak following purification; the complex elutes together over gel filtration column (Superdex S200 increase analytical column). Although some Glo3 fragments are unstable over time, the recombinant fragments used for ITC runs exhibit high purity and stability.

The strongest interaction between β'-COP double propeller domains and Glo3 regions was observed to be with by Glo3 residues 230-290, with an average K_D of 0.8 ± 0.2 µM in 3 runs (Figure 2-6A; Table A2-2). We saw no obvious difference in binding affinity when Glo3 residues 220-230 are removed, but loss of Glo3 residues 230-240 almost completely abrogated measurable ITC binding (Figure 2-6B). Serial truncations from the C-terminus resulted in progressively weaker interactions (Figure 2-5A). Together, these data define Glo3 residues 230-290 as the key region mediating the direct interaction with the β'-COP propeller domains.

We then tested which β'-COP propeller domain is required for the interaction with Glo3 (Figure 2-5B). We generated and purified β'-COP constructs containing either one of the two individual propellers (β'-COP residues 1-304 or residues 300-604), and tested their binding affinities with Glo3 residues 230-290. The results showed that neither the N-terminal nor C-terminal β'-COP propeller domains alone have

sufficient affinity to measure binding using ITC (K_D < ~ 300 μM). However, when both propeller domains are present, β'-COP binds Glo3 residues 230-290 with a K_D of around 0.6 μM and 1:1 stoichiometry. These data suggest the Glo3 interaction requires the surface of both β'-COP propeller domains, in contrast to the dilysine cargo motifs, which interact only with the N-terminal propeller domain (Jackson et al., 2012; Ma and Goldberg, 2013).

Point mutations in β'-COP or Glo3 abrogate binding in vitro

ITC experiments revealed that Glo3 residues 230-290 exhibits the greatest binding affinity with β'-COP, and therefore may be a good candidate for co-crystallization experiments. However, all initial attempts to determine the β'-COP/Glo3 structure using X-ray crystallography structure failed, as we repeatedly found β'-COP double propeller packing within the crystal lattice excluded the flexible Glo3 fragment (discussed later chapter). Instead, we utilized a systematic mutagenesis approach to identify the key residues in β'-COP and Glo3 that mediate the interaction between the two proteins.

To investigate the type of interaction between β'-COP and Glo3, we first tested the salt dependence of the β'-COP/Glo3 interaction in ITC. The results showed that high salt concentration (500 mM NaCl) substantially weaken the interaction compared to a low salt condition (100 mM) (Figure 2-7B), suggesting the interaction was likely to be mediated by electrostatic contacts. Through sequence alignment, we discovered two highly conserved clusters of lysine residues located inside the BoCCS region of Glo3 (Figure 2-7A). The first cluster (K233/K234/K235) was previously proposed to interact with COPI in cell lysates (Schindler et al., 2009), though the corresponding COPI subunit remained unidentified. The second cluster (K251/K252/K255) had not been previously identified.

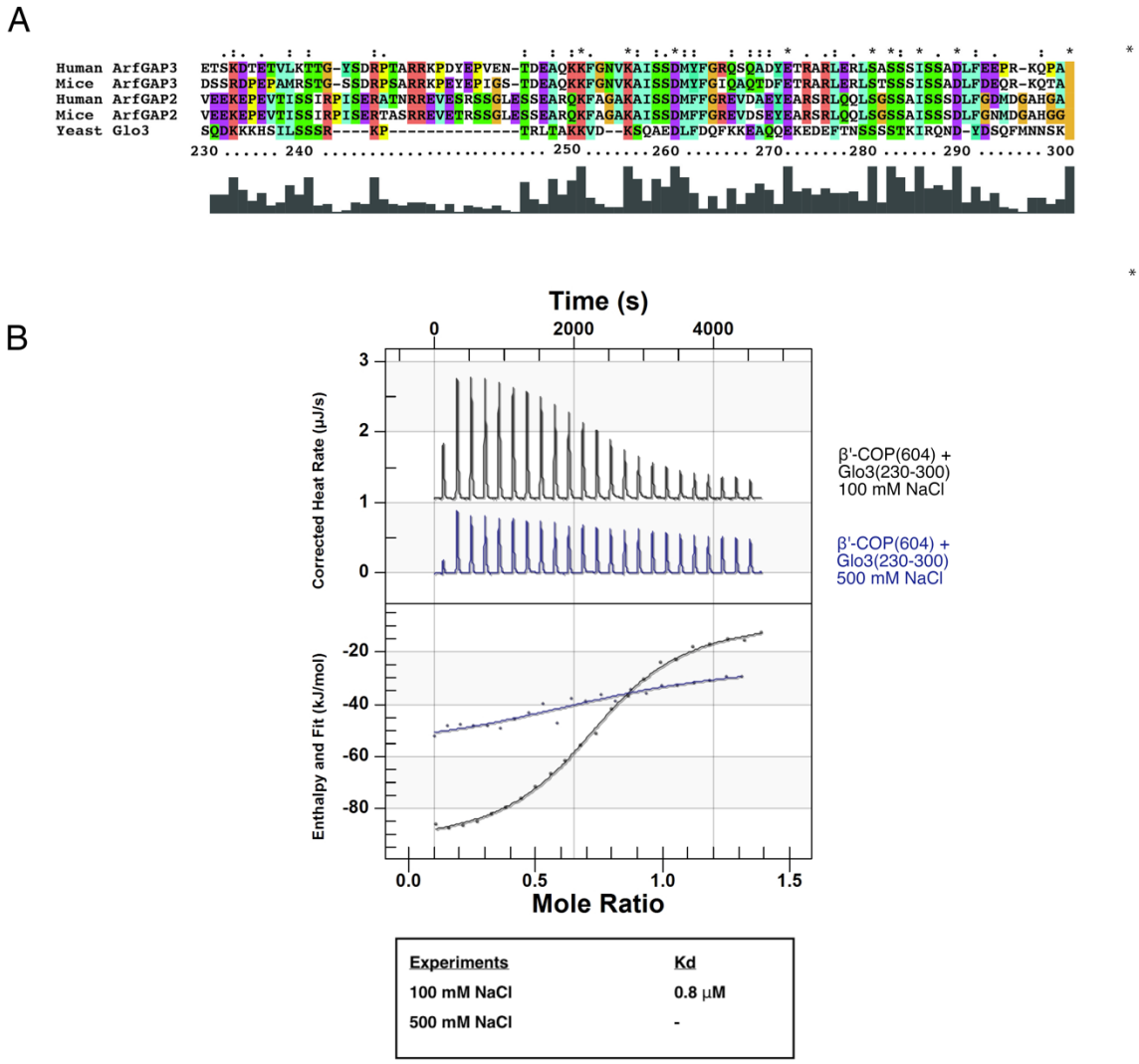

Figure 2-7. Conserved Glo3 lysine residues mediate an electrostatic interaction with β'-COP C-terminal propeller domain. (A) Glo3 partial sequence alignment highlighting key conserved residues between *S. cerevisiae* Glo3 and mammalian ArfGAP2/3 homologs in *M. musculus* and *H. sapiens*. Glo3 residues 230-300 are labeled. (B) ITC experiments between wild-type β'-COP residues 1-604 and Glo3 residues 230-270 in 100 mM NaCl and 500 mM NaCl. Near physiological salt concentrations (100 mM NaCl), the two proteins interact with a low micromolar K_D. The same experiment in high-salt buffer (500 mM NaCl) disrupts the interaction, since binding was too weak to determine a K_D. Together these data suggest electrostatic residues play an important role in the β'-COP/Glo3 interaction.

To test these lysine patches, we generated mutant Glo3 fragments with one of the patches mutated. We then purified the fragments and tested their binding affinities using calorimetry (Figure 2-8A). The K_D between Glo3 K233E single mutant and β'-COP is around 40-fold weaker than wild-type, and

mutating the entire first cluster (the Glo3 BoCCS K233E/K234E/K235E triple mutant) reduces binding affinity below the detection limit (Figure 2-8A). Mutating the second cluster (the Glo3 BoCCS K251E/K252E/K255E triple mutant) also reduced the binding affinity by about 40 fold. Together, these data suggest both lysine clusters within the Glo3 BoCCS region are import in mediating the interaction between β'-COP and Glo3, and the first lysine patch is especially important.

After identifying the key residues in Glo3, we then set out to find their counterparts on β'-COP, which are likely acidic residues such as aspartate or glutamate residues. We investigated the electrostatic surface of the β'-COP double propeller domains and systematically mutated multiple acidic patches located throughout both the N-terminal and C-terminal propellers. We changed the aspartate and glutamate residues in the acidic patches to alanine residues. Most of the β'-COP mutants bound to wild-type Glo3 BoCCS fragment with similar affinities as wild-type β'-COP (Table A2-3), except for one patch located on the C-terminal propeller (D437/D450) (Figure 2-8B). Mutating the aspartate residues to alanines (D437A/D450A) reduced binding affinity with Glo3 by around 60 fold (K_D = 18 μM) (Figure 2-8C; Table A2-2). In addition to this patch, several N-terminal mutants exhibited weaker effects (~ 8-fold weaker) (Table A2-3), with the R15A/K17A/R59A mutant having the largest effect (~ 16-fold weaker) (Table A2-1; Table A2-3). Interestingly, the R15A/K17A/R59A mutant was previously shown to disrupt dilysine cargo motif binding (Jackson et al., 2012), indicating the dilysine binding site may be close to the Glo3 binding site on the β'-COP N-terminal propeller domain.

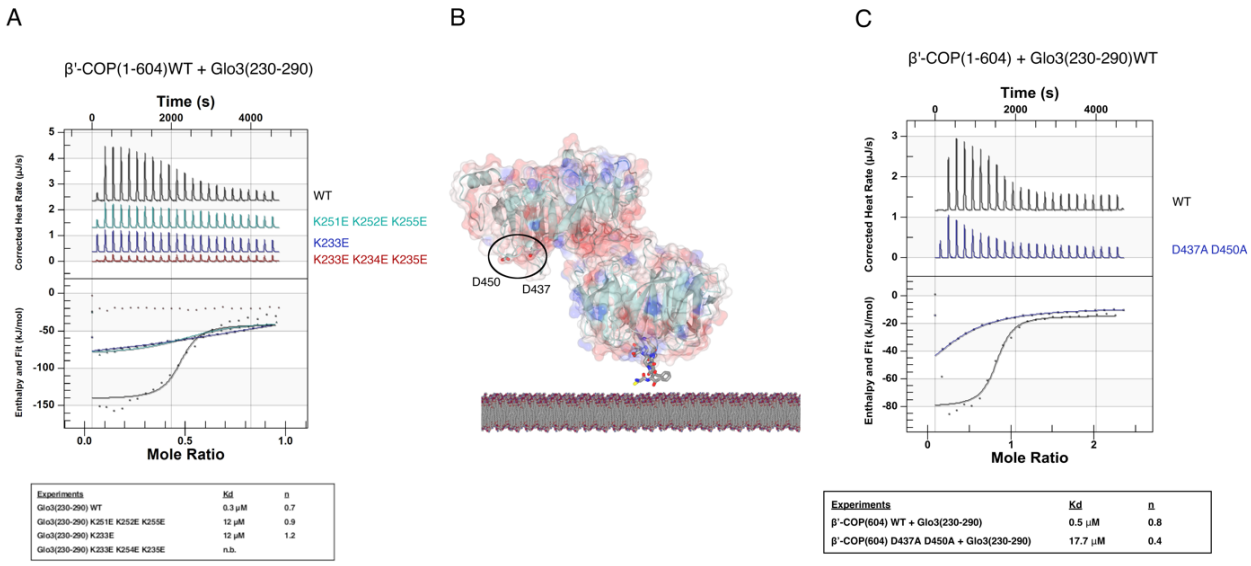

Figure 2-8. Key Glo3 lysine residues mediate an electrostatic interaction with an acidic patch on β'-COP. (A) Representative ITC experiments between wild-type β'-COP (residues 1-604) and mutant versions of Glo3 (residues 230-290). Two Glo3 mutants substantially reduce binding in ITC: a single point mutation at K233E and the K251E/K252E/K255E triple mutant. Both mutants exhibit 40-fold weaker binding as compared to wild-type Glo3 (K_D ~ 12 µM; Table A2-2). The Glo3 K233E/K234E/K235E triple mutant exhibits no measurable binding in ITC (K_D <300 µM). (B) The electrostatic surface of β'-COP propeller domains with acidic patch (D437/D450) and dilysine binding site (grey cylinders) highlighted with respect to membrane. β'-COP is shown in a membrane-bound side view with a dilysine cargo motif shown in grey cylinders. (C) Representative ITC experiment with wild-type untagged Glo3 (residues 230-290) and mutant β'-COP double propellers (D437A/D450A) (residues 1-604), with a K_D of 18 µM. The D437/D450 mutant exhibits 60-fold weaker binding to Glo3, suggesting this acidic patch plays a critical role in the interaction.

The interaction between β'-COP and Glo3 is required for Glo3 binding to the COPI coat

We then set out to test whether the key lysine residue patches on Glo3 are required only for binding with isolated β'-COP, or they are also important for Glo3 engagement with the COPI coatomer (Figure 2-9). We used purified GST-tagged Glo3 fragments in both wild-type and mutant forms as bait in pulldown experiments from budding yeast cell lysates that contain His and FLAG tagged β-COP. Our data indicate mutating the two lysine patches (K233E/K234E/K235E/K251E/K252E/K255E) on the Glo3 BoCCS region that mediate interaction with β'-COP abrogated Glo3 binding to the entire COPI coatomer *in vitro*. Our results suggested that although Glo3 was found to interact with both the β'-COP and γ-COP subunits of COPI (Eugster et al., 2000), Glo3 engages with the COPI coat mainly through the β'-COP subunit and the β'-COP/Glo3 interaction is required for Glo3 to stably associate with the COPI coat.

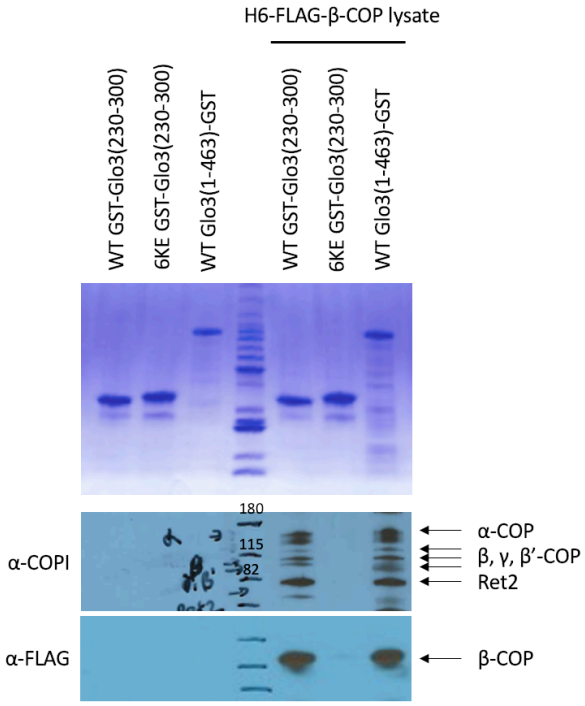

Figure 2-9. Glo3 associates with COPI coat through β'-COP. GST-pulldown experiments using GST tagged Glo3 fragments that contain the BoCCS region (N-terminal tagged wild-type residues 230-300, N-terminal GST-tagged residues 230-300 with K233E/K234E/K235E/K251E/K252E/K255E mutations, C-terminal GST-tagged wild-type residues 1-463) as bait for yeast cell lysates containing His6- and FLAG-tagged β-COP. Glo3 BoCCS fragments pulls down the COPI coat (both the B- and F-subcomplexes), and disrupting the lysine residues that are known to mediate β'-COP binding abrogated Glo3 association with the COPI coat. Cell lysates were provided by Swapneeta Date in the Graham lab at Vanderbilt University.

Structure approaches

Crystallography. In order to obtain structural information about the interaction between β'-COP and Glo3, we tried multiple crystallography approaches to obtain a co-crystal of the β'-COP propeller domains and Glo3 BoCCS region. We first tried co-crystallizing the β'-COP double propeller domains with Glo3 fragments of different lengths that contained the minimal β'-COP binding region. However, we repeatedly found β'-COP double propeller domains pack next to the D437/D450 patch within the crystal lattice, which excluded the flexible Glo3 fragment from the crystals. Fusing the Glo3 fragments with β'-COP into a single polypeptide did not yield any crystals. We then designed several shorter peptides encompassing one of the lysine patches and set up crystallization trials with β'-COP double propellers as well as individual single propellers, since sometimes even weak binding partners may be promoted to co-

crystallize in crystallization drops by high concentrations. In this way, we were able to obtain a crystal that exhibited a potential density for one of the Glo3 lysine patches near the dilysine binding site of the N-terminal propeller domain of β'-COP (Figure 2-10), which agrees with our ITC data (Table A2-2; Table A2-3). Though the current dataset is not of high enough quality to allow peptide building, we are engaging in ongoing crystallization efforts.

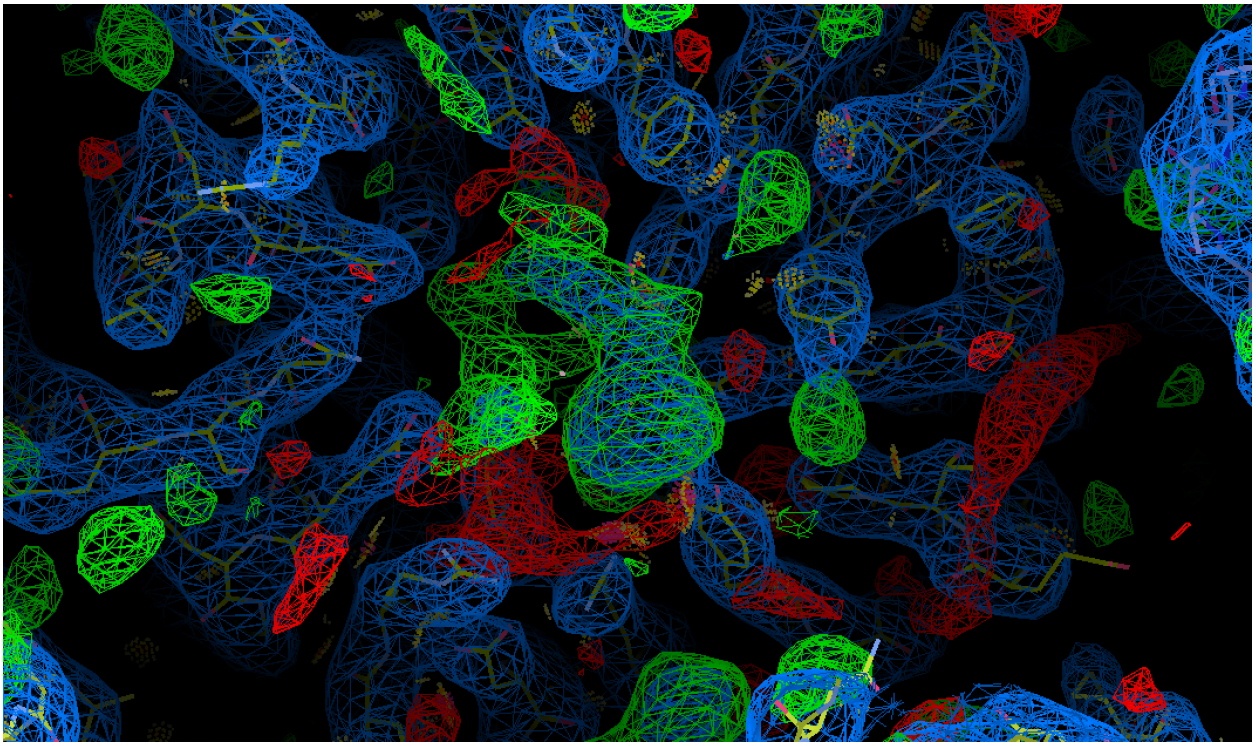

Figure 2-10. The electron density map for potential Glo3 peptide. Representative $2mF_O$-DF_C electron density (contoured at 0.51 electrons/Å^3 in Coot) near the dilysine binding site on β'-COP following molecular replacement in Phaser. The potential density for Glo3 peptide that contains a lysine patch locates near the N-terminal propeller domain of β'-COP (green).

Cryo-EM. Efforts to obtain the β'-COP/Glo3 BoCCS structure by cryo-EM are also underway (Figure 2-11). Four datasets were initially collected, one dataset was collected with the FEI Technai T30 Polara cryo-transmission electron microscope at Vanderbilt University, two datasets were collected with ThermoFisher FEI Titan Krios microscopes at the NCCAT, and the other dataset was collected with ThermoFisher FEI Titan Krios microscope at Vanderbilt University. Because the β'-COP/Glo3 BoCCS protein complex is relatively small, the pixel size from the first NCCAT dataset was too large and the micrographs

were too crowded. The second NCCAT dataset features a more dilute sample and a much smaller pixel size, with defocus values to match. The β'-COP double propellers also exhibit preferred orientation, which posed challenges in data processing and limited the resolution of our model. Traces of the Glo3 BoCCS peptide are visible in the 3D construction but will need further processing to be resolved.

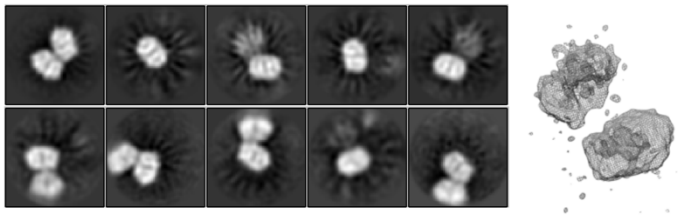

Figure 2-11. Representatives of 2D class averages and a recent 3D reconstruction from the β'-COP/Glo3 complex. Image processing is complicated by the small size of the complex and the pseudosymmetry between the two propellers. Figure courtesy of Amy Kendall.

β'-COP can bind Glo3 and dilysine motifs simultaneously in vitro

We have presented here a new direct interaction between β'-COP and Glo3 with biochemical and biophysical evidence. It is known that COPI picks up a range of cargoes and SNAREs from the Golgi and the endosomes through short cargo sorting motifs (Jackson et al., 1990b; Letourneur et al., 1994; Townsley and Pelham, 1994). The β'-COP subunit of COPI recognizes transmembrane proteins that require recycling to the ER through dilysine motifs (KKxxx or KxKxx) (Jackson et al., 2012; Ma and Goldberg, 2013). To investigate whether Glo3/β'-COP interaction is related to dilysine cargo binding, we first tested whether β'-COP can interact with dilysine cargo motif and Glo3 simultaneously *in vitro* using ITC. Previous β'-COP structures obtained from both X-ray crystallography and cryo-ET revealed that β'-COP can exist in various conformations, and we wondered whether β'-COP could be "locked" into a certain conformation that favors cargo-binding by Glo3, or if nGlo3 and dilysine cargo might compete for binding to the same site on β'-COP.

ITC data showed no difference in the affinity of purified wild-type β'-COP double propeller domains for dilysine cargo motif peptides when Glo3 is present or absent (Figure 2-12A). However, the

published β'-COP RKR dilysine binding mutant binds Glo3 with a slightly weaker affinity and the D98A/D117A mutant binds Glo3 with the same affinity as wild-type (Jackson et al., 2012) (Figure 2-12B). These data suggest dilysine cargo and Glo3 can bind β'-COP simultaneously at least *in vitro*, and Glo3 may bind to the N-terminal propeller domain of β'-COP near the dilysine binding site. The RKR patch may be part of the Glo3 binding position on the N-terminal propeller. Alternatively, the mutation might have altered the overall electrostatic distribution across the propeller surface and therefore affected the Glo3 binding site. Since both β'-COP propeller domains are required for binding Glo3, we speculate there must be a second patch on the N-terminal propeller and the data suggest it is likely located close to the dilysine binding site, though we have not yet definitively identified the patch.

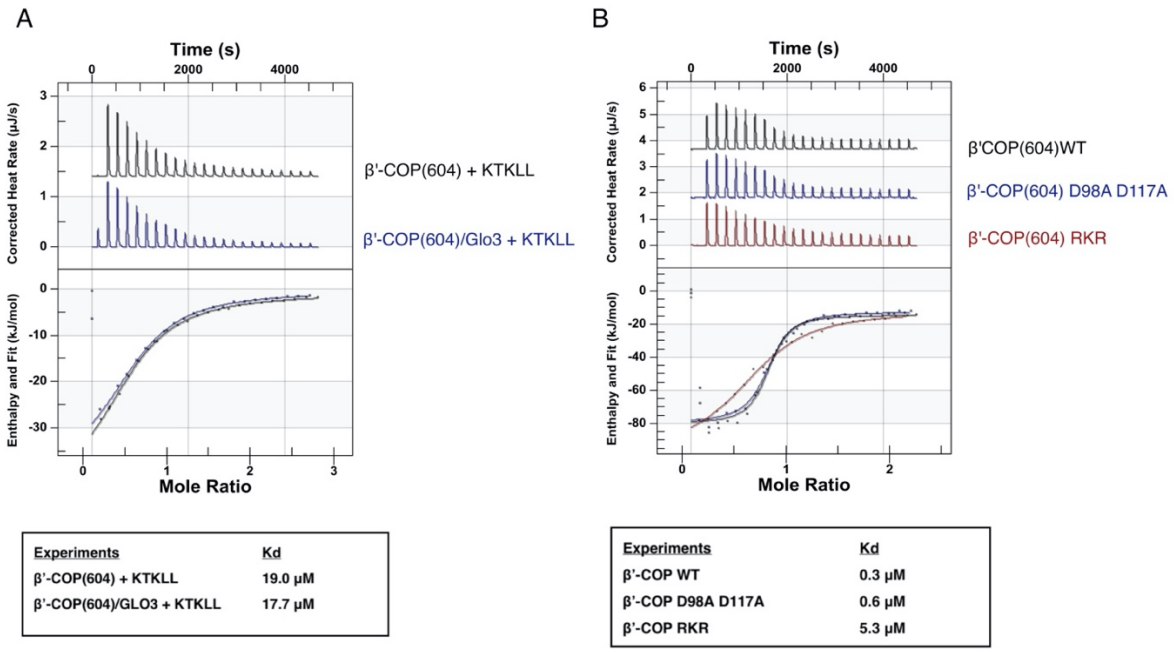

Figure 2-12. Glo3 BoCCS and dilysine cargo motifs bind β'-COP simultaneously in vitro. (A) Representative ITC experiments with untagged β'-COP residues 1-604; Glo3 residues 230-290; and dilysine motif (KTKLL) peptide. The presence of Glo3 does not alter the binding affinity of β'-COP to dilysine motifs *in vitro*. (B) ITC experiments with β'-COP dilysine binding mutants. The R13A/K15A/R59A (RKR mutant) disrupts binding to the dilysine motif carboxy-terminus, while D98A/D117A disrupts binding to the two lysine residues in the dilysine motif. The RKR mutant exhibits weaker binding to Glo3, while D98A/D117A binds Glo3 as well as wild-type protein. These data suggest Glo3 and dilysine motifs do not compete for binding β'-COP *in vitro*. However, disrupting the overall charge distribution on the N-terminal propeller in the RKR mutant suggests it may play a role in Glo3 binding or it locates close to the Glo3 binding site on β'-COP.

COPI cargo sorting in yeast

To investigate whether abrogating the β'-COP/Glo3 interaction would affect Glo3 function or COPI-dependent cargo transport *in vivo*, we used budding yeast as a model to test whether this interaction would affect cell viability and tested multiple known COPI-dependent cargoes, including Ste2, Rer1, Emp47, and SNARE proteins.

Growth assays. We first set out to test if disrupting the β'-COP/Glo3 interaction would affect the growth of yeast cells. We used the *glo3 K233E/K234E/K235E* and *glo3 K251E/K252E/K255E* mutants in a *glo3Δgcs1Δ* strain background (Figure 2-14A). The *glo3Δgcs1Δ* double deletion is inviable but can be sustained with a wild-type copy of *GLO3* on a *URA3* labeled pRS416 plasmid. Both wild-type *GLO3* and mutant *GLO3* forms were then introduced into the *glo3Δgcs1Δ* background on a *LEU2* labeled pRS315 plasmid. On the selection media that selects for both plasmids, all transformed strains grow in the same manner as a wild-type strain, since they all contain the wild-type pRS416-*GLO3* plasmid. Upon transforming onto the 5-FOA (5-fluoro-orotic acid) media, which selects against the pRS416-*GLO3* plasmid, the *glo3Δgcs1Δ* strain harboring an empty pRS415 plasmid became inviable. However, we observed no obvious difference in growth between the wild-type *GLO3* strain and strains that harbor either form of *glo3* mutation at normal temperature (30°C). Therefore, disrupting the β'-COP/Glo3 interaction does not abrogate the essential growth function of Glo3.

Ste2. Ste2 is a yeast α-factor receptor and transmembrane GPCR that initiates the signaling response that leads to mating between yeast haploid a and α cells. Ste2 cycles between the cell surface and internal compartments in yeast cells. Previous work has demonstrated the Glo3-dependent trafficking of post-endocytic Ste2-GFP to the cell surface (Kawada et al., 2015). We examined Ste2-GFP localization in both the *glo3 K233E/K234E/K235E* and *glo3 K251E/K252E/K255E* mutants in the *glo3Δgcs1Δ* strain background (Figure 2-13), and observed a significant difference in the amount of Ste2-GFP at the plasma

membrane in wild-type *GLO3* and *glo3* mutants: less Ste2-GFP was observed at the plasma membrane in both mutant strains relative to wild-type, and Ste2 is obviously mis-localized to the vacuole.

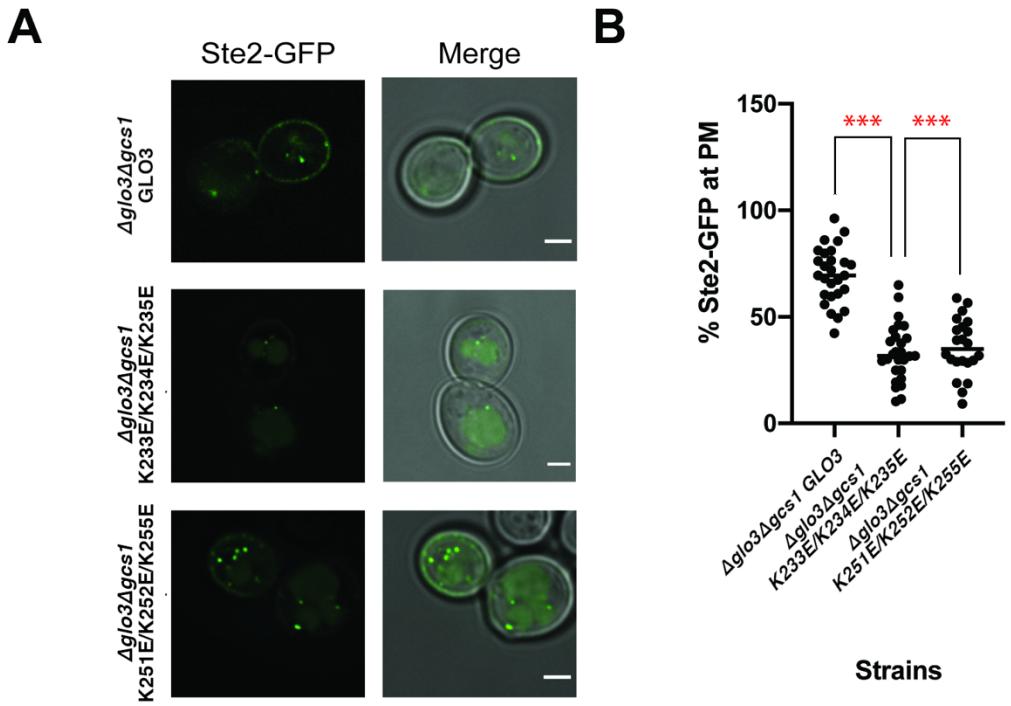

Figure 2-13. Ste2 is mis-sorted to the vacuole when the β'-COP/Glo3 interaction is disrupted in *S. cerevisiae*. (A) Fluorescence imaging of Ste2-GFP in *glo3Δgcs1Δ* strains with wild-type *GLO3* or *glo3* mutants (K233E/K234E/K235E or K251E/K252E/K255E) introduced on a pRS135 plasmid. Scale bar represents 2 µm. (B) Box plots showing percentage of Ste2-GFP observed at the plasma membrane in each strain with median marked as black line. Mutating either lysine cluster in yeast cells causes a significant difference in Ste2-GFP sorting compared to the wild-type *GLO3* strain. Statistical comparisons were pairwise between *GLO3* and mutants; data were analyzed using a one-way ANOVA (Prism); and probability values of less than 0.001 are represented by ***. Figure generated by Clara Guillem in the Graham lab at Vanderbilt University.

Emp47. We then set out to test whether disrupting the β'-COP/Glo3 interaction would affect protein cargoes that cycle between the Golgi and ER in COPI coated vesicles. Previous studies have established that both α-COP and β'-COP N-terminal propeller domains recognize the dilysine sorting motifs (KxKxx or KKxx) located at the C-terminus of transmembrane cargo proteins. Emp47 is a published COPI dilysine cargo with a cytosolic KxKxx motif that is mainly picked up by β'-COP, thus it is an excellent cargo candidate to investigate COPI-dependent retrieval from the Golgi to the ER, especially involving β'-COP. When Emp47 sorting into the COPI vesicles is disrupted, Emp47 mis-localizes to the vacuole where

it is degraded. To test Emp47 sorting in the mutant cells, we examined the stability of Emp47-myc over time in the *glo3Δgcs1Δ* strain background after inhibiting protein synthesis with cycloheximide. We observed stable Emp47 over time in the *glo3 K233E/K234E/K235E* and *glo3 K251E/K252E/K255E* cells (Figure 2-14B). The results indicate disrupting the β'-COP/Glo3 interaction does not seem to affect Emp47 sorting. Such result is not surprising since we showed earlier that β'-COP likely binds Glo3 and dilysine cargoes simultaneously *in vitro,* suggesting that dilysine cargo recognition through β'-COP and Glo3 binding with β'-COP seem to be separate processes.

Rer1. We then examined the localization of GFP-Rer1 (Figure 14C). Rer1 is a retrieval receptor that localizes to early Golgi cisternae at steady-state, but cycles rapidly between the ER and early Golgi in COPI and COPII coated vesicles. Disrupting COPI function can cause mis-localization of Rer1-GFP to the vacuole (Sato et al., 2001). However, we found no difference in Rer1-GFP localization between wild-type *GLO3* and either of the *glo3* mutants. Together, the data on Emp47 and Rer1 suggest disrupting the β'-COP/Glo3 interaction does not appear to disrupt COPI function in cargo retrieval from the Golgi to the ER.

SNARES. As mentioned in the introduction chapter, COPI is engaged with SNARE proteins and recycles v-SNAREs back to donor membranes. We first looked at Snc1, a yeast R-SNARE/v-SNARE. Snc1 is an exocytic SNARE that cycles between the Golgi and the plasma membrane. Snc1 has been previously shown to be mis-localized when COPI is deleted (Kawada et al., 2015; Schindler and Spang, 2007; Schindler et al., 2009). We examined the localization of mNG-Snc1 in the *glo3Δgcs1Δ* background in both the wild-type and *glo3* mutant strains (Figure 2-15 A/B/C). mNG-Snc1 normally localizes to punctate structures inside the cell and at the plasma membrane. We found no significant difference in the amount of mNG-Snc1 at the plasma membrane puncta relative to internal locations. However, the *glo3 K233E/K234E/K235E* cells have more mNG-Snc1 localized to ring or tubule structures that are not common in cells with wild-type *GLO3*, and both mutants exhibit more ring structures on average than wild-type. These structures may indicate abnormal Golgi and endosome morphology, and such phenotypes suggest

that disrupting the β'-COP/Glo3 interaction affects the maintenance of Golgi morphology that requires COPI function.

We also looked at Bet1, a Q-SNARE/v-SNARE protein that localizes to the early Golgi and is required for vesicular transport between ER and the Golgi. Bet1 has been previously found to interact with the Glo3 BoCCS region (Ossipov et al., 1999; Schindler et al., 2009). We examined the localization of mNG-Bet1 in the *glo3Δgcs1Δ* background in both the wild-type and *glo3* mutant strains and observed a small number of abnormal ring structures in the *glo3 K233E/K234E/K235E* strain, but the difference from the mutants and the wild-type did not reach the significance level (Figure 2-15 D/E/F). The number of abnormal structures in total (tubules and rings) was on the edge of significance, in contrast to the mNG-Snc1 data.

Together, *in vivo* data from multiple types of COPI cargoes and receptors suggest β'-COP/Glo3 interaction likely plays more important role in cargo recycling via the endosomes and plasma membrane and plays less an important role in cargo cycling between the *cis*-Golgi and the ER.

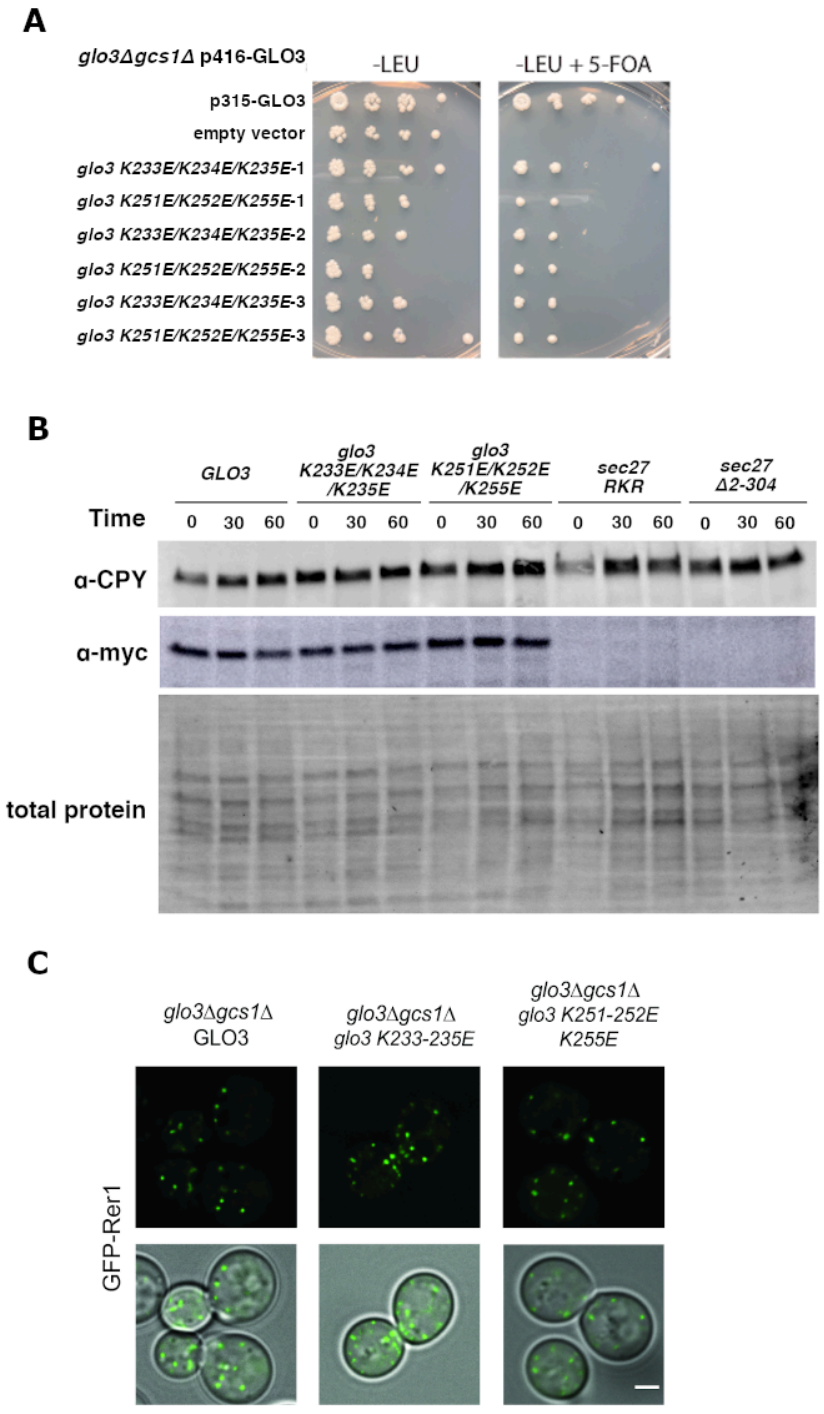

Figure 2-14. Yeast growth assays and Golgi/ER COPI cargo trafficking data. (A) Yeast growth assays in *glo3Δgcs1Δ* background strains with *GLO3* or *glo3* mutants (K233E/K234E/ K235E or K251E/K252E/K255E). Mutant strains do not show growth defects comparing to the wild-type strain. (B) The Emp47-myc reporter construct (visualized using α-myc) remains stable over time in both wild-type *GLO3* and mutant *glo3* strains. In contrast, the reporter is sent to the vacuole and degraded when the dilysine binding site on *sec27* is mutated (*sec27RKR*; R13A/K15A/R59A) or the first propeller of *sec27* is deleted (*sec27 Δ2-304*). (C) Representative fluorescence images of GFP-Rer1 in *glo3Δgcs1Δ* strains with *GLO3* or *glo3* mutants introduced on a plasmid. GFP-

Rer1 trafficking does not appear to change when the β'-COP/Glo3 interaction is disrupted. Thanks to Clara Guillem and Todd Graham lab at Vanderbilt University.

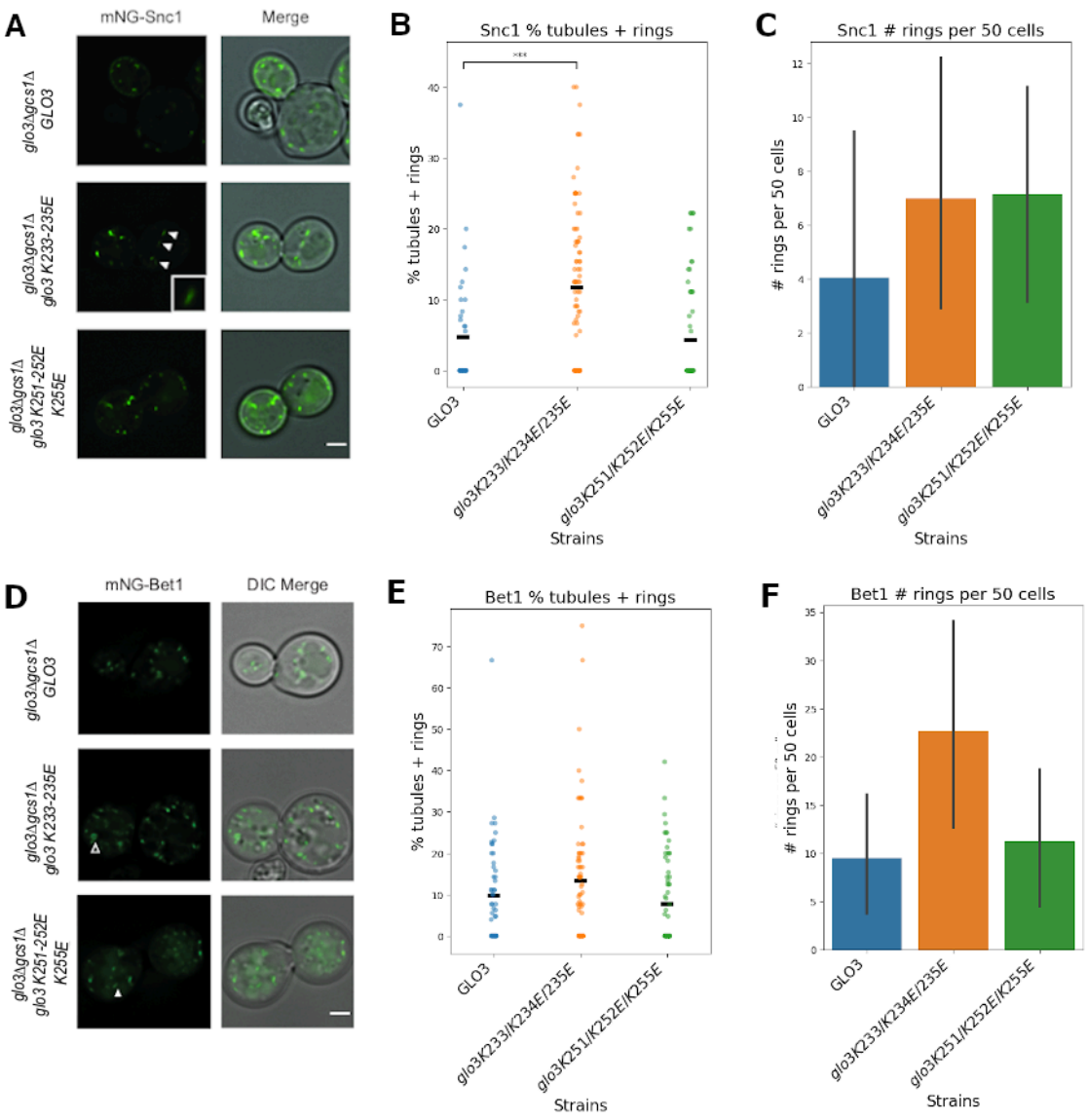

Figure 2-15. SNARE localization and Golgi morphology data. (A) Fluorescence imaging of mNG-Snc1 in glo3Δgcs1Δ strains with *GLO3* or *glo3* mutants (K233E/K234E/K235E or K251E/K252E/K255E) on a plasmid. (B) Strip plot showing percentage of abnormal structures (tubules and rings) with mean (black bar) observed in each strain. Mutating the first lysine cluster (K233E/K234E/K235E) resulted in cells exhibiting a significant difference from wild-type. Significance was determined using a Mann-Whitney test comparing wild-type and mutant strains. (C) Bar plot showing number of mNG-Snc1 ring structures with standard deviation (black lines) in each strain. (D) Fluorescence imaging of mNG-Bet1 in *glo3Δgcs1Δ* strains with *GLO3* or *glo3* mutants (K233E/K234E/K235E or K251E/K252E/K255E) on a plasmid. (E) Strip plot showing percentage of abnormal structures (tubules and rings) with mean (black bar) observed in each strain. Although we sometimes observe abnormal structures in the *glo3 K233E/K234E/K235* strain, the number does not reach significance level, as determined by a Mann-Whitney test. (F) Bar plot showing number of mNG-Bet1 ring structures with standard deviation (black lines) in each strain. Thanks to Clara Guillem and Todd Graham lab at Vanderbilt University.

Discussion

Molecular details of the β'-COP/Glo3 interaction

Previous studies have demonstrated that Glo3, not Gcs1, stably associates with COPI using affinity purification from yeast cell lysates (Arakel et al., 2019a). Here we show for the first time that Glo3 stably associates with COPI through a direct molecular interaction with the β'-COP subunit, and that this interaction exhibits a low micromolar K_D. We mapped key residues in both Glo3 and β'-COP propeller domains that mediate the interaction. We identified two lysine residue patches (K233/K234/K235 and K251/K252/K255) in the Glo3 BoCCS region that interact with two propeller domains of β'-COP and an acidic patch (D436/D450) on the β'-COP C-terminal propeller domain that binds the lysine residues on Glo3. The two lysine residue patches are separated by ~20 amino acids and could potentially span up to 50 Å if this region is unconstrained by any secondary structures. Through ITC experiments, we showed both β'-COP propeller domains are required to bind Glo3 BoCCS.

It is tempting to speculate each β'-COP propeller domain binds each one of the Glo3 lysine cluster through an acidic patch, suggesting there is a second acidic patch on the N-terminal domain of β'-COP waiting to be discovered. We have been unable to identify the exact residues involved in this acidic patch through systematic mutagenesis, but ITC and structural data implies that the second patch is likely located near the dilysine cargo motif binding site (E15/K17/R59). Our ongoing efforts to optimize the crystallography and cryo-EM experiments will likely provide more structural information about the second acidic patch and therefore uncover the precise molecular details of the Glo3 interaction with the N-terminal propeller domain of β'-COP.

β'-COP emerges as a potential molecular platform in COPI

Together with previously published studies, multiple lines of data suggest the β'-COP subunit of COPI may be a potential molecular platform to coordinate interactions with different protein regulators within the COPI coat. Propeller domains in other trafficking proteins often act as molecular platforms; for

example, clathrin contains a propeller domain called terminal domain (TD). The terminal domain in clathrin consists of four interaction site for protein binding partners (Ter Haar et al., 2000; Miele et al., 2004; Muenzner et al., 2017; Willox and Royle, 2012). There are four propeller domains in the COPI coat: two in β'-COP and two in α-COP. β'-COP propeller domains are located near the γ-appendage in the F-subcomplex and α-COP is located near the β-appendage in the reconstituted coat (Dodonova et al., 2017). Until now, only two functions have been discovered to be related to the propeller domains of COPI: the N-terminal propeller domain of β'-COP is related to the recycling of ubiquitinated Snc1, though the molecular details remains unidentified (Xu et al., 2017); and the only identified binding sites on both the α-COP and β'-COP N-terminal propeller domains bind the dilysine cargo motifs (KKxx or KxKxx) found in transmembrane protein cargoes cycling between the Golgi and the ER (Jackson et al., 2012; Ma and Goldberg, 2013).

In this work, we identified two new direct binding partners for β'-COP: the Arf1 and the ArfGAP, Glo3. Through ITC experiments, we showed that the Glo3 BoCCS region interacts with both the N-terminal and C-terminal propeller domains of β'-COP, therefore identifying the first binding site and ascribing the first function to the C-terminal propeller domain. In previous cryo-ET reconstructions, β'-COP is located adjacent to both Arf1 and the ArfGAP2/3 GAP domain (Dodonova et al., 2015, 2017), though the molecular details about the interfaces were not reported. Here we also showed for the first time that β'-COP directly interacts with Arf1. Together, this information suggests that β'-COP performs as a molecular platform that coordinates key events in the COPI life cycle, especially coupling cargo recognition with F-subcomplex binding and Arf1 hydrolysis though interaction with Arf1 and Glo3. It will be interesting to test in the future whether Arf1(GTP) hydrolysis by Glo3 can be influenced by cargo binding though β'-COP.

Cargo sorting and Golgi morphology

ArfGAPs play critical roles in COPI mediated membrane trafficking other than just providing GAP activity. Yeast ArfGAPs of Glo3 and Gcs1 form an essential pair, where loss of either ArfGAP is tolerated,

but losing both is lethal to the cell. It has been proposed that Glo3 and Gcs1 are both overlapped and separated in locations and functions (Arakel et al., 2019a). However, despite their important roles, the molecular mechanisms and roles of these ArfGAPs have been difficult to dissect. In this study we identified a new molecular interaction between Glo3 and β'-COP, which provides great molecular tools to better understand the functions of Glo3 and Gcs1 more precisely.

It has been established that β'-COP recognizes the dilysine cargoes, here we observed β'-COP can bind Glo3 BoCCS region and the dilysine cargo motif simultaneously, which supports the idea that β'-COP can engage with ArfGAP and dilysine cargoes simultaneously. Alternatively, β'-COP recognition of dilysine cargoes and interaction with the Glo3 BoCCS region may happen in separate time or space. In our experiments, Glo3 engagement does not seem to be required to maintain proper cargo sorting between the *cis*-Golgi and ER, since we did not observe mis-trafficking of Emp47, a well-characterized COPI dilysine cargo that cycles between the *cis*-Golgi and ER, and Rer1, another cargo that cycles between the *cis*-Golgi and ER. In contrast, we observed two distinct phenotypes related to the Golgi. First, we imaged SNARE proteins of Snc1 and Bet and found abnormal Golgi morphology when disrupting the β'-COP/Glo3 interaction, and defects appeared to exist when imaging Snc1, which primarily localized in the Golgi. Second, Ste2, a yeast α-factor receptor, exhibits a trafficking defect and tends to be mis-sorted to the vacuole instead of its normal post-endocytic cycling to the plasma membrane. Together, these data implicated that the β'-COP/Glo3 interaction may not be involved in the dilysine cargo sorting between the ER and the *cis*-Golgi, but instead is required in maintaining proper steady-state levels receptor cargoes (*e.g.* Ste2) and SNAREs (*e.g.* Snc1) that cycle from the endosomes via the TGN to the plasma membrane, suggesting a possible separation of function between Glo3 and Gcs1, which is worthy to be further investigated.

Altogether, our data have implications in the functional, and possibly the spatial separation of Glo3 and Gcs1 in the COPI coat. Arakel and colleagues previously demonstrated the GAP-dead mutant

version of Glo3 (R59K) is lethal to yeast cells while cells bearing the GAP-dead version of Gcs1 (R54K) are viable, and re-introducing the BoCCS region alone rescues growth in the Glo3 GAP-dead mutant strain (Arakel et al., 2019a). Previous data also showed Glo3 BoCCS region co-immunoprecipitates Emp47, Bet1, and Bos1 (Schindler et al., 2009). These studies have established that Glo3 BoCCS plays an important regulatory role in COPI transport. Our data suggest that instead of engaging directly, Glo3 BoCCS likely engages with Emp47 indirectly though β'-COP. In addition, Glo3 has also been implicated in Sec22 binding, though molecular details remain unclear (Rein et al., 2002). Based on both published data and new data from our studies, we speculate that the β'-COP/Glo3 interaction is important to ensure proper sorting and trafficking of SNAREs and receptors, especially via the TGN, even in the absence of a functional GAP domain.

Our data also raise multiple new questions about how and why the COPI coat couples Glo3 binding to Arf1(GTP) hydrolysis and recognition of cargo and SNARE proteins. Previous publications have showed how the β/δ-COP and γ/ζ-COP interact directly with Arf(GTP) to form an "open" conformation similar to AP-1 and AP-2 in clathrin coated vesicles (Jackson et al., 2010; Ma and Goldberg, 2013; Ren et al., 2013), and the presence of the COPI coat F-subcomplex promotes Arf1(GTP) hydrolysis. Our data suggest β'-COP does not have preference for either Arf1 nucleotide-bound state *in vitro*, thus it is possible that only the F-subcomplex senses Arf1 status and promotes the open or hyper-open conformations observed in crystal structure (Yu et al., 2012) or cryo-ET reconstructions (Dodonova et al., 2015, 2017). Though our data is different from a previous study where crosslinked β'-COP/Arf1 has strong signal in the presence of GTPγS (Sun et al., 2007), this previous study was conducted using the whole coatomer and is therefore possible that such preference to GTP indirectly come from the F-subcomplex subunits (Yu et al., 2012). β'-COP, instead, may further stabilize an assembled coat or regulate Arf1 hydrolysis indirectly through Glo3, and the interface between β'-COP and Arf1 must be located on the opposite of the Arf1 switches. The tripartite

interaction bears further investigation on how β'-COP couples Glo3 regulation on the COPI coat to cargo and SNARE recognition.

Acknowledgements

We sincerely thank David Owen and members of the Jackson and Graham labs for helpful feedback, discussion, and critical reading of the manuscript. BX, CJ, and AK performed protein expression, protein purification, biochemical, and biophysical experiments. BX, CG, and JB undertook yeast experiments, including growth and cargo sorting assays, and imaging experiments. BX and LPJ wrote the paper with input from all authors. LPJ conceived the project. BX, CJ, AK, and LPJ are supported by NIH R35GM119525. LPJ is a Pew Scholar in the Biomedical Sciences, supported by the Pew Charitable Trusts. CG, JB, and TRG are supported by NIH R01GM118452. The authors declare no competing conflicts of interest.

Materials and methods

Reagents and antibodies

Unless otherwise noted, all chemicals were purchased from Fisher (Chicago, IL) or Sigma (St. Louis, MO). The following antibodies were used in this study: anti-His (abcam), rabbit anti-Arf1 (Graham lab), rabbit anti-COPI (Barlowe lab and Spang lab), anti-myc (Invitrogen).

Cloning and mutagenesis

For structural and biochemical analyses, C-terminal His-tagged β'-COP and Glo3 were placed into the NdeI/BamHI or NdeI/HinDIII sites of an in-house vector pMW172 (Owen and Evans, 1998) under control of the T7 promoter. N-terminal His-tagged yeast Arf1 was placed into pET-21a (+) vector in the NdeI/BamHI sites. The Glo3 BoCCS and GRM regions and β'-COP (residues) were ligated into BamHI/NotI sites of pGEX-6P-1 (GE Healthcare), resulting in N-terminal GST-tagged proteins with a 3C-protease cleavage site. Other GST-tagged Glo3 and β'-COP constructs were sub-cloned into NdeI/BamHI or

NdeI/HinDIII sites of pMWGST, a modified form of pMW172 incorporating a C-terminal, thrombin cleavable GST tag.

For mutagenesis, a two-stage quick-change protocol adapted from Wang and Malcolm (1999) was used to introduce mutations in Glo3 and β'-COP proteins. In this protocol, mutagenic primers (St. Louis, MO, USA) were created for the desired mutations. In the first step, two polymerase chain reactions (PCRs), with either the mutagenic 5' or 3' primer, were amplified around the plasmid. The two reactions were then combined in an additional PCR step, followed by DpnI digest and transformation. All constructs were verified by sequencing (GENEWIZ) prior to use.

Protein expression and purification

All constructs were expressed in BL21(DE3)pLysS cells (Invitrogen) for 16-20 hours at 22°C following induction with 0.4 mM IPTG. His-tagged Arf1 constructs were purified in 20 mM Tris-HCl (pH 8.0), 200 mM NaCl, 0.5 mM TCEP, and 5 mM $MgCl_2$. Full-length Glo3 was purified in 20 mM HEPES (pH 7.5), 500 mM NaCl, and 1 mM DTT. Other Arf1 and Glo3 constructs and all β'-COP constructs were purified in 20 mM HEPES (pH 7.5), 200 mM NaCl, and 1 mM DTT. AEBSF (Calbiochem) or cOmplete ULTRA Tablets (Roche) was incorporated at early stages of all purifications. Cells were lysed by a disruptor (Constant Systems Limited) and proteins were affinity purified using glutathione sepharose (GE Healthcare) or HisPur cobalt resin (Thermo Scientific) in buffers listed above. GST-tagged proteins were cleaved overnight with thrombin (Recothrom, The Medicine Company) or 3C-protease (made in-house) at 4°C and eluted in batch. All proteins were further purified by gel filtration on a Superdex S200 preparative or analytical column (GE Healthcare).

GST pulldown assays

GST or GST-tagged β'-COP (residues 1-604), Arf1, or Glo3 constructs (GAP domain, BoCCS region, GRM region) were immobilized on glutathione sepharose resin (GE Healthcare) for one hour on ice. The resin was incubated for one hour on ice with prey proteins (Glo3-His8; T31N or Q71L Δ18Arf1-His6; or β'-

COP (1-604)-His6) in 20mM HEPES (pH7.5), 200mM NaCl, 10mM MgCl, 2mM DTT, and 0.5% NP40. Samples were washed three times with the same buffer. Proteins were eluted from the resin using buffer plus 30 mM reduced glutathione. Gel samples were prepared from the supernatant following elution, and the assay was analyzed by Commassie staining of SDS-PAGE gels. The gels were further analyzed by western blotting, using anti-His (Abcam, NB100-63173) and rabbit anti-Arf1 antibodies (from Todd Graham, Vanderbilt University). Yeast cell lysates were provided by Todd Graham lab at Vanderbilt University.

Isothermal titration calorimetry (ITC)

ITC experiments were conducted on a NanoITC instrument (TA Instruments) at 20°C. The molar concentration of protein in the syringe was at least 5 times that of protein in the cell. All experiments were carried out in 10 mM HEPES (pH 7.5), 100 mM NaCl, and 0.5 mM TCEP, filtered and degassed. All proteins had purification tags removed and were gel filtered into the ITC buffer. Incremental titrations were performed with baseline of 100 seconds, injection volume of 2 µL, and injection intervals of 200 seconds. Titration data was analyzed in NanoAnalyze (TA instruments) to obtain a fit and value for stoichiometry (n) and equilibration association constant (K_a). K_D values were then calculated from the association constant. The dilysine peptide RQEIIKTKLL was used in ITC experiments testing dilysine cargo binding.

Sequence alignments

In order to map residue conservation of Glo3, sequences of full-length and the BoCCS region alone of Glo3 from *S. cerevisiae, M. musculus, H. sapiens, B. Taurus, P. troglodytes, G. gallus, D. melanogaster, C. elegans, S. pombe,* and *A. thaliana* were aligned using ClustalW (Madeira et al., 2019) and PRALINE (Simossis and Heringa, 2005a).

Yeast strains and plasmids

Standard media and techniques for growing and transforming yeast were used. Glo3 mutant strains were constructed by plasmid shuffling (PXY51) on 5'-fluoro-orotic acid (5-FOA) plates. Yeast strains

used in this study are listed in Table A2-4. Plasmids constructions were performed using standard molecular manipulation. Wild-type *GLO3* gene were cloned into pRS315 yeast vectors with endogenous promoter and terminator sequences. Mutations were introduced using the two-stage quick-change mutagenesis protocol.

Yeast growth assays

Strains containing pRS416-*GLO3* (wild-type) and pRS315-*glo3* (mutant constructs) were grown at 30°C. Cells were then sub-cultured, and an equal OD of each strain was loaded into a 96-well plate. Using a prong replicator, strains were stamped onto both appropriate synthetic media and 5-FOA plates to select against the pRS416-*GLO3* plasmid. Cells were grown for four days and images of these plates were captured.

Fluorescence imaging

Three biological replicates of transformed strains were sub-cultured for imaging in appropriate synthetic media. Cells at mid-log phase were then mounted on glass slides and observed immediately at room temperature. Images were acquired using a DeltaVision Elite Imaging System (GE Healthcare Life Sciences, Pittsburgh, PA) equipped with a 100x objective lens. Z-stack of images were collected for Green channel and DIC. All images were de-convolved using softWoRx software (GE Healthcare Life Sciences). Cells were chosen using green fluorescence expression.

Data analysis and statistics

To quantify levels of Ste2-GFP at the cell surface, traces were drawn just outside and inside the plasma membranes using the freehand drawing tool in ImageJ to measure the total cellular fluorescence ($Cell_{fl}$) and Internal fluorescence (Int_{fl}), respectively. The percent of Ste2-GFP at the plasma membrane was then calculated by ($Cell_{fl}$ - Int_{fl})/$Cell_{fl.}$ Statistical differences were determined using a one way ANOVA test in GraphPad Prism version 8.0 (GraphPad Software, San Diego, California, USA, www.graphpad.com). Images of fluorescently tagged SNARE proteins and Rer1 were coded, and the number of tubules, puncta,

and rings were counted in a blinded experiment. Statistical differences against wild-type were determined using Mann-Whitney test, and data were visualized using Python. Probability values of less than 0.04, 0.01, or 0.001 were used to show statistically significant differences and are represented with *, **, or *** respectively.

Dilysine reporter construct trafficking in yeast

Yeast Emp47 under control of its endogenous promoter was used as the backbone for reporter constructs, and a myc-tag was incorporated following the transmembrane domain to facilitate Western blotting. The KxKxx reporter contained endogenous Emp47 transmembrane domain followed by the cytoplasmic sequence (RQEIIKTKLL). The reporter was introduced into appropriate *GLO3* wildtype and *glo3* mutant strains. Reporter levels were monitored by Western blotting against the myc tag both prior to and following a 20 µg/mL cycloheximide chase at time points equal to 0, 30, and 60 minutes. Cells were lysed using glass beads with SDS buffer and then boiled at 95°C for 5 minutes. Western blots were probed with mouse monoclonal anti-myc (Invitrogen 9E10) for the reporter and with mouse anti-CPY (Invitrogen 10A5B5) as a loading control. The membrane was then incubated with HRP-goat anti-mouse IgG secondary antibody (Invitrogen) or IRDye 800CW goat anti-mouse IgG secondary antibody (LI-COR) to visualize.

Crystallography attempts

Purified Yeast β'-COP single propeller or double propellers domains were concentrated to 15-20 mg/mL. Purified or chemically synthesized (GenScript, NJ) Glo3 peptides were added at 10-20 fold molar ratio to β'-COP and incubated to bind. The β'-COP/Glo3 complex was crystalized in 400 nL drops in crystallization trays set up on a Mosquito robot (LLP Lab Tech). Crystals were observed in multiple conditions in Hampton PEG/Ion HT, JSCG+, and ProPlex HT-96 screenings. Crystals were harvested directly from 96-well plates into 500 nL drops in reservoir buffer with Glo3 peptide plus 25% glycerol for cryo-protection. Crystallographic datasets were collected at Argonne National Laboratory sector LS-CAT,

beamline 21-ID-G or 21-ID-F, from crystals flash frozen by plunging into liquid nitrogen. Data were collected at a wavelength of λ=1Å. The space group was P65 for peptide-bound double propeller and P42 for peptide-bound N-terminal propeller. The data were integrated and merged in HKL2000 (Otwinowski and Minor, 1997) or Dials (Beilsten-Edmands et al., 2020) and further processed using the CCP4 (Winn et al., 2011) and PHENIX (Liebschner et al., 2019) suites. The structures was phased using molecular replacement methods in Phaser (McCoy et al., 2007) with the yeast β'-COP double propeller as initial models (PDB ID: 2YNP). Rounds of manual model building were undertaken in Coot (Emsley et al., 2010) with iterative rounds of refinement using PHENIX or REFMAC5 (Nicholls et al., 2012).

Cryo-EM

For negative stain electron microscopy, 10 µl of the β'-COP/Glo3 complex at concentrations between 5 µg/mL and 10 µg/mL were applied to continuous carbon film on 400 square mesh copper EM grids (Electron Microscopy Sciences, Hatfield, PA) and washed twice with water. The grids were stained with 2% uranyl formate and 1% uranyl acetate and air dried overnight. The grids were screened on a ThermoFisher FEI Morgagni microscope operating at 100kV with a AMT 1k × 1k CCD camera (Vanderbilt University CryoEM facility) to verity protein quality. For cryo-electron microscopy, β'-COP/Glo3 complex at 50 µg/mL or 100 µg/mL was applied to freshly glow discharged CF-2/2-2C C-Flat grids (Protochips, Morrisville, NC) or Quantifoil 1.2/1.3 300 mesh grids (Quantifoil), and the grids were vitified in liquid ethane using a ThermoFisher FEI MarkIV Vitrobot. The grids were first screened on a ThermoFisher FEI Tecnai F20 operating at 200kV with a 4k × 4k CCD camera (Vanderbilt University CryoEM facility). Working datasets were collected at the NIH National Center for CryoEM Access and Training (NCCAT) in two different data collection sessions using ThermoFisher FEI Titan Krios microscopes. Ongoing data processing is carried out using RELION-3 (Zivanov et al., 2018).

CHAPTER III

THE GLO3 GAP CRYSTAL STRUCTURE SUPPORTS THE MOLECULAR NICHE MODEL FOR ARFGAP3 IN COPI COATS

Boyang Xie[1,2], Christian Jung[1], Mintu Chandra[1], Andrew Engel[1], Amy K. Kendall[1,2], and Lauren P. Jackson[1,2,3]

[1]Department of Biological Sciences, Vanderbilt University, Nashville, TN, USA
[2]Center for Structural Biology, Vanderbilt University, Nashville, TN, USA
[3]Department of Biochemistry, Vanderbilt University, Nashville, TN, USA

[†]Correspondence to lauren.p.jackson@vanderbilt.edu

This article has been published under the same title in

Advances in Biological Regulation, 79, 1 2021

Abstract

Arf GTPase activating (ArfGAP) proteins are critical regulatory and effector proteins in membrane trafficking pathways. Budding yeast contain two ArfGAP proteins (Gcs1 and Glo3) implicated in COPI coat function at the Golgi, and yeast require Glo3 catalytic function for viability. A new X-ray crystal structure of the Glo3 GAP domain was determined at 2.1 Å resolution using molecular replacement methods. The structure reveals a Cys4-family zinc finger motif with an invariant residue (R59) positioned to act as an "arginine finger" during catalysis. Comparisons among eukaryotic GAP domains show a key difference between ArfGAP1 and ArfGAP2/3 family members in the final helix located within the domain. Conservation at both the sequence and structural levels suggest the Glo3 GAP domain interacts with yeast Arf1 switch I and II regions to promote catalysis. Together, the structural data presented here provide additional evidence for placing Glo3 near Arf1 triads within membrane-assembled COPI coats and further support the molecular niche model for COPI coat regulation by ArfGAPs.

Introduction

Arf GTPase activating proteins (ArfGAP) comprise a family of regulatory and effector proteins defined by the presence of the ArfGAP domain that is approximately 130-150 amino acids in length. ArfGAPs are found across eukaryotes: yeast contain five ArfGAPs, while mammalian cells contain over thirty (Kahn et al., 2008). ArfGAPs utilize their GAP domains to promote GTPase hydrolysis on small GTPases in the Arf family (Cherfils, 2014; Gillingham and Munro, 2007; Jackson and Bouvet, 2014). Arf proteins are sub-classified based on sequence homology and structural features (Jackson and Bouvet, 2014). Arfs undergo well-documented conformational changes in their switch I and switch II regions upon shifting nucleotide state (Goldberg, 1998; Pasqualato et al., 2002), when a β hairpin between switch I and switch II regions allows communication from the protein N-terminus to the nucleotide binding site. In

general, structural evidence suggests catalytic activity by GAP domains (Vetter and Wittinghofer, 2001) relies on two key residues: an invariant ''arginine finger'' residue in the GAP and a conserved catalytic glutamine residue in its cognate GTPase. When GAP domains bind a GTPase, the GAP stabilizes the otherwise flexible switch II region, which in turn allows the catalytic glutamine residue to align a nucleophilic water molecule and promote hydrolysis (Vetter and Wittinghofer, 2001).

Five ArfGAPs have been identified in the yeast *Saccharomyces cerevisiae* and shown to display a combination of redundant and unique functions (Spang et al., 2010). Mammalian cells express an array of ArfGAPs ranging from relatively small proteins resembling those found in yeast to the large, multi-domain ArfGAPs that are proposed to function as scaffolds for cell signaling. Among the ArfGAPs discovered, there are eleven ArfGAP subfamilies, and members of two ArfGAP families specifically bind and regulate the small GTPase, Arf1 (Jackson and Bouvet, 2014). Arf1 plays critical roles in multiple membrane trafficking pathways mediated by vesicular coats, including a role in inducing membrane curvature (Makowski et al., 2020). On the Golgi apparatus, Arf1(GTP) recruits multiple coat protein complexes to promote and regulate vesicle formation. Intrinsic GTP hydrolysis on Arf1 occurs slowly, so ArfGAPs are needed in cells to promote timely hydrolysis (Kahn and Gilman, 1986). ArfGAP proteins are critical regulators and effectors of COPI coat function (Arakel et al., 2018; Duden, 2003; Jackson, 2014). COPI is essential for vesicular membrane trafficking in eukaryotes and has many established roles, including retrieval of endoplasmic reticulum (ER) proteins from the Golgi; ER/Golgi protein recycling from endosomes to the TGN (Popoff et al., 2011; Xu et al., 2017; Yang et al., 2011). Despite their cellular importance, the precise molecular role of ArfGAPs in regulating coats remains poorly understood. ArfGAPs are implicated in COPI coat assembly (Lewis et al., 2004; Yang et al., 2002); cargo/SNARE sorting (Lee et al., 2005; Robinson et al., 2006; Schindler et al., 2009); and coat disassembly (Reinhard et al., 2003). Budding yeast has two essential ArfGAP proteins, Glo3 and Gcs1, which have overlapping functions (Poon et al., 1999). Both yeast ArfGAPs have homologs/orthologs in mammalian cells: Gcs1 corresponds to ArfGAP1, while Glo3

corresponds to the ArfGAP2/3 family (Kahn et al., 2008). Yeast tolerate deletion of either of *GLO3* or *GCS1* genes individually, but deletion of both genes is lethal (Schindler et al., 2009).

Glo3 has been shown to play important roles in COPI coat assembly. Apart from a GAP domain it also includes an internal BoCCS (Binding of Coatomer, Cargo, and SNAREs) region and a C-terminal GRM (Glo3 regulatory motif) region (Schindler et al., 2009). Yeast require both a functional Glo3 GAP domain and BoCCS region (Arakel et al., 2019a; Schindler et al., 2009). Recent data indicate yeast especially require the Glo3 GAP activity, as strains harboring the GAP-dead version of Glo3 (R59K) are not viable, even in the presence of functional Gcs1 (Arakel et al., 2019a; Lewis et al., 2004). Biochemical data using yeast cell lysates suggest only Glo3 stably associates with the COPI coat, although Gcs1 is also proposed to interact with COPI through a short hydrophobic motif (Arakel et al., 2018; Cosson et al., 1998; Rawet et al., 2010; Suckling et al., 2015). Recent studies from the Briggs and Schwappach labs together proposed the ''molecular niche'' hypothesis: this suggests Gcs1 (ArfGAP1) and Glo3 (ArfGAP2/3) occupy different positions within assembled COPI coats (Arakel et al., 2019a; Dodonova et al., 2017). Taken together, data indicate the ArfGAP1 and ArfGAP2/3 families may exhibit separation of function.

There are limited published structural data available on ArfGAP proteins that engage COPI coats. This part of work reports the first X-ray crystal structure of the yeast Glo3 GAP domain (residues 1-150). The structure reveals a Cys4-type zinc finger motif and the position of the invariant arginine residues (R59) essential for function in budding yeast (Arakel et al., 2019a). As expected, the Glo3 GAP domain exhibits sequence and structural similarity to other GAP domains in the ArfGAP family. However, comparison among available structures reveals ArfGAP2/3 family members contain an extended helix as compared to ArfGAP1 domains. Combining sequence and structural conservation with modeling suggests how Glo3 GAP likely engages Arf1(GTP) using a highly conserved interface. This new structure provides evidence for placement of the Glo3 GAP domain within assembled COPI coats on membranes

and further supports the recently proposed molecular niche model (Arakel et al., 2019a; Dodonova et al., 2017).

Results

X-ray crystal structure of Glo3 GAP domain

The structure of *S. cerevisiae* Glo3 GAP domain (residues 1-150, Figure 3-2) was determined to 2.1 Å resolution (Figure 3-1A; Table A3-1; Figure 3-2) using molecular replacement methods with human ArfGAP2 (PDB ID: 2P57; unpublished model) as an initial search model. The dataset was originally intended for S-SAD method, but was later used for molecular replacement since the anomalous signal was beyond detection limit. The needle shaped crystals belonged to space group $P2_1$ and contained four molecules in the asymmetric unit (Figure 3-1C). All four copies show clear and well-ordered density from residues 8 to 145; additional density for residues 4-7 is visible in chain B only (Figure 3-3). There is no significant difference between the four copies, and they overlay with a root mean square deviation (RMSD) value of 0.58 Å in CCP4 Superpose (Krissinel and Henrick, 2004). Following several rounds of iterative refinement in PHENIX (Adams et al., 2010; Liebschner et al., 2019), the final model demonstrated excellent overall geometry (Table A3-1) with 99% resides in Ramachandran favored regions and final R_{work}/R_{free} values of 0.191/0.247.

Overall, the Glo3 GAP domain (Figure 3-1A) is composed of a central core of five β-strands and six α-helices. Secondary structure prediction program PSIPRED (Buchan and Jones, 2019) successfully predicted all six helices but failed to predict the first three very short β-strands (β1, β2, β3). An additional short strand was predicted (Figure 3-1C) following helix α6, which we were unable to visualize in the density. Strand β3 makes hydrogen bonding contacts with β4 and β5 to form the central three-stranded β sheet. The Glo3 GAP domain comprises a Cys_4 zinc finger containing the sequence C-XX-C-X_{16}-C-XX-C. the zinc finger is composed of three β strands (β1, β2, β4) together with adjoining loops and the N-

terminal end of helix α2. The zinc ion is tetrahedrally coordinated by four conserved cysteine residues (Cys31, Cys34, Cys51, and Cys54), which each exhibit a distance between 2.3-2.5 Å from the zinc ion (Figure 3-1B). The domain further contains a conserved arginine residue (R59) located in helix α2. This residue is predicted to act as an ''arginine finger'' during Arf1 catalysis (Scheffzek et al., 1997), and comparison among ArfGAP structures reveals it is well-positioned to play this role.

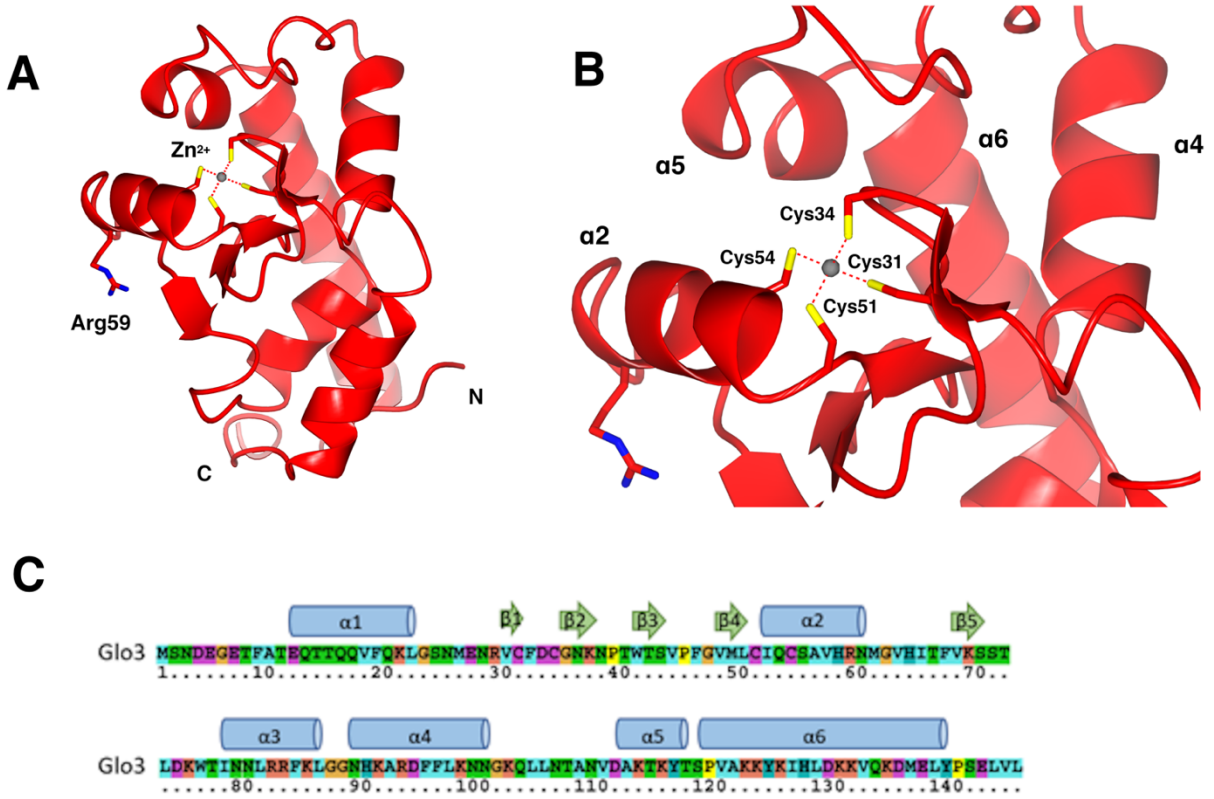

Figure 3-1. Glo3 GAP domain X-ray crystal structure. (A) The Glo3 GAP domain (residues 1-150) X-ray crystal structure determined at 2.1 Å resolution is shown as a ribbon diagram with N- and C-termini, coordinated zinc ion (grey sphere), and conserved residues (Arg59, Cys residues as red cylinders) highlighted. (B) Close-up view of zinc finger: the conserved Arg59 side chain is shown as cylinders, and the location of the zinc ion (Zn^{2+}) within the zinc finger is shown as a grey sphere coordinated to four Cys residues. (C) The Glo3 GAP sequence marked with secondary structural elements. The GAP domain contains six α-helices and five β-strands.

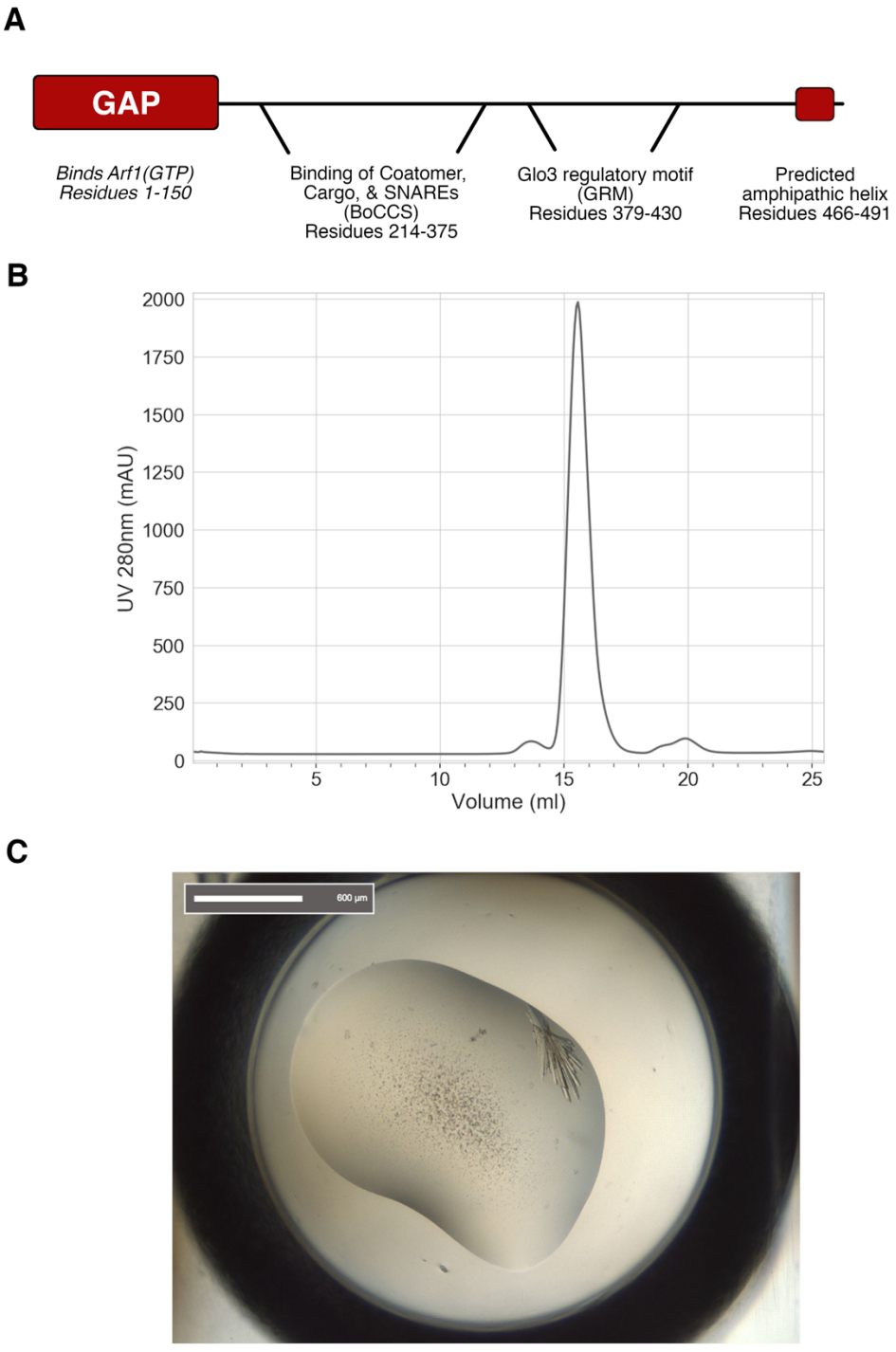

Figure 3-2. Glo3 domain architecture and purification. (A) Glo3 contains an N-terminal GAP domain (residues 1-150; shown as red box). The middle portion of Glo3 has been defined as the "Binding of Coatomer, Cargo, and SNAREs" region (residues 214-375), while the C-terminus contains a "Glo3 regulatory motif" (GRM; residues 379-430). The C-terminus (residues 466-491) is predicted to contain an amphipathic helix. (B) Representative gel filtration profile from purified Glo3 GAP domain used in crystallization trials. The GAP domain was purified over a Superdex S200 Increase 10/300 GL column (GE Healthcare) and elutes at a volume consistent with its predicted molecular weight (18 kDa). (C) Representative image of the Glo3 GAP domain crystal.

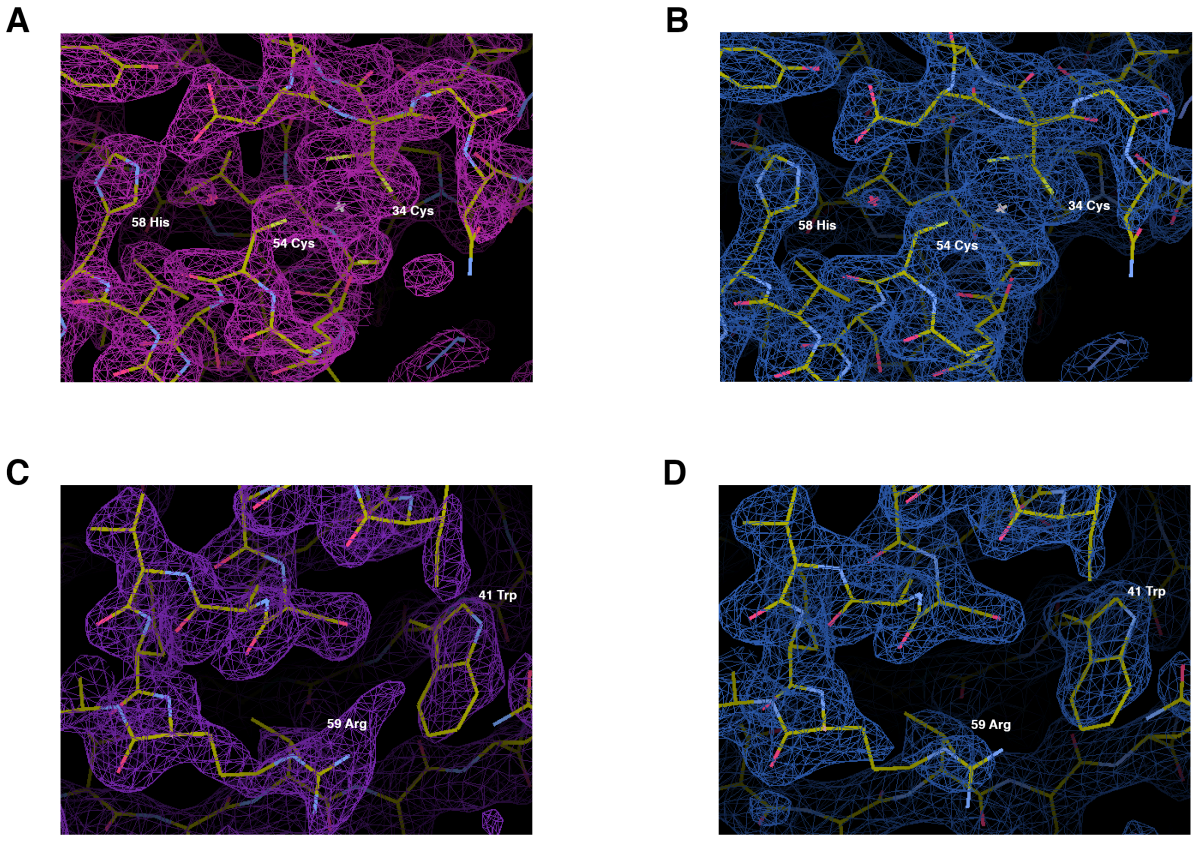

Figure 3-3. Glo3 GAP domain experimental and refined electron density maps. (A) Representative 2mFO-DFC electron density (contoured at 0.51 electrons/Å3 in Coot) near the zinc ion is shown in magenta following molecular replacement in Phaser. (B) Final refined 2mFO-DFC density near the zinc ion is shown in blue. (C) Representative 2mFO-DFC electron density (contoured at 0.51 electrons/Å3 in Coot) near Arg59 ion is shown in purple following molecular replacement in Phaser. (D) Final refined 2mFO-DFC density near Arg59 is shown in blue.

Comparison among ArfGAP domain structures

The Glo3 GAP domain was compared with thirteen ArfGAP domain structures deposited in the PDB using CCP4 Superpose (Krissinel and Henrick, 2004) (Table A3-2) and Consurf (Ashkenazy et al., 2010) to evaluate conservation (Figure 3-4A); many of the available structures were deposited but remain unpublished. We first compared domains that the overall secondary structural level. Glo3 GAP domain is most similar to human ArfGAP2 (also called ZNF289; PDB ID: 2P57) and *P. falciparum* ArfGAP (PDB ID: 3SUB) based on overall RMSD (RMSD: 1.4 Å; Table A3-2). All thirteen structures align well in the region that comprises the first four α-helices (α1- α4) and β-strands (β1-4), while α5 and α6 in the C-termini

exhibit more variability among GAP domains. Globally, the Glo3 GAP looks similar to human GAP domains found in ArfGAP1, ArfGAP2, and ASAP2 (Figure 3-4B).

We further compared the highly conserved zinc finger core (TABLE A3-2) found in ArfGAP domains; this specifically includes three β-sheets (β1, β2, β4), adjoining loops, and the N-terminal end of helix α2. All ArfGAP domain zinc fingers align well with Glo3 GAP domain (RMSD: 0.5 – 1.4 Å; TABLE A3-2). As expected, the zinc finger is a conserved structural feature among ArfGAP proteins (Goldberg, 1999; Kahn et al., 2008). Furthermore, the invariant arginine residue (Glo3 R59) proposed to act as a catalytic "arginine finger" is conserved at both the sequence (Figure 3-5A) and structural levels: this residue aligns very closely across multiple structures of GAP domains deposited in the PDB (Figure 3-5A). This residue has previously been reported to play either catalytic (Ismail et al., 2010) or structural roles (Goldberg, 1999) in different ArfGAP proteins.

However, there is one notable difference in the final helix located at the C-terminus of these GAP domains (Figure 3-5B). Helix α6 is especially different among ArfGAP proteins. The GAP domains from multiple human ArfGAPs lack helix α6 altogether; examples include ASAP3 (PDBs: 2B0O, 3LVQ), SMAP1 (PDB: 2CRR), and ACAP1 (PDB: 3JUE). The human ArfGAP, Hrb (PDBa: 2D9L, 2OLM), contains an extremely short helix α6 with only a single turn. All of these ArfGAP domains are found in human proteins that lie outside the ArfGAP1 or ArfGAP2/3 families (Kahn et al., 2008).

In addition, there appears to be a difference between the ArfGAP1 and ArfGAP2/3 family members. Two human ArfGAP1 crystal structures (PDBs: 3DWD, 3O47) reveal only four turns in helix α6. In contrast, helix α6 in the Glo3 GAP domain contains six turns and is therefore longer (Figure 3-4B). Like Glo3, human ArfGAP2 (PDB ID: 2P57) and ArfGAP3 (PDB ID: 2CRW) each contain an extended helix α6. The ArfGAP3 structure (PDB: 2CRW) was determined using NMR, and it is clear from the data where helix α6 ends and leads into a region of high flexibility. The X-ray crystal structure of human ArfGAP2 is more ambiguous; there are clearly five turns in helix α6, and the last few residues suggest one more turn is

possible. Overall, currently available GAP structures from different family members support the idea that ArfGAP2/3 proteins may differ at the C-terminus of the GAP domain, in addition to overall domain architecture. This has implications for COPI coat assembly.

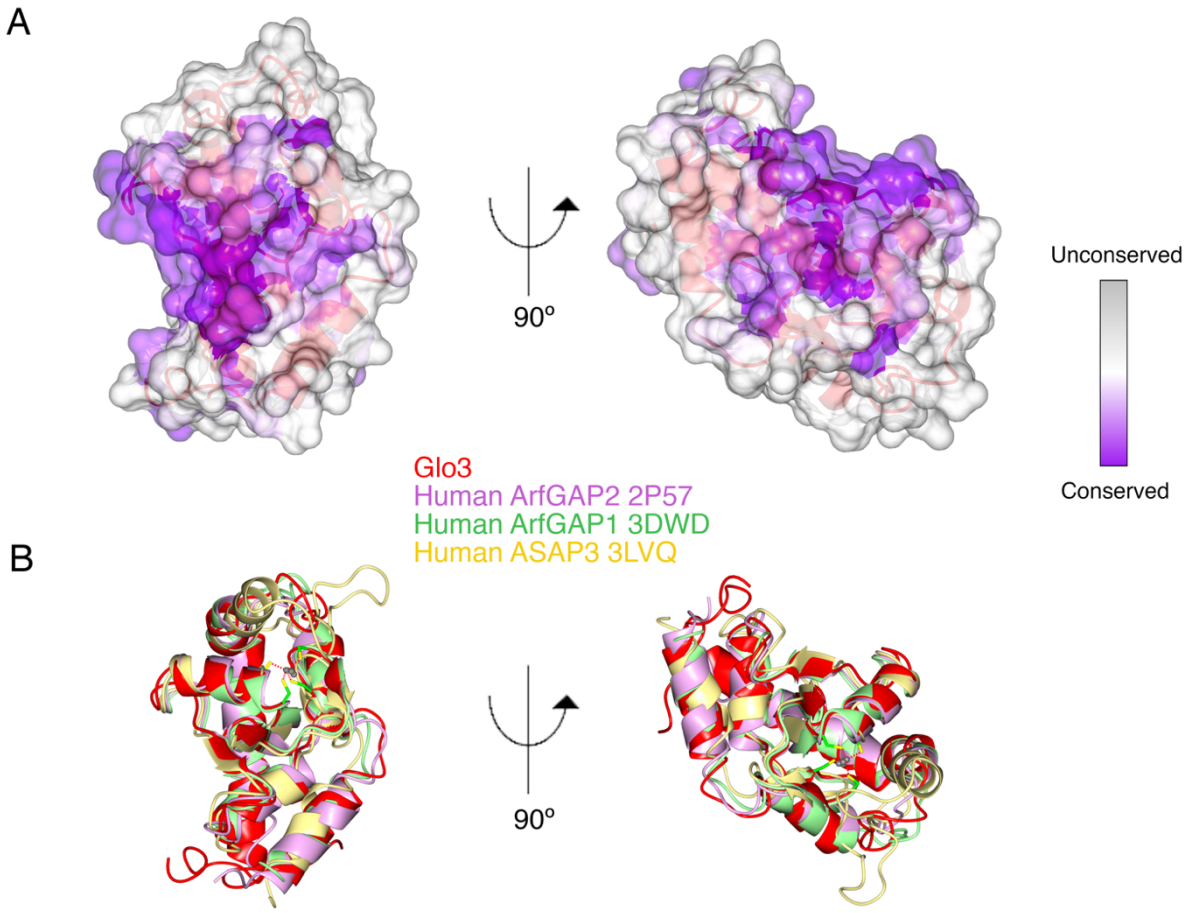

Figure 3-4. Glo3 GAP domain structural conservation. (A) Two views (rotated 90 degrees) showing overall Glo3 GAP conservation mapped onto its X-ray crystal structure (shown as a surface). Grey areas denote no conservation, while purple represents identity. (B) Two views (rotated 90 degrees) showing overall structural conservation between yeast Glo3 GAP and three human ArfGAP domain structures (ArfGAP1, ArfGAP2, and ASAP3).

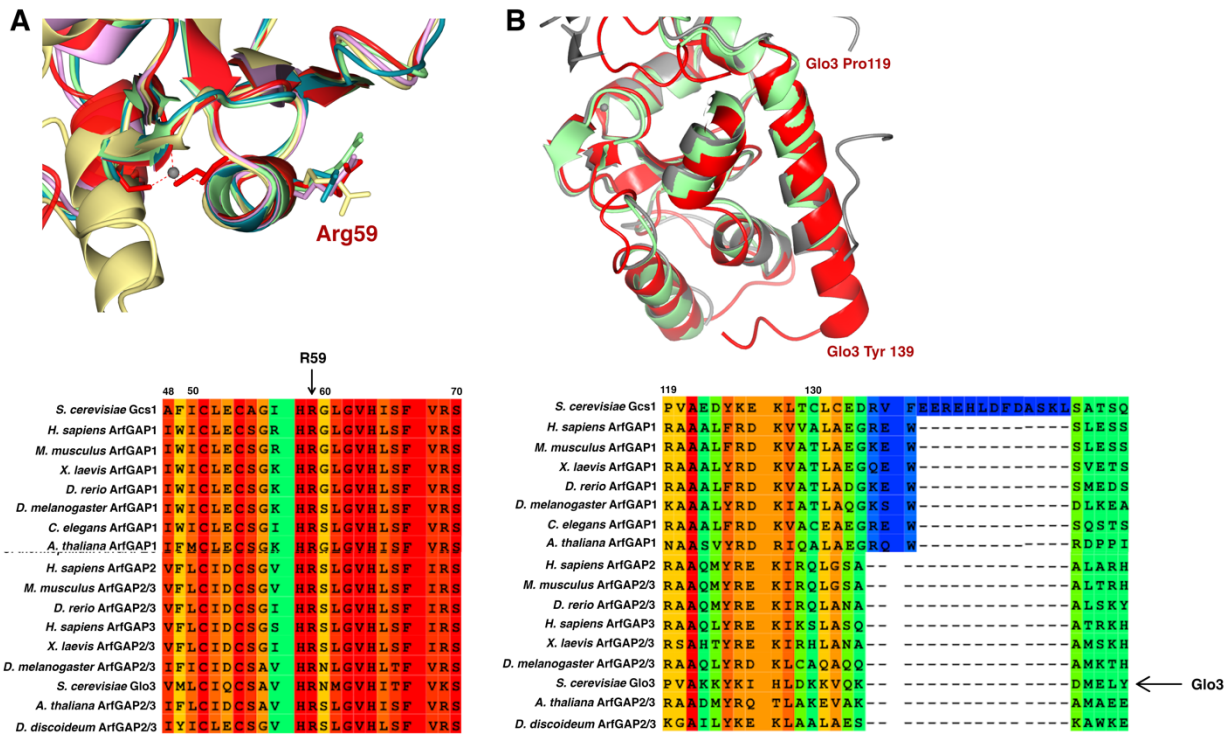

Figure 3-5. Structural conservation among ArfGAP family proteins. (A) Top: Overlay of invariant "arginine finger" in GAP domain structures with side chains shown as cylinders. Glo3 is shown as red ribbons; ArfGAP1 as green ribbons (PDB: 3DWD); ArfGAP2 as pink ribbons (PDB: 2P57); ASAP3 GAP as yellow ribbons (PDB: 3LVQ). Bottom: partial sequence alignment showing invariant arginine residue across species and ArfGAP families. This region is highly conserved at both the sequence and structural levels (B) Top: Overlay of two ArfGAP1 X-ray crystal structures (grey ribbons, PDB: 3O47; green ribbons, PDB: 3DWD) with Glo3 GAP domain determined in this work (red ribbons). Glo3 contains a longer C-terminal helix (helix a6) as compared to ArfGAP1 family proteins; this helix is two turns longer in Glo3 GAP. Bottom: partial sequence alignment comparing Glo3 helix a6 (residues 119-139) with other ArfGAPs. The ArfGAP1 family appears to have an insert that breaks the helix in this family.

Generation of yeast Glo3 GAP/Arf1 model

Controversy exists regarding how ArfGAP proteins engage Arf1 (Goldberg, 1999; Ismail et al., 2010). Here we report the first yeast GAP domain structure, but there are two relevant published mammalian X-ray structural models for Arf/ArfGAP interactions. The first is for murine ArfGAP1/Arf1 (Goldberg, 1999) (PDB coordinates not available), and the second is for human ASAP3/Arf6 (Ismail et al., 2010) (PDB ID: 3LVQ). We note that ArfGAP1 is the mammalian homologue of yeast Gcs1, which differs structurally and functionally from Glo3. Overall, the two models differ in where the GAP domain binds its Arf. Briefly, we combined conservation analysis in Consurf (Ashkenazy et al., 2010) with structural

modeling in CCP4MG (McNicholas et al., 2011) and propose the yeast Glo3 GAP/Arf1 interaction (Figure 3-6) likely resembles the ASAP3/Arf6 interaction, and this model has implications for assembly within the COPI coat on membranes (Figure 3-7).

The mouse ArfGAP1/Arf1•GDP co-crystal X-ray structure (Goldberg, 1999) reveals ArfGAP1 binds Arf1 on a surface located away from the central zinc finger; in this model, coatomer was proposed to provide the arginine finger required for catalysis. Specifically, ArfGAP1 binds the Arf1 switch II region and helix α3, which are located on the opposite face from the zinc finger, and does not engage switch I. The Arf1 switch II interaction occurs via ArfGAP1 residues located on helices α3 and α6 (residues K68, I70, A116, E120, K122). This switch II interaction appears unlikely to happen with Glo3, because some residues are not conserved (K68, I70) while others have no equivalent.

The second part of the interaction requires both electrostatic and hydrophobic interactions between ArfGAP1 and Arf1 helix α3. The hydrophobic residues in ArfGAP1 (V54, H55, and F58) are conserved in Glo3 (V63, H64, F67; Figure 3-6), but critical ArfGAP1 residues (R60, K68, and E71) that mediate salt bridge formation are not (Glo3 K69, T77, and N80). The ArfGAP1 lysine (K68) and glutamate (E71) residues are conserved among ArfGAP1 family members (Figure 3-5), which highlights a potential sequence and structural difference that delineates ArfGAP1 domains from the ArfGAP2/3 family and may have functional implications.

The structure of ASAP3 with Arf6 reveals a different mechanism (Ismail et al., 2010). In this model (Figure 3-8), Arf6 is bound to GDP•AlF_3 to capture the complex in the transition state, where ASAP3 uses its zinc finger to bind Arf6 switch I and II regions. ASAP3 GAP domain residues contributing to the buried interface are located on sheets β1 and β3, helices α2 and α4, and adjoining loops. The proposed arginine finger in ASAP3 is R469, which corresponds to Glo3 R59 in sequence alignments and structural superposition. R469 protrudes into the active site, where it is positioned to act as an arginine finger to further stabilize the transition state and orient the nucleophile during catalysis. This ASAP3/Arf6 model

(Ismail et al., 2010) is similar to reported interactions between Ras and RasGAP proteins (Scheffzek et al., 1997).

The Glo3 GAP/Arf1 interaction appears more likely to resemble the ASAP3/Arf6 interaction (Figure 3-6; Figure 3-8). The most highly conserved portion of Glo3 GAP across eukaryotes encompasses strands β3, β4, β5 and parts of helix α2. This region superposes well with the ASAP3 GAP domain (Figure 3-4B), indicating both sequence and structural conservation. Multiple ASAP3 residues required to interact with GTP-bound Arf6 switch I and II regions are conserved in the Glo3 GAP domain (residues Trp41, Ile52, Arg59, Val63, Leu73, Asp74; Figure 3-6B). We generated a yeast Arf1•GDP•AlF_3 model based on the Arf6•GDP•AlF_3 structure (3VLQ) using MODELLER (Webb and Sali, 2016). This model superposes well (RMSD = 0.66 Å) with an X-ray structure of human GTP-bound Arf1 (PDB ID: 2J59), and Arf1 is highly conserved across eukaryotes (sequence identity= 77 %; sequence similarity= 96%), which gives confidence in this model for yeast Arf1(GTP). The model suggests key conserved Arf1 switch I (Thr45, Ile46, Pro47, Ile48) and switch II residues (Gln71, Asp72, Arg73) are positioned to interact with Glo3 (Figure 3-4B). The ASAP3 GAP domain was reported to promote hydrolysis on Arf1 (Ismail et al., 2010), lending further support to this model. Overall, we favor this model, but there are some caveats (see Discussion).

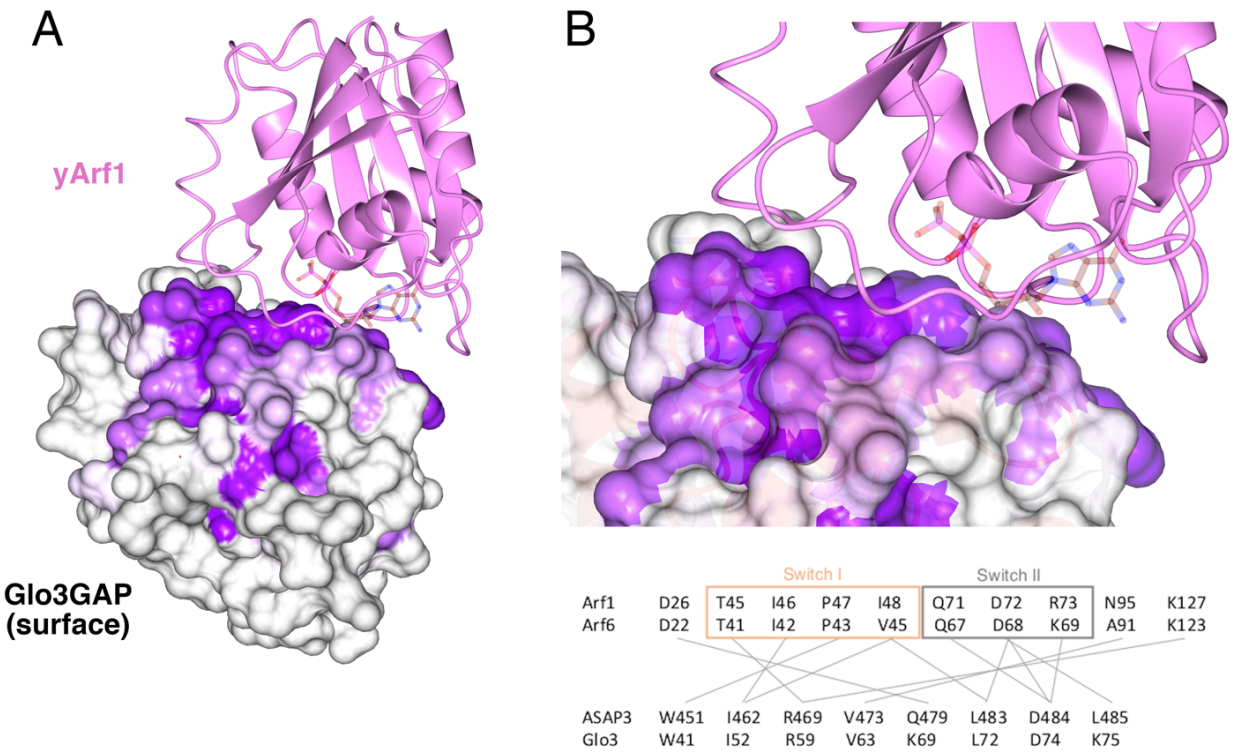

Figure 3-6. Model for yeast Glo3 GAP binding to Arf1. (A) Model of Glo3 GAP/yeast Arf1 generated using ASAP3/Arf6 crystal structure as a model (PDB: 3LVQ; Figure 3-8). Yeast Arf1 (yArf1) is shown as pink ribbons and Glo3 GAP domain is shown as a surface colored by conservation. The predicted Arf1 binding interface (dark purple) is highly conserved in the Glo3 GAP domain, which supports a model resembling the ASAP3/Arf6 interaction. The nucleotide from 3LVQ is shown as transparent cylinders to denote its binding site. (B) Upper panel: Close-up view of Glo3 GAP/yArf1 model interface; the nucleotide from 3LVQ is shown as transparent cylinders to delineate the binding site. Lower panel: Residues in the proposed interaction interface are conserved, including key Arf switch I and II residues and the arginine finger in both GAP domains (Glo3 Arg59/ASAP3 Arg469). Grey lines represent proposed molecular interactions between Arf switch I/switch II residues and their counterparts on each GAP domain.

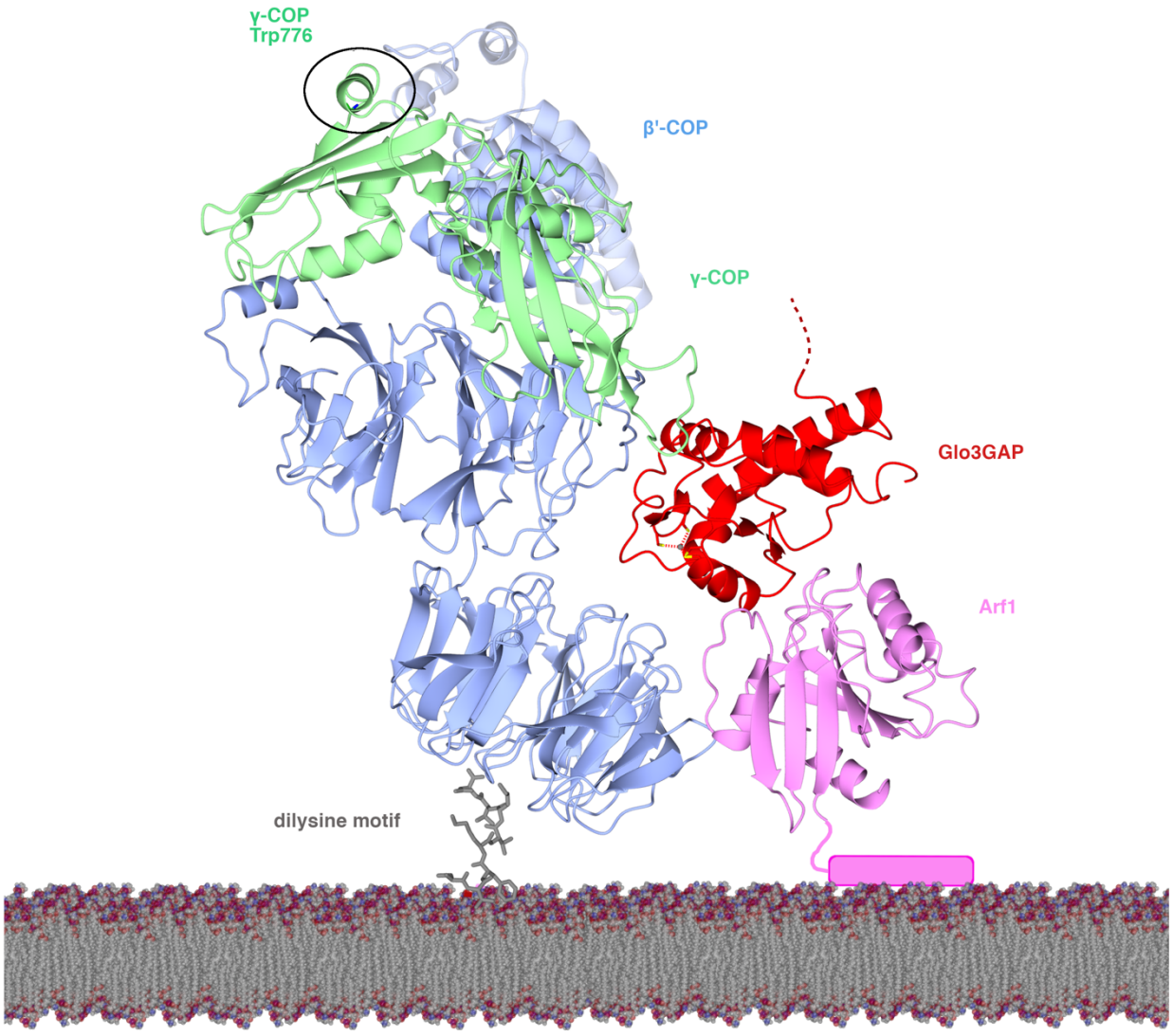

Figure 3-7. Model for Glo3 GAP domain within membrane-assembled COPI coats. Model for the interaction of Glo3 GAP (red ribbons) with -Arf1 (pink ribbons with N-terminal amphipathic helix shown as cylinder). Two different Arf1 positions are proposed in COPI coats; this view represents one copy of γ-Arf1 within a triad (see text for details). This model shows Glo3 GAP acting on γ-Arf1, which is located in Arf1 triads found adjacent to β'-COP subunits (blue ribbons; WD-repeat domains and solenoid). The γ-COP appendage domain (green ribbons) is also shown. This model was generated by combining the Glo3 GAP/γArf1 model presented in Figure 3-6 with cryo-ET reconstructions (PDB ID: 5NZS) of reconstituted COPI coats. The Glo3 BoCCS region begins at the red dashed/dotted line. The precise molecular position of the Glo3 BoCCS and GRM regions are unknown, but the known Glo3 binding site on γ-COP appendage domain is marked as a black circle. (Figure 3-9 and Figure 3-10 show models for Glo3 GAP interacting with β-Arf1 positions at different linkages within the COPI coat.)

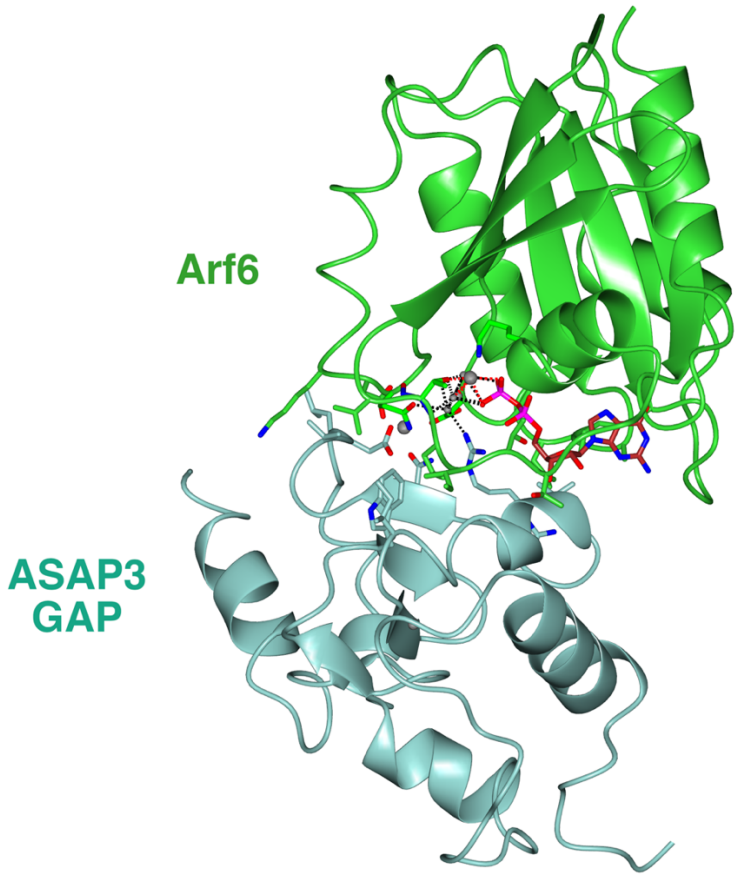

Figure 3-8. Generation of yeast Glo3 GAP/Arf1 model. Experimentally determined ASAP3/Arf6 X-ray crystal structure (PDB ID: 3LVQ) used to generate the yeast Glo3GAP/ Arf1 model in Figure 6. The ASAP3 GAP domain is shown in sea green ribbons with Arf6 in green ribbons. Key side chains in both ASAP3 and Arf6 that mediate the interaction are highlighted as cylinders, and the nucleotide is shown as red cylinders.

Discussion

Differences among ArfGAP proteins

ArfGAP domains contain a C_4-type zinc finger motif and conserved arginine residue that may act as an "arginine finger" during catalysis. Based on structures for GAP domains that act on Ras and Rab GTPases (Vetter and Wittinghofer, 2001), these structural features have been proposed to explain catalysis on Arf1. However, an X-ray structure of mammalian ArfGAP1 with Arf1 (Goldberg, 1999) suggested the zinc finger played a structural rather than catalytic role. There are currently no structural

data for yeast Gcs1, but there are multiple structures for the GAP domain in human ArfGAP1, which is thought to be functionally equivalent (Kahn et al., 2008) to yeast Gcs1.

The Glo3 GAP structure presented here adds the first GAP structure for yeast ArfGAP domains and allows comparison among eukaryotic ArfGAP1 and ArfGAP2/3 family members. The conserved invariant arginine has now been visualized in multiple structures and appears to occupy the same position in GAP domains found in a variety of ArfGAPs (Figure 3-5A); data from yeast further suggest this is a catalytic arginine in Glo3 (Arakel et al., 2019a). Together, the Glo3 GAP domain structure and Arf1 modeling in this work further support a canonical role for this residue as the "arginine finger" required for catalysis. In contrast, data from yeast suggest Gcs1 GAP activity is non-essential (Arakel et al., 2019a), and alignments reveal ArfGAP1 and ArfGAP2/3 family members have diverged in sequence immediately following the invariant arginine. Together, these data may further support the proposed structural role for this residue in the published mammalian ArfGAP1/Arf1 structure (Goldberg, 1999). However, it should be noted the ArfGAP1/Arf1 structure was determined in the presence of GDP rather than GTP, and therefore depicts product rather than a transition state. Finally, there are conflicting data regarding whether or not COPI is required to promote catalysis by either ArfGAP1 or ArfGAP3 *in vitro* (Goldberg, 1999; Ismail et al., 2010; Kliouchnikov et al., 2009). It will be important to follow up with structural and biophysical studies in yeast.

Structural comparisons suggest there may be one difference in GAP domains from different families: ArfGAP1 family members appear to have a shorter helix α6 than do ArfGAP2/3 members (Figure 3-5B). The presence of this extended helix in Glo3 has important implications for where it can be accommodated in the membrane-assembled COPI coat.

Model for Arf1 binding

The zinc finger catalytic core and potential Arf1 binding residues are highly conserved in Glo3 GAP domain at both the sequence (Figure 3-5) and structural (Figure 3-4) levels, which supports the model for

Arf1 binding proposed in Figure 3-6. However, there are caveats to this proposed model. First, the model was generated using human ASAP3 GAP, which exhibits some structural differences from Glo3 GAP. The Arf6 binding surface on ASAP3 (helix α2 and strand β5) is highly conserved with Glo3. The primary difference between the two domains is that ASAP3 GAP lacks helix α6. Second, the overall domain architecture for ASAP3 differs from Glo3. ASAP3 contains an ankyrin repeat domain following its GAP domain, and some residues within the ankyrin domain make minor interactions with Arf6. Glo3 does not contain an ankyrin domain, so there are no equivalent residues. Finally, ASAP3 contains a calcium binding site; the GAP domain uses two residues (Gln479/Leu485) to coordinate a calcium ion. These residues are not conserved in Glo3 or other ArfGAP2/3 family members. Overall, despite these differences, the key residues and surface required for Arf binding are highly conserved between these two GAP proteins. Two additional pieces of data further support the model: ASAP3 was reported to promote catalysis on Arf1 (Ismail et al., 2010), and cryo-ET reconstructions (Dodonova et al., 2017) from reconstituted mammalian COPI show a similar binding mode.

Placement of Glo3 within membrane-assembled COPI coat

The Glo3 GAP/Arf1 structural model presented in Figure 3 provides evidence for placement of Glo3 GAP within the COPI coat (Figure 3-6). Based on cryo-electron tomographic reconstructions from reconstituted coats, there are two proposed "types" of Arf1. The first (called γ-Arf1 (Arakel et al., 2019a)) forms a triad with roughly three-fold symmetry (Dodonova et al., 2015, 2017) and is located adjacent to β'-COP and γ-COP subunits. The second (called β-Arf1) is located next to β-COP subunits; this interaction has been visualized using both X-ray crystallography (Yu et al., 2012) and cryo-electron tomography (cryo-ET) (Dodonova et al., 2015). The presence of these two Arf1s is the basis for the "molecular niche" model, which proposes that Gcs1 binds β-Arf1 and Glo3 binds γ-Arf1 (Arakel et al., 2019a). This model places Gcs1 near δ-COP subunits, which is consistent with independent X-ray crystal data.(Suckling et al., 2015)

The model presented here (Figure 3-7) supports cryo-ET reconstructions at low resolution placing human ArfGAP2 adjacent to γ-Arf1 (Dodonova et al., 2017), since Glo3 is the yeast equivalent of mammalian ArfGAP2. Superposing the yeast Glo3 GAP/Arf1 model presented in Figure 3-6 onto γ-Arf1 located in triads reveals the Glo3 GAP domain could be accommodated at this position (one copy within the triad is shown in (Figure 3-7). In contrast, modeling suggests the Glo3 GAP domain would experience clashes with the β-COP subunit while binding the β-Arf1 in multiple linkages (Figure 3-9); the GAP could only be accommodated at one observed linkage (linkage IV; Figure 3-10). In particular, the extended helix α6 in Glo3 appears to clash with β-COP (Figure 3-9). Dodonova and colleagues reported the ArfGAP1/Arf1 interaction (Goldberg, 1999) could not be accommodated at the γ-Arf1 site in reconstituted COPI coats (Dodonova et al., 2017). Together, current structural data from multiple groups support the molecular niche model, in which Glo3 (ArfGAP2/3 in humans) binds γ-Arf1. It remains to be confirmed structurally whether Gcs1 or ArfGAP1 specifically binds β-Arf1, and it will be important to test these structural hypotheses in vitro and in vivo.

Overall, in yeast, Glo3 appears to be the ArfGAP required for cell viability and function: GAP-dead Glo3 (R59K) cells cannot survive (Arakel et al., 2019a), while GAP-dead Gcs1 (R54K) cells are viable. The structural data presented here further support this invariant residue acting as the arginine finger required for catalysis. Data increasingly suggest Glo3 plays the more vital role in COPI coat function. One interpretation is that Glo3 is required to hydrolyze Arf1(GTP) to promote coat recycling, although Glo3 certainly has additional important functions (Schindler et al., 2009). The Glo3 GAP-dead mutant may “lock” assembled COPI coats onto membranes since Glo3 is known to stably associate with COPI (Arakel et al., 2019a), thereby preventing recycling of a coat that is essential for cellular function. Further structural studies on complexes will be required to understand molecular details of how Glo3 regulates coat assembly and function.

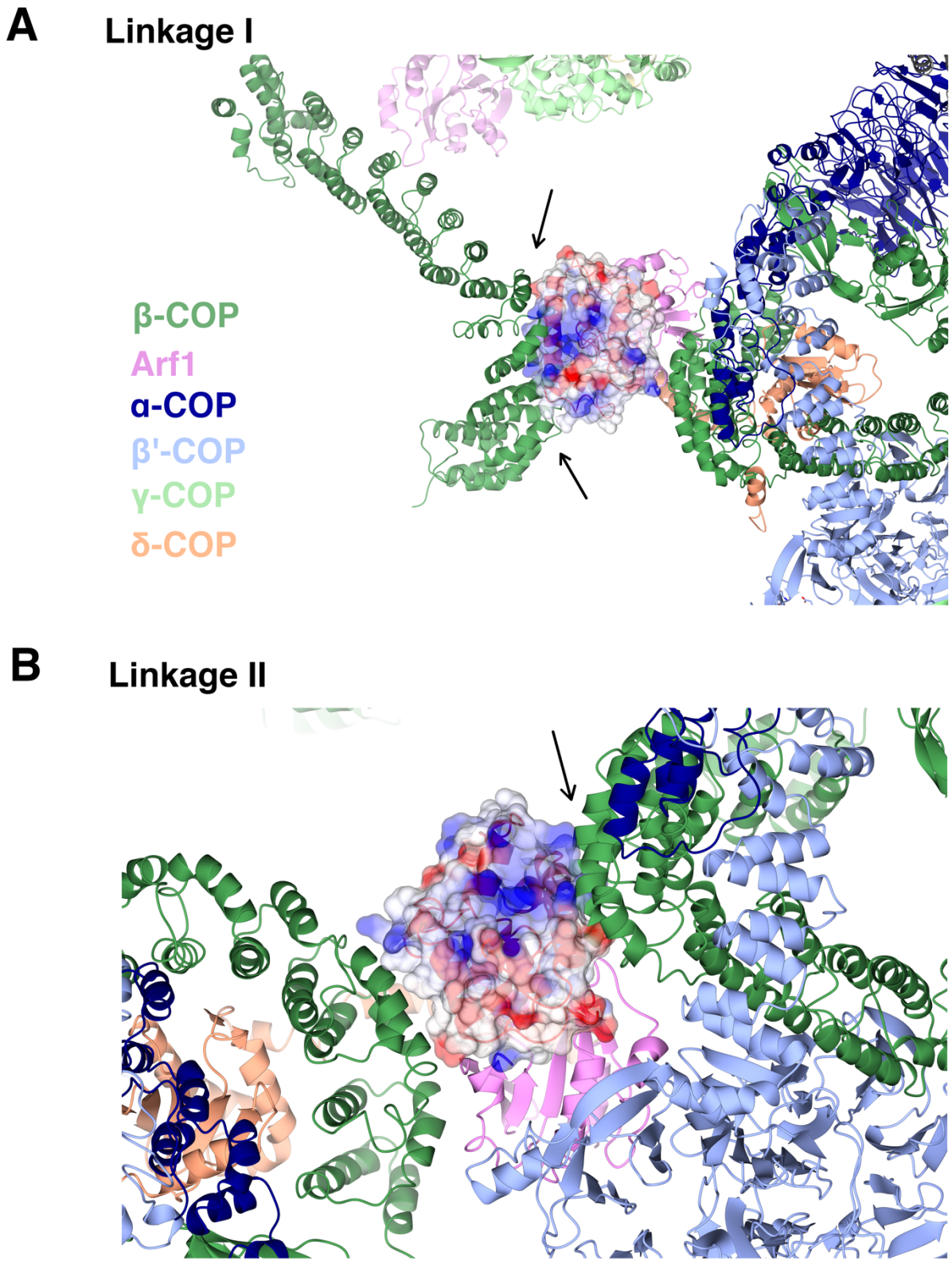

Figure 3-9. Glo3 GAP domain modeled at linkages I and II in assembled COPI coats. (A) View of Glo3 GAP domain (shown as surface) modeled at β-Arf1 site in linkage I (PDB: 5NZT). The GAP domain would clash with the β-COP subunit (green ribbons);

specific clashes are marked by black arrows. (B) View of Glo3 GAP domain modeled at β-Arf1 in linkage II (PDB: 5NZU). The GAP domain would clash with the β-COP subunit (green ribbons); specific clashes are marked by black arrows.

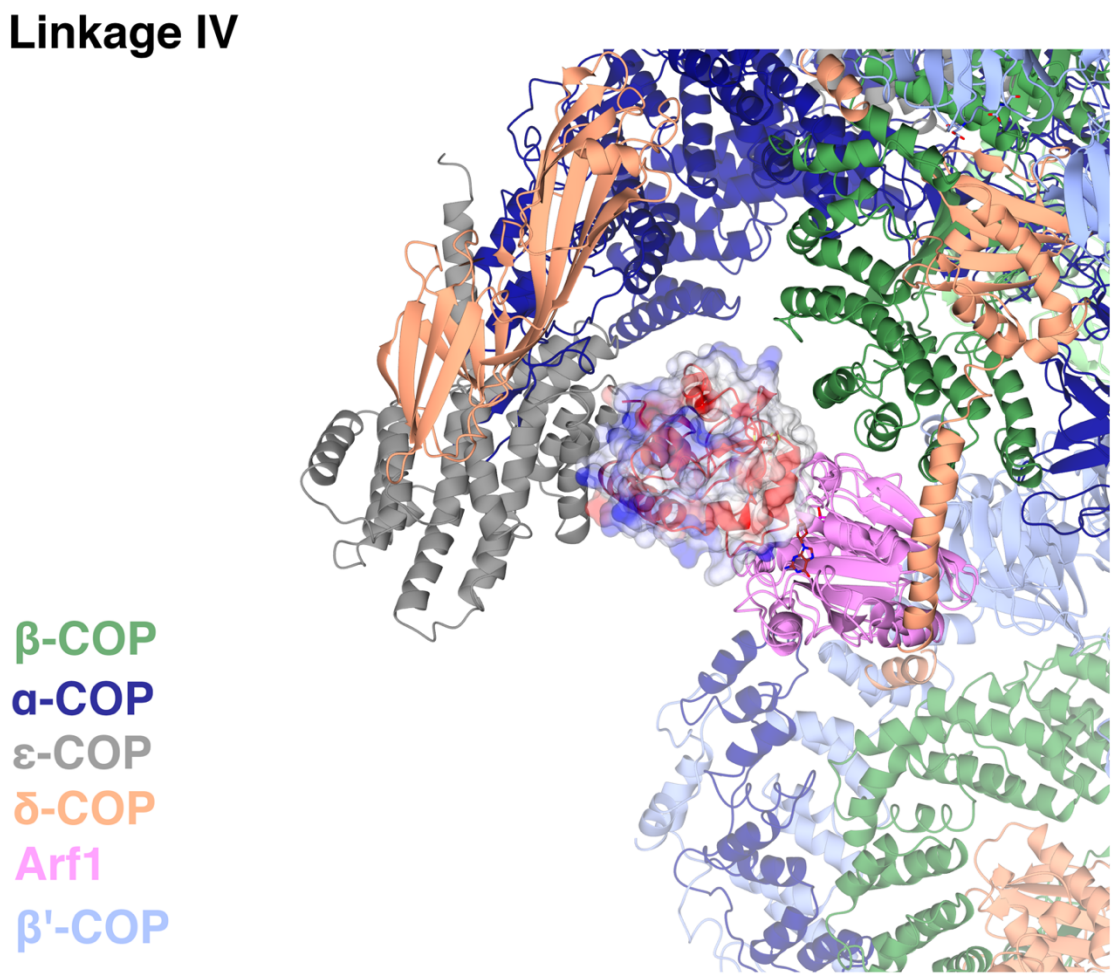

Figure 3-10. Glo3 GAP domain modeled at linkage IV in assembled COPI coats. Modeling suggests the Glo3 GAP domain (shown as surface) could be accommodated near β-Arf1 sites in linkage IV. At this position, it is unclear whether helix α6 in the GAP domain would clash with either the ε-COP (grey ribbons) or β-COP (green ribbons) subunits located nearby.

Acknowledgements

BX, CJ, and AK performed protein expression and protein purification experiments. BX, AE, MC, and LPJ collected X-ray data and undertook structure determination and refinement. AE generated sequence alignments. BX and LPJ wrote the paper with input from all authors. LPJ conceived the project. BX, CJ, MC,

AK, and LPJ are supported by NIH R35GM119525. LPJ is a Pew Scholar in the Biomedical Sciences, supported by the Pew Charitable Trusts. The authors declare no competing conflicts of interest.

Materials and methods

Reagents.

Unless noted otherwise, all chemicals were purchased from Sigma (St. Louis, MO).

Cloning and plasmids.

An C-terminal GST-tagged fusion protein of Glo3 GAP domain (residues 1-150) was sub-cloned from full-length Glo3 into NdeI/BamHI sites of in-house vector pMWGST under control of a T7 promoter; this vector is a modified form of pMW172 (Owen and Evans, 1998) Full-length *S. cerevisiae* Glo3 was amplified by PCR from cDNA generated from the yeast genome kindly provided by the Graham lab (Vanderbilt University).

Protein expression and purification.

S. cerevisiae Glo3 GAP domain (residues 1-150) was expressed in and purified from *E. coli* BL21(DE3)pLysS cells (Invitrogen) for 16 to 20 hours at 22°C following induction with 0.4 mM Isopropyl β-D-1-thiogalactopyronoside (IPTG) at OD_{600} = 1.0. The protein was purified in buffer containing 10 mM HEPES (pH 7.5), 200 mM NaCl, 1 mM DTT with AEBSF protease inhibitor (Calbiochem) used at all stages of purification. Cells were lysed by a disruptor (Constant System Limited), and proteins were affinity purified using glutathione sepharose (GE Healthcare) in the purification buffer. The GST-tagged protein was cleaved overnight at 4°C by thrombin protease (Recothrom, The Medicine Company) and batch eluted. Eluted protein was further purified by gel filtration on a Superdex S200 Increase 10/300 GL column (GE Healthcare).

Crystallization, data collection, and structure determination.

Purified yeast Glo3 GAP domain (residues 1-150) was concentrated to 5-10 mg/mL and crystallized in 2.0 M ammonium sulfate and 0.1 M sodium acetate pH 4.6 (Molecular Dimensions screen JCSG+ condition 35). Crystallization trays were set up using 400 nL drops on a Mosquito robot (LLP Lab Tech). Crystals were harvested directly from 96-well plates into 500 nL drops in reservoir buffer plus 25% glycerol for cryo-protection. Crystallographic datasets were collected at Argonne National Laboratory, sector LS-CAT, beamline 21-ID-D, from crystals flash frozen by plunging into liquid nitrogen. Data were collected at a wavelength of λ=1.77 Å. Detailed data collection settings are shown in Table A3-3. Two datasets were collected on the same needle shaped crystal, then trimmed and merged to become one complete dataset.

Crystals diffracted to 2.07 Å resolution and were of monoclinic space group $P2_1$ with unit cell dimensions a = 54.4 Å, b = 74.0 Å, c = 77.9 Å, α = 90.00°, β = 105.34°, γ = 90.00°. The data were integrated and merged in HKL2000 (Otwinowski and Minor, 1997) and further processed using the CCP4 (Winn et al., 2011) and PHENIX (Liebschner et al., 2019) suites. The structure was phased using molecular replacement methods in Phaser (McCoy et al., 2007) with the GAP domain from human ArfGAP2 as an initial model (PDB ID: 2P57). The Glo3 GAP model was first built using PHENIX AutoBuild (Terwilliger et al., 2008), and the built model was then used as a new molecular replacement model in Phaser. Additional rounds of manual model building were undertaken in Coot (Emsley et al., 2010) with iterative rounds of refinement using in PHENIX. Structure coordinates and maps have been deposited at the PDB (PDB ID: 7JTZ)

Sequence alignments.

In order to map conservation, GAP domain sequences from the ArfGAP1 and ArfGAP2/3 sub-families were aligned using Praline (Simossis and Heringa, 2005b). The following species were used in alignments: *S. cerevisiae, S. pombe, C. thermophilum, D. discoideum, C. elegans, A. thaliana, D. melanogaster, D. rerio, X. laevis, M. musculus,* and *H. sapiens.* A spreadsheet containing accession numbers for all genes used in the alignments is provided as Table A3-4.

Structural comparisons and visualization.

Superpose (Krissinel and Henrick, 2004) in the CCP4 suite was used to compare structures of Glo3 GAP domain with other ArfGAP domains deposited in the PDB. The SSM algorithm was used to align the structures, and to determine RMSD and number of residues aligned between structures. The structure comparison was carried out on the complete GAP domain based on the overall secondary structure, as well as on the catalytic core (defined as Glo3 residues 27 – 65), which includes the zinc finger and arginine finger. All structural images or electron density maps presented in figures were generated using either the CCP4 Molecular Graphics (CCP4MG) program (McNicholas et al., 2011) or Coot (Emsley et al., 2010).

CHAPTER IV

DISCUSSION AND FUTURE DIRECTIONS

The molecular niche model of ArfGAPs in the COPI coat

Both previous studies and our studies have demonstrated that Arf1, COPI coatomer, and ArfGAPs co-exist in one complex (Szafer et al., 2000; Weimer et al., 2008) (Chapter II), and previous reconstitution assays demonstrated both Gcs1 and Glo3 can initiate COPI vesicle uncoating (Weimer et al., 2008). Multiples studies have shown Glo3 stably associates with COPI; while there's controversy whether Gcs1 really interacts with the COPI subunit of δ-COP, it is certain Gcs1 exist in the vesicle coat, perhaps mainly through Arf1 and the membrane. Why COPI utilizes more than one ArfGAP is a mystery, but there's substantial evidence suggesting Glo3 and Gcs1 fulfill different functions in the COPI vesicle cycle, and correspondingly, occupy different niches in the COPI coat. Our data described in Chapter II and Chapter III support this hypothesis from different angles.

The molecular niches of ArfGAPs are fundamentally implicated by the two different niches of Arf1 molecules in the COPI coat. Recent cryo-ET reconstructions have shed some light on the organizations of the complicated COPI coat (Bykov et al., 2017; Dodonova et al., 2015, 2017). In the reconstructions, an adaptor-like F-subcomplex and an outer-coat-like B-subcomplex form a highly intertwined COPI heptameric coatomer, and three heptameric coatomers form a symmetric triad, which is the basic unit of the COPI coat. Triads are connected by flexible domains from different coatomer subunits, forming different dimeric or homotrimeric linkage patterns in the coat (Figure 1-10). In each heptameric coatomer, two molecules of Arf1 are located on the opposite sides of the heptameric coatomer, in the vicinity of β-COP and γ-COP, respectively, with almost equivalent surfaces (Figure 1-9; Figure 1-10) (Dodonova et al.,

2015, 2017; Yu et al., 2012). Therefore, the two molecules of Arf1 in each coatomer are named β-Arf1 and γ-Arf1 in reference to their distinct locations, or niches, in the coat.

The GAP domains

When forming a triad, three molecules of γ-Arf1 are in proximity at the center of the triad, and the GAP domain of ArfGAP2 (or Glo3) preferentially binds γ-Arf1 and occupies the niche near the tri-Arf1 triad center (Dodonova et al., 2017). In contrast, the peripheral β-Arf1 does not recruit the ArfGAP2 GAP domain. It seems surprising such preference even exists without the presence of C-terminal non-GAP domains of the ArfGAPs, considering the GAP domains of ArfGAPS are highly conserved and similar. However, our data described in Chapter III, together with previous studies, support the possibility that this preference results from the interplay of different geometric environments of different Arf1 niches and the subtle but important variations in the GAP domains. According to the cryo-ET reconstruction (Dodonova et al., 2017), β- and γ-Arf1 molecules interact with different coatomer subunits and therefore in geometry have different space available for GAP binding in the triads as well as different linkages. This geometric requirement seems to be accommodated by the GAP domains of ArfGAP1/Gcs1 or ArfGAP2/3/Glo3 types: the variations in Arf1-binding residues and helix 6 enable two types of GAP domains to interact with Arf1 molecules on different surfaces, therefore the γ-Arf1 niche accommodates ArfGAP2/3/Glo3 type GAP domain well but placing this type of GAP domain near the β-Arf1 niche will cause clashes in multiple linkages (Dodonova et al., 2017; Goldberg, 1998) (Chapter III). This geometric difference between two types of GAP domains also explains previous findings where mutating the supposed arginine finger of Glo3 GAP (R59) causes more severe phenotype than that of Gcs1 GAP (R54): Gcs1 GAP likely utilizes the arginine finger provided by coatomers while the Glo3 GAP likely utilizes its own intrinsic arginine finger (Arakel et al., 2019b; Goldberg, 1998) (Chapter III).

The non-GAP regions in ArfGAPs

The different niches of two types of ArfGAPs may also result from the different properties of their C-terminal non-GAP regions. In contrast to γ-Arf1 and ArfGAP2/3/Glo3, Gcs1 has been proposed to occupy the niche near β-Arf1, taking into the consideration the interaction between Gcs1 and δ-COP and the positional restrictions imposed by the flexible, interacting domains of γ-COP and δ-COP (Cosson et al., 1998; Rawet et al., 2010; Suckling et al., 2015). The interaction between δ-COP appendage domain and Gcs1 at the membrane may help orient Gcs1 within the assembled coat and stabilize Gcs1 in the vicinity of β-Arf1. The fact that three β-Arf1 molecules are separately located in periphery of the triads where the membrane is more exposed may also add to the probability of Gcs1 being located near β-Arf1 since Gcs1 has two ALPS motifs that are membrane associated.

Similarly, interactions with the COPI coatomer subunits through the BoCCS region of Glo3 could also help bring Glo3 GAP domain closer to γ-Arf1. It was previously reported that purified ArfGAP2 has little activity compared to purified ArfGAP1 (Luo et al., 2009a). We also consistently found in pulldowns, ITC experiments, and crystallography trials that neither Glo3 nor its GAP domain have very high affinity with Arf1 (Chapter II and Chapter III). Multiple lines of studies have suggested the presence of coatomer stimulates the GAP-activated GTP hydrolysis on Arf1 and this stimulation is especially enhanced for ArfGAP2 (Kliouchnikov et al., 2009; Luo et al., 2009a; Weimer et al., 2008; Yu et al., 2012). Since β'-COP interacts with both Glo3 and Arf1 at the same time as shown in Chapter II, it is possible that this stimulation effect partially comes from coatomer/Glo3 interactions bringing the Arf1 and Glo3 and other effector coatomer subunits closer together.

Functional implications and future directions

Apart from geometric aspects, there are also functional implications of the molecular niche model. Based on the pulldown results in Chapter II (Figure 2-3) and the model created in Chapter III (Figure 3-7; Figure 4-1), β'-COP alone seems to have no preference for either GTP-or GDP-bound Arf1 and it locates on the back side of the nucleotide/GAP binding sites of Arf1. This is different from the result of a previous

study where crosslinked β'-COP/Arf1 has strong signal in the presence of GTPγS (Sun et al., 2007). But this study was conducted using the whole coatomer and such preference to GTP may indirectly come from the F-subcomplex subunits (Yu et al., 2012). Despite that β'-COP locates on the back side of the nucleotide/GAP binding sites of Arf1, losing a functional BoCCS region or GRM region could rescue the cells harboring a dead Glo3 GAP domain (Arakel et al., 2019b). These data indicate the propeller domains of β'-COP may have effects on the GAP activity and GTP hydrolysis at some point in the COPI cycle, but it probably happens indirectly through binding the BoCCS region and then was communicated by the GRM region. This is different from the F-subcomplex subunits, which have direct effects on the GAP activity and GTP hydrolysis (Ma and Goldberg, 2013) as well as the Gcs1 GAP domain, which is able to be directly stimulated by coatomer (Goldberg, 1998, 1999).

To better refine the model shown in (Figure 4-1), it would be helpful to understand where the rest of the Glo3 sequence lies within the COPI coat, since the GAP domain makes up only a small portion of the full Glo3 sequence. In addition to the Glo3 residues 230-290 that we have revealed to engage with the β'-COP propeller domains (Chapter II), it has also been demonstrated that Glo3 binds a hydrophobic residue on the γ-COP appendage domain (Watson et al., 2004), though it is unclear what residues in Glo3 interact with γ-COP appendage domain. It's worth investigating the γ-COP/Glo3 interaction in the future, since γ-COP is known to recognize cargoes with aromatic motifs, as well as binding and regulating the γ-Arf1 (Bermak et al., 2002; Gommel et al., 2001; Yu et al., 2012), therefore it is possible that cargo binding is communicated to GAP-stimulated GTP hydrolysis through γ-COP interaction with Glo3.

It was also previously reported that Glo3 BoCCS region binds cargoes and SNARE proteins, though the data were always acquired by pulling the complex from the cell and not by using purified proteins (Schindler et al., 2009), therefore it is not clear whether the interactions are direct or though interactions with other coatomer components. We speculate cargo proteins and SNAREs likely interact with Glo3 indirectly through its engagement with β'-COP, because Glo3 association is lost when the Glo3/β'-COP

interaction is disrupted (Chapter II). However, to better understand whether and how Glo3 regulates the COPI through multiple types of coat components, it would still be interesting to investigate whether Glo3 interacts directly with these proteins, such as Sec22, using purified recombinant proteins.

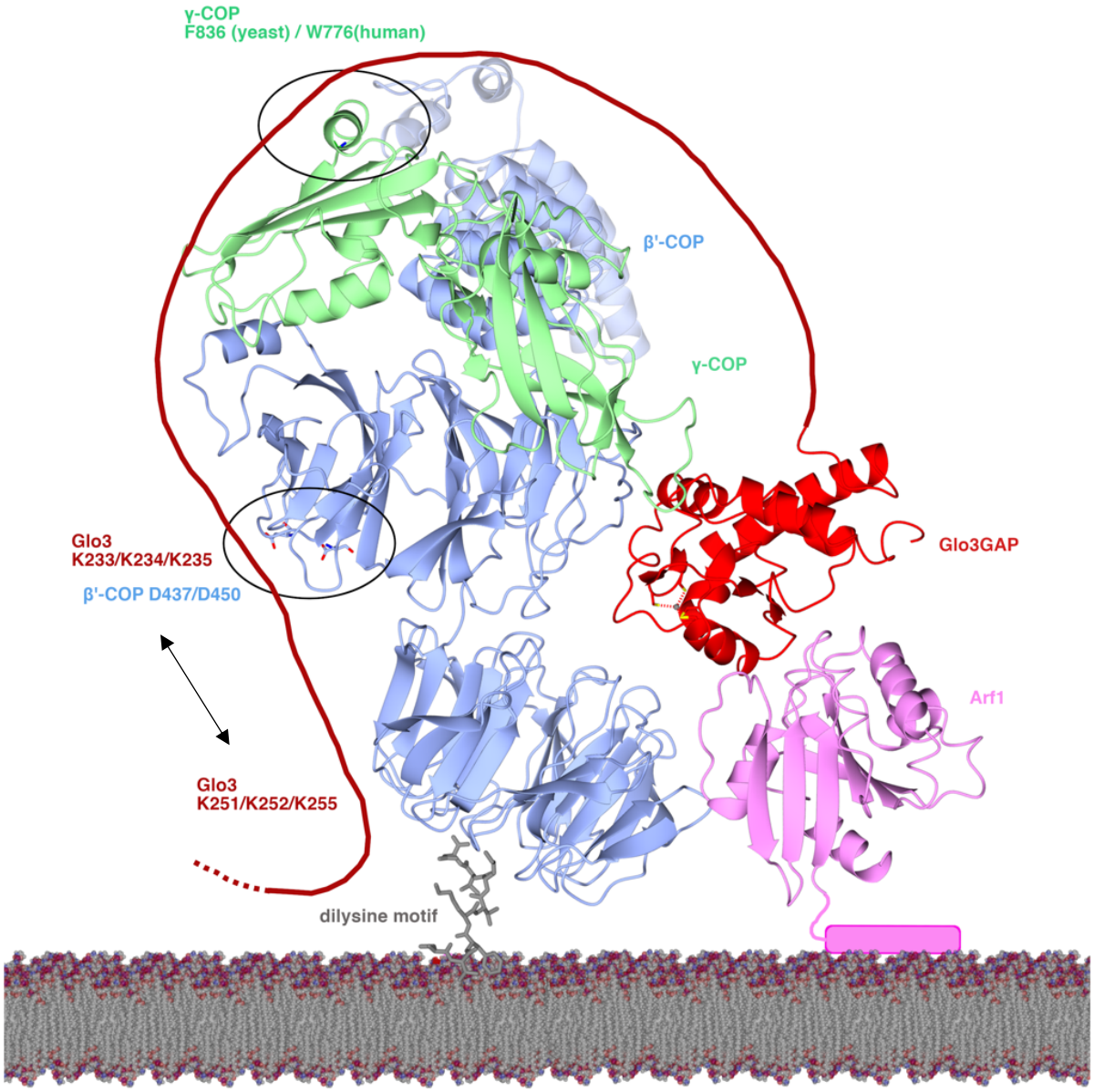

Figure 4-12. Model for the interaction between β'-COP (blue ribbons; WD-repeat domains and solenoid shown); Arf1 (pink ribbons with N-terminal amphipathic helix shown as cylinder); γ-COP appendage (green ribbons); and Glo3 (GAP domain as red ribbons and BoCCS region as red line). The dashed line marks the start of Glo3 GRM region; its position and orientation remain unknown, but it is predicted to have a C-terminal amphipathic helix. The dilysine motif in transmembrane cargoes is shown as grey cylinders. The position of γ-COP was generated based on cryo-ET reconstructions of COPI (PDB: 5NZS). Our data suggest the first Glo3 lysine cluster (K233/K234/K235) may interact with the D437/D450 patch on the C-terminal β'-COP propeller, and the second cluster (K251/K252/K255) may interact with the N-terminal β'-COP propeller. γ-COP appendage also binds Glo3; γ-COP F836 is implicated in binding, but the Glo3 residues remain unknown. Depending on the results of our structural

approaches, which lysine patches of Glo3 (K233/K234/K235 or K251/K252/K255) bind which propeller domains of β'-COP may have implications in whether Glo3 binds γ-COP downstream or upstream of its β'-COP binding sites.

The roles of ArfGAPs in COPI

It has long been established that the cycle of GTP binding and hydrolysis by Arf1 is essential in the coat association and dissociation from the membranes. The life of a COPI-coated vesicle begins with the recruitment of cytoplasmic COPI coatomer to the site of emergence by a small GTPase, Arf1, though other members of Arf-family GTPase, such as Arf2, have also been indicated in COPI trafficking (Popoff et al., 2011). Arf1 functions as a "glue" that holds the protein coat on to the membrane (Reviewed in Bonifacino and Glick, 2004; Nie and Randazzo, 2006). COPI coat proteins and GTP-bound Arf1 alone can drive the formation of vesicles *in vitro* (Bremser et al., 1999; Spang et al., 1998). Though the importance of ArfGAPs have long been well accepted, studying the detailed functions and their mechanisms has been a long arduous journey.

In the classic model, nucleotide exchange from GDP to GTP on Arf1 causes coat association with the membrane and activated GTP hydrolysis on Arf1 is a terminator of Arf1 signaling that triggers coat dissociation, and it must be delayed until the COPI coat is fully assembled (Reinhard et al., 2003). The presence of GAP protein is essential for this process, since Arf1 lacks detectable intrinsic GTPase activity; ArfGAP1, the mammalian homologue of yeast Gcs1, is the first GAP identified to carry out this function. This model was formed based on previous studies using non-hydrolysable GTP, GTPγS, or GTP-locked Arf1 with a Q71L mutation (Donaldson et al., 1990; Serafini et al., 1991; Tanigawa et al., 1993; Teal et al., 1994), where COPI-coated vesicles were trapped when GTP hydrolysis was disabled. However, further investigations on the GTP hydrolysis in COPI revealed a regulatory role for ArfGAP during the cargo sorting process. Multiple studies have found using GTPγS or GTP-locked Arf1 causes less cargo to be packaged into the COPI vesicles (Lanoix et al., 2001a; Nickel et al., 1998; Pepperkok et al., 2000), suggesting the GTP hydrolysis function of Arf1 either facilitates the coat-cargo interaction, or serves as a check point to ensure

enough cargo is packed into the vesicles before release. Lee and colleagues also found ArfGAP1 displays a GAP-dependent function of increasing the affinity of coatomer for cargo proteins (Lee et al., 2005). In addition, previous genetic studies found overexpressing Glo3 or Gcs1 suppressed a loss-of-function allele of Arf1, suggesting ArfGAPs also function as downstream effectors of Arf1 (Zhang et al., 2003, 1998). Because otherwise the negative regulatory GAP function of ArfGAPs would have no effect or exacerbating effect on Arf1 insufficiency.

Together, the fact that ArfGAPs are involved in both cargo sorting and coat dissociation processes in a temporally regulated manner suggest ArfGAPs possess important regulatory roles in COPI-coated vesicle trafficking from vesicle formation to coat removal. And based on past findings, two possible models for controlling the appropriate timing of GTP hydrolysis on Arf1 by GAP can be proposed.

ArfGAP regulations by membrane curvature

In one model, the GAP activity is controlled by membrane curvature sensing by Gcs1 or ArfGAP1. Gcs1 contains two ALPS motifs that form amphipathic helix with exposed to lipid bilayer in membrane when curvature is driven by coatomer polymerization (Bigay et al., 2003, 2005; Mesmin et al., 2007; Drin et al., 2005; Yang et al., 2005). However, this curvature sensing model is not well reproduced and it cannot be applied to understanding the mechanism of Glo3 or ArfGAP2/3 in COPI, since they do not possess ALPS motifs (Luo and Randazzo, 2008). Another shortcoming of this model is that it does not have any implications in how ArfGAP regulates the cargo sorting process of COPI and therefore cannot explain why GTP hydrolysis deficiency would cause COPI vesicles to contain less cargo.

ArfGAP regulations by COPI coatomer, cargo, and SNAREs

In the other model, COPI coatomer promotes GAP activity and cargo proteins inhibit GAP activity (Goldberg, 2000a; Lee et al., 2005; Weiss and Nilsson, 2003; Yang et al., 2002). Though one study by Szafer and colleagues believed the proximity between Arf1 and ArfGAP1 may be sufficient for stimulation of GTP hydrolysis (Szafer et al., 2000).

Both Glo3 and Gcs1 have been proposed to be stimulated by the COPI coatomer (Frigerio et al., 2007; Kliouchnikov et al., 2009; Luo and Randazzo, 2008; Weimer et al., 2008). This could happen through direct modulation of the GAP activity, since the COPI coatomer was proposed to provide the essential Arginine required for GAP activity in a previous study revealing the structure of the GAP domain of an ArfGAP1 in complex with Arf1 (Goldberg, 1998). In this model, the ArfGAP1 GAP domain binds Arf1 on a surface located away from the arginine finger and COPI coatomer promotes the GAP activity by providing the arginine finger. However, this mechanism may not be applied to the Glo3 type of ArfGAP based on the structural analysis work described in Chapter III: the GAP domain of Glo3 lacks the important residues that mediate the interaction between ArfGAP1 GAP domain and Arf1 in the same manner as proposed (Goldberg, 1998). Instead, the Glo3 GAP domain likely possesses the ability to bind Arf1 in a different mechanism proposed by Ismail and colleagues, where the zinc finger binds the switch I/II region of Arf1 and the arginine finger on the GAP domain promotes GTP hydrolysis on Arf1 (Ismail et al., 2010). This mechanism variation present in the GAP domains suggests Gcs1 and Glo3 types of ArfGAP adopt different behaviors in COPI and their non-GAP region are different in both sequence and function to coordinate with their GAP domains.

The ArfGAP regulation by COPI coatomer can also happen through the non-GAP region of the ArfGAPs, especially for Glo3 (or ArfGAP2/3), which has lower intrinsic GAP activity and greater affinity for COPI coatomer than Gcs1 (or ArfGAP1) (Kliouchnikov et al., 2009; Luo et al., 2009a; Weimer et al., 2008). It was proposed that ArfGAP1/Gcs1 is recruited to the membrane without the coatomer whereas the membrane recruitment of ArfGAP2/3/Glo3 is coatomer-dependent (Frigerio et al., 2007; Kliouchnikov et al., 2009; Lee et al., 2005; Schindler et al., 2009; Weimer et al., 2008). Both Glo3 and Gcs1 types of ArfGAPs have been proposed to bind COPI coat proteins. A tryptophan-based δL-motif in ArfGAP1/Gcs1 was previously proposed to interact with the COPI δ-COP subunit with low affinity (Cosson et al., 1998; Rawet et al., 2010; Suckling et al., 2015), though not reproduced in a later study (Arakel et al., 2019b).

ArfGAP2/3/Glo3, instead, stably associates with COPI coatomer and interacts with γ-COP appendage domain and β'-COP propeller domains through the internal BoCCS region (Arakel et al., 2019b; Eugster et al., 2000; Lewis et al., 2004; Schindler et al., 2009; Watson et al., 2004) (Chapter II). It was also proposed to interact with β-COP (Arakel et al., 2019b). As described in Chapter II, we showed biochemical evidence that Glo3 interacts directly with β'-COP through key lysine residues and this interaction is essential for Glo3 to associate with the rest of the COPI coat, therefore the interactions between Glo3 and other COPI coatomer components must be weaker. It has been previously shown that Glo3 needs both a functional GAP domain as well as a functional BoCCS region and the C-terminal GRM region was proposed to communicate between the GAP and BoCCS region (Arakel et al., 2019b; Schindler et al., 2009). It is possible that Glo3 performs its regulatory functions mainly through sensing the changes from β'-COP by recognizing an occupied BoCCS region. Since β'-COP is known to be important in cargo recognition, especially dilysine cargoes and ubiquitinated SNARE cargoes (Cosson and Letourneur, 1994; Gaynor et al., 1994; Jackson et al., 2012, 1990a; Ma and Goldberg, 2013; Xu et al., 2017), we may speculate that Glo3 couples cargo recognition with GTP hydrolysis or COPI formation through coordination with β'-COP. And all together, these data may suggest Gcs1 regulates more than COPI in the Golgi/EE and Glo3 is more COPI-specialized.

Apart from binding the COPI coatomer, it has been reported that ArfGAP activity can be regulated by cargoes and SNAREs. Though it is not completely clear how exactly cargo and SNAREs affect ArfGAPs and what the molecular mechanism might be. Some studies for the role of ArfGAP-dependent GTP hydrolysis in cargo sorting with appropriate timing were performed using the cytoplasmic tails of cargo proteins and ArfGAP1. In earlier reports, the GAP activity of the GAP domain from ArfGAP1 was inhibited by the presence of p24 cargo proteins, but remained unaffected by the dilysine cargo proteins, suggesting the activation of ArfGAP occurs after vesicle assembly and the delay in activation is achieved by appropriate cargo proteins regulating the GAP domain directly in a coatomer-independent manner

(Goldberg, 2000a; Luo and Randazzo, 2008). Another study, however, found peptides from p24 cargo proteins increased the activity of full-length ArfGAP2 (Luo et al., 2009a). This difference may be caused by the differences in the GAP domains or regulation by the BoCCS and GRM regions in ArfGAP2. In addition, both Glo3 and Gcs1 are able to interact with SNARE proteins and induce a conformational change that would allow the recruitment of Arf1 and COPI coatomer to SNAREs (Rein et al., 2002; Schindler and Spang, 2007; Schindler et al., 2009).

Models for ArfGAP functions in COPI and future directions

Altogether, these findings suggest the Gcs1 type of ArfGAP may control GTP hydrolysis with membrane curvature change and regulation from the cargo and coatomer on the GAP domain, while the Glo3 type of ArfGAP may be capable of performing a "switch" type of coordination or regulation that can couple GTP hydrolysis with different activities. One possibility is that Glo3 serves as a "checkpoint" to proofread the cargo sorting process: when the right amount and type of cargo proteins are picked up by the COPI coatomer, GAP activity and GTP hydrolysis is inhibited and vesicle formation continues; and when not enough cargo or the wrong type of cargo is detected, GAP activity and GTP hydrolysis is activated and coat dissembles before vesicle formation is complete. Another possibility is that when the right cargo type or concentration is reached, GTP hydrolysis happens on some molecules of Arf1 in COPI and serves as a signal to proceed with vesicle formation; therefore GTP-hydrolyzed Arf1(GDP) molecules remain in the coat since β'-COP and Glo3 continues to form a complex with Arf1(GDP) (Chapter II), and other molecules of Arf1(GTP) in the coat are responsible for later coat removal.

To better understand the functions and test the model, a GAP-mediated GTP hydrolysis assay combined with lipid pelleting assays or liposome assays could be conducted. By attaching the cargo peptides to Ni-NTA-DOGS through a His tag and attaching Arf1 through its myristoylated N-terminal helix, we can add different purified components of COPI, such as the coatomer subunits and SNAREs, to investigated under what conditions GAP activity will be triggered. To explore the regulation functions and

interplay of different parts of the ArfGAP2/3/Glo3 sequence, we could use constructs containing different regions of ArfGAP2/3/Glo3. For example, using GAP domain alone will give us information about the simple GAP activity; using GAP-BoCCS could show how coatomer, cargo, and SNARE bindings affect GAP activity; and adding GRM will help reveal how Glo3 translates differences in COPI status into different binding status in the BoCCS and communicate this signal with the GAP domain to execute.

Alternatively, Glo3 may play a structural role in COPI. It has been discussed in Chapter II that Glo3 interacts with both propeller domains of β'-COP, thus it is possible Glo3 coordinates the conformational change of COPI coatomer during recruitment and locks the COPI coatomers in the "hyper-open" conformation by interacting with β'-COP and other proteins. The BoCCS region of Glo3 may also confine the relative position of β'-COP, cargo, GAP domain, and SNAREs, and brings them in proximity for complex interactions and synergy. This could potentially be studied using cryo-electron tomography or *in situ* cryo-electron tomography.

However, we cannot clearly decide how exact the model should be, given the high complexity and redundancy of the COPI system. Further investigation will be needed to better understand ArfGAPs in COPI-mediated trafficking.

The functional and spatial separation of Glo3 and Gcs1 in COPI trafficking

The distinct niches of Glo3 and Gcs1 in the COPI coat and the variations in both the GAP domain and non-GAP regions indicate a functional and spatial separation of Glo3 and Gcs1 in COPI mediated trafficking. Multiple lines of evidence indicate Gcs1 could play a more general role in vesicle formation or other activities in the Golgi and the early endosomes, though not all Arf1-dependent vesicle budding events require Gcs1 function. In contrast, Glo3 might be more COPI specific. The first line of evidence comes from the genetic interactions so far tested, where deleting individual types of ArfGAP is viable to cells, only *Δgcs1Δage2* and *Δgcs1Δglo3* are lethal (Poon et al., 2001). They seem to have overlapping

functions in exit of the TGN. Hence the function of Gcs1 may be more generic than Age2 and Glo3. Secondly, Gcs1 has limited interaction with the COPI coat and relies largely on membrane curvature sensing for functional regulation, while Glo3 has several contact site with the coatomer and stably associates with the COPI coat (Arakel et al., 2019b; Bigay et al., 2003, 2005; Bruno Mesmin et al., 2007; Drin et al., 2005; Schindler et al., 2009; Watson et al., 2004; Yang et al., 2005) (Chapter II). Finally, the GAP activity of Gcs1 is intrinsically stronger than Glo3 GAP and is less dependent on the presence of the COPI coatomer (Luo et al., 2009a; Weimer et al., 2008).

Separation based on cargoes and pathways

In eukaryotic cells, COPI is known to carry out multiple vesicular membrane trafficking pathways: retrieval of ER proteins from the Golgi, retrograde and anterograde trafficking within the Golgi compartments (Popoff et al., 2011), and cargo recycling from early endosomes to the TGN (Xu et al., 2017). Different types of cargoes are involved in different pathways and therefore may need COPI to choose the right type of cargo to carry out trafficking in the correct pathway. It is possible that the ArfGAPs Glo3 and Gcs1 play a role in this by preferentially participating in the trafficking of different cargoes. As described in Chapter II, our data showed disrupting the Glo3/β'-COP interaction affected transport of cargoes and SNAREs in the TGN/post-Golgi pathways and this interaction seemed to have little or no effect on ER-Golgi cargoes, including the dilysine cargoes, suggesting Glo3 is likely more engaged with cargoes that cycle via the late-Golgi through its interaction with β'-COP. Together with the recent data showing Gcs1 plays an important role in the retrieval of HDEL/KDEL-containing cargoes to the ER, we may speculate there's a possibility that Glo3 and Gcs1 are functionally separated in cargoes and pathways. Despite the fact that losing either one of them is not lethal to cells and they both are capable of performing COPI-mediate retrieval, maybe Glo3 is more involved with late-Golgi/post-Golgi cargoes and Gcs1 with ER-early-Golgi cargoes. However, there is still not enough knowledge about cargo preferences of Gcs1 to fully support this, and interactions between Glo3 and other components of the COPI could also be a factor that hasn't

been taken into consideration. In addition to this, previous studies showed members of the p24 family could inhibit the GAP activity of the Gcs1-type GAP domain while dilysine cargo imposes no effect (Goldberg, 2000a), it has also been shown that full length ArfGAP2 (or Glo3) can be activated by members of the p24 family (Luo et al., 2009a). The p24 family members are considered to cycle between the ER-Golgi interface, hence these results could suggest a "checkpoint" behavior of Gcs1 and a "discard" behavior of Glo3 for the p24 family cargoes in the ER/Golgi pathway. However, this may also be affected by other factors, such as the regulations by non-GAP regions of the ArfGAPs or the ubiquitination of p24 family members.

Apart from these, it's surprising that neither our data or previous studies on ArfGAPs showed regulations on the dilysine cargoes, even though Glo3 directly interacts with the dilysine binding subunit of β'-COP likely near the dilysine binding site. Again, this could be potentially explained if Glo3-mediated regulation does not happen in the same COPI vesicles that transport dilysine cargoes between the ER and the Golgi, but more investigations are needed in the future. Another possibility is that our current way of testing the dilysine cargo trafficking is not capable of capturing a specific phenotype of mis-sorting. Our cycloheximide chase experiment to test the Emp47 cargo was designed based on the assumption that mis-sorted Emp47 goes to the vacuole and is then hydrolyzed. However, if Emp47 mis-sorting caused by the loss of β'-COP/Glo3 interaction leads to accumulation of Emp47 in a different compartment such as the Golgi, we would not be able to observe that with our current experimental design. To better investigate the trafficking of dilysine cargoes in the future, we could potentially follow the path of their trafficking by GFP-tagging the cargoes and visualizing them under the microscope. In addition to this, improving our current structural efforts on the Glo3/β'-COP structure and understanding where β'-COP interacts with Glo3 and the dilysine motif, respectively, may also be helpful.

Separation based on functions in a COPI cycle

Alternatively, COPI may associate with Glo3 and Gcs1 simultaneously, akin to the two Arf1 niches to perform different functions in the same COPI cycle. COPI vesicles need to coordinate multiple GAP-stimulated GTP hydrolysis events in each COPI cycle, since it has been shown that GAP stimulated GTP-hydrolysis happens at both the cargo sorting stage and the coat removal stage (Donaldson et al., 1990; Lanoix et al., 2001a; Nickel et al., 1998; Pepperkok et al., 2000; Serafini et al., 1991; Tanigawa et al., 1993; Teal et al., 1994). Even though Gcs1 and Glo3 types of ArfGAPs were both discovered to be capable of stimulating coat disassembly and to function in cargo sorting-related GTP hydrolysis (Arakel et al., 2019b; Luo et al., 2009a; Weimer et al., 2008), they might still have a different preference in performing at the cargo sorting stage or the coat removal stage. This can be supported by previous data from Arakel and colleagues, which suggested the Gcs1-mediated GTP hydrolysis on β-Arf1 and Glo3-midiated GTP hydrolysis on γ-Arf1 trigger mechanistically distinct outcomes, with the assumption that the arginine fingers in both GAP domains are functional in a physiological state (Arakel et al., 2019b). This could potentially be further investigated using *in vitro* constructed COPI vesicles or liposomes with different purified coat components (such as coatomer, cargo peptides, Arf1, GAP, SNAREs, etc.) added at different stages to see under what conditions the ArfGAP molecules will stimulate GTP hydrolysis. And by utilizing GAP-dead versions of Gcs1 or Glo3, it may be possible to separate the functions of these two ArfGAPs in COPI.

The functional separation of ArfGAPs in the same COPI cycle may also happen during the uncoating process. Previous cryo-ET reconstruction of the *in vivo* COPI vesicles suggested the uncoating process starts soon after vesicles leave the site of emergence (Bykov et al., 2017), another study, however, showed the α-COP is needed for tethering (Travis et al., 2019). Together, these data indicate coat disassembly happens in steps, where part of the coat is removed after budding and the other remaining coat components leave after tethering. It raises the question whether the step-wise process also needs

separate GAP activities. Though currently there's not much data available, it's worth performing more investigations into this, perhaps using the *in situ* cryo-ET method.

Possible roles of Glo3 in COPI-mediated trafficking

The COPI-mediated retrograde transport from the Golgi to the ER and within the Golgi has long been established. In contrast, the COPI-mediated retrieval pathway involving the endosomes was poorly defined and only attracted attention in recent years when Xu and colleagues found Snc1, a SNARE protein that cycles between the Golgi and the plasma membrane, to be dependent on COPI through a ubiquitin signal (Aniento et al., 1996; Kawada et al., 2015; Schindler and Spang, 2007; Whitney et al., 1995; Xu et al., 2017).

In retrieval of ubiquitinated endocytic cargoes

At the earlier stage of my project, given our findings that Glo3 interacts directly with β'-COP, and β'-COP being the COPI subunit that recognizes the classic ER/Golgi dilysine cargoes of COPI, we suspected Glo3 could function as a regulator between the dilysine cargo recognition event, SNARE/coatomer recruitment, and GTP hydrolysis. Based on this idea, we hypothesized binding either one of Glo3 or dilysine cargo might affect β'-COP's ability to bind the other, either through inhibition or promotion. However, we found that even though dilysine motif and Glo3 likely bind β'-COP N-terminal propeller at adjacent sites, β'-COP seems to interact with both Glo3 and dilysine motif simultaneously *in vitro*, and prebinding either one of the two proteins had little effect on binding the other (Chapter II). Such result seems to implicate that β'-COP/Glo3 and β'-COP/dilysine interactions are independent processes. Our trafficking assays also seemed to agree with this and showed no phenotype in dilysine cargo transport when β'-COP/Glo3 interaction is disrupted (Chapter II). Other ER related COPI cargoes like Rer1 also seem to remain unaffected.

In contrast to the ER/Golgi cargoes, we noticed disrupted trafficking patterns of endocytic cargoes, including Ste2 and Snc1, when the β'-COP/Glo3 interaction is lost. Furthermore, the post-Golgi cargoes whose trafficking were disrupted by the disabled β'-COP/Glo3 interaction are also found to be modified by ubiquitylation (Swaney et al., 2013). Ubiquitylated residues have also been found in the β'-COP N-terminal propeller and Glo3 (Swaney et al., 2013). In a previous study, a similar Snc1 phenotype was observed to be caused by the loss of the ubiquitin binding site on β'-COP N-terminal propeller (Xu et al., 2017). These findings led us to form a hypothesis that Glo3 is important in mediating the ubiquitinated COPI cargo trafficking in endocytic trafficking via the late Golgi. And it is possible that the mutations perturbing the β'-COP/Glo3 interaction do not cause a more general trafficking defect because Glo3 could still have weak communication with COPI via the ubiquitin modifications.

To further shed light on this, in the future we could test other potentially ubiquitinated endocytic SNARE proteins and other cargoes, for example Sec22, *in vivo* to see whether they experience issues with trafficking when disrupting the β'-COP/Glo3 interaction. Though there is a possibility that Glo3 and β'-COP have different specificity towards different types of ubiquitin chains and therefore have different level of influence on cargoes with different ubiquitin chains. Another area that could be investigated in the future is the separation or coordination of the roles of the β'-COP/Glo3 interaction and β'-COP ubiquitylation in Snc1 trafficking. A previous study has shown that restoring the ubiquitylation on β'-COP could restore Snc1 recycling caused by the loss of β'-COP N-terminal propeller domain (Xu et al., 2017). It will also be interesting to see whether the phenotype of aberrant Snc1 recycling caused by the loss of N-terminal propeller could be rescued by an artificial Glo3 connection. In addition to this, once both the Glo3 binding site and ubiquitin binding site on β'-COP N-terminal propeller domain have been identified, it may be interesting to see whether disrupting either the ubiquitylation site or the Glo3 binding site on β'-COP N-terminal propeller could cause similar phenotype.

In maintaining the Golgi-localized glycosyltransferases

However, the above theory does not explain the Glo3 localization in the cells as reported by Kawada and colleagues (Kawada et al., 2015). According to their studies, though Glo3 partially localizes at the TGN, the majority of Glo3 localizes at the *cis*-to-*medial* Golgi compartments, suggesting that Glo3 must play significant roles in the retrograde transport from the *cis*-Golgi back to the ER and within the Golgi. Ste2 as an α-receptor has been known to undergo several forms of post-translational modifications, including phosphorylation, ubiquitination, and N-glycosylation, and it was previously reported to need N-glycosylation for proper sorting inside the cell (Mentesana and Konopka, 2001).

An alternative hypothesis to interpret our data is that Ste2 mis-sorting might not be caused directly by disrupting the endocytic retrieval mediated by COPI. Instead, Ste2 might have been mis-sorted to the vacuole because it was not properly modified due to disrupted N-glycosylation functions in the Golgi, which could have been caused by insufficient retrieval of glycosyltransferases within the Golgi stacks by COPI in our mutant cells. Many Golgi-localized N-glycosylation related glycosyltransferases are COPI cargoes recognized via Vps74, such as the Mnn9. To further investigate this area, future experiments may include trafficking assays looking at the localizations and retention of cargoes like Mnn9 in the mutant cells.

BIBIOGRAPHY

Adams, P.D., Afonine, P. V, Bunkóczi, G., Chen, V.B., Davis, I.W., Echools, N., Headd, J.J., Hung, L.-W., Kapral, G.J., Grosse-Kunstleve, R.W., et al. (2010). PHENIX: a comprehensive, Python-based system for macromolecular structure solution. Acta Cryst D *66*, 213–221.

Adolf, F., Herrmann, A., Hellwig, A., Beck, R., Brügger, B., and Wieland, F.T. (2013). Scission of COPI and COPII Vesicles Is Independent of GTP Hydrolysis. Traffic *14*, 922–932.

Aguilera-Romero, A., Kaminska, J., Spang, A., Riezman, H., and Muñiz, M. (2008). The yeast p24 complex is required for the formation of COPI retrograde transport vesicles from the Golgi apparatus. J. Cell Biol. *180*, 713–720.

Ahmadian, M.R., Stege, P., Scheffzek, K., and Wittinghofer, A. (1997). Confirmation of the arginine-finger hypothesis for the GAP-stimulated GTP-hydrolysis reaction of Ras. Nat. Struct. Biol. 1997 49 *4*, 686–689.

AJ, N., and SM, S. (2015). STRUCTURAL BIOLOGY. COPI gets a fancy new coat. Science *349*, 142–143.

Amor, J.C., Harrison, D.H., Kahn, R.A., and Ringe, D. (1994). Structure of the human ADP-ribosylation factor 1 complexed with GDP. Nat. 1994 3726507 *372*, 704–708.

and, P.E.M., and Konopka*, J.B. (2001). Mutational Analysis of the Role of N-Glycosylation in α-Factor Receptor Function†. Biochemistry *40*, 9685–9694.

Aniento, F., Gu, F., Parton, R.G., and Gruenberg, J. (1996). An endosomal beta COP is involved in the pH-dependent formation of transport vesicles destined for late endosomes. J. Cell Biol. *133*, 29–41.

Antonny, B., Beraud-Dufour, S., Chardin, P., and Chabre, M. (1997). N-terminal hydrophobic residues of the G-protein ADP-ribosylation factor-1 insert into membrane phospholipids upon GDP to GTP exchange. Biochemistry *36*, 4675–4684.

Aoe, T., Cukierman, E., Lee, A., Cassel, D., Peters, P.J., and Hsu, V.W. (1997). The KDEL receptor, ERD2, regulates intracellular traffic by recruiting a GTPase-activating protein for ARF1. EMBO J. *16*, 7305–7316.

Arakel, E.C., Brandenburg, S., Uchida, K., Zhang, H., Lin, Y.-W., Kohl, T., Schrul, B., Sulkin, M.S., Efimov, I.R., Nichols, C.G., et al. (2014). Tuning the electrical properties of the heart by differential trafficking of KATP ion channel complexes. J. Cell Sci. *127*, 2106–2119.

Arakel, E.C., Richter, K.P., Clancy, A., and Schwappach, B. (2016). δ-COP contains a helix C-terminal to its longin domain key to COPI dynamics and function. Proc. Natl. Acad. Sci. *113*, 6916–6921.

Arakel, E.C., Schwappach, B., Arakel, E.C., and Schwappach, B. (2018). Correction : Formation of COPI-coated vesicles at a glance (doi : 10 . 1242 / jcs . 209890) Formation of COPI-coated vesicles at a glance.

Arakel, E.C., Estrada, A.F., Rau, E.-M., Spang, A., and Schwappach, B. (2019a). Dissection of GTPase activating proteins reveals functional asymmetry in the COPI coat.

Arakel, E.C., Huranova, M., Estrada, A.F., Rau, M.E., Spang, A., and Schwappach, B. (2019b). Dissection of GTPase-activating proteins reveals functional asymmetry in the COPI coat of budding yeast. J. Cell Sci.

132.

Ashkenazy, H., Erez, E., Martz, E., Pupko, T., and Ben-Tal, N. (2010). ConSurf 2010: calculating evolutionary conservation in sequence and structure of proteins and nucleic acids. Nucleic Acids Res. *38*, W529–W533.

Bai, M., Gad, H., Turacchio, G., Cocucci, E., Yang, J.-S., Li, J., Beznoussenko, G. V, Nie, Z., Luo, R., Fu, L., et al. (2011). ARFGAP1 promotes AP-2-dependent endocytosis. Nat. Cell Biol. *13*, 559–567.

Barlowe, C.K., and Miller, E.A. (2013). Secretory protein biogenesis and traffic in the early secretory pathway. Genetics *193*, 383–410.

Barlowe, C., Barlowe, C., Schekman, R., Ravazzola, M., Helms, J.B., Rothman, J.E., Wieland, F.T., Tanigawa, G., Rothman, J.E., and Balch, W.E. (1994). COPII: A membrane coat formed by Sec proteins that drive vesicle budding from the endoplasmic reticulum. Cell *77*, 895–907.

Beacham, G.M., Partlow, E.A., and Hollopeter, G. (2019). Conformational regulation of AP1 and AP2 clathrin adaptor complexes.

Beck, R., Sun, Z., Adolf, F., Rutz, C., Bassler, J., Wild, K., Sinning, I., Hurt, E., Brügger, B., Béthune, J., et al. (2008). Membrane curvature induced by Arf1-GTP is essential for vesicle formation. Proc. Natl. Acad. Sci. *105*, 11731–11736.

Beck, R., Prinz, S., Diestelkötter-Bachert, P., Röhling, S., Adolf, F., Hoehner, K., Welsch, S., Ronchi, P., Brügger, B., Briggs, J.A.G., et al. (2011). Coatomer and dimeric ADP ribosylation factor 1 promote distinct steps in membrane scission. J. Cell Biol. *194*, 765–777.

Beilsten-Edmands, J., Winter, G., Gildea, R., Parkhurst, J., Waterman, D., and Evans, G. (2020). Scaling diffraction data in the DIALS software package: algorithms and new approaches for multi-crystal scaling. Urn:Issn:2059-7983 *76*, 385–399.

Beller, M., Sztalryd, C., Southall, N., Bell, M., Jäckle, H., Auld, D.S., and Oliver, B. (2008). COPI Complex Is a Regulator of Lipid Homeostasis. PLOS Biol. *6*, e292.

Benmerah, A., Gagnon, J., Bègue, B., Mégarbané, B., Dautry-Varsat, A., and Cerf-Bensussan, N. (1995). The tyrosine kinase substrate eps15 is constitutively associated with the plasma membrane adaptor AP-2. J. Cell Biol. *131*, 1831–1838.

Bermak, J.C., Li, M., Bullock, C., Weingarten, P., and Zhou, Q.Y. (2002). Interaction of γ-COP with a transport motif in the D1 receptor C-terminus. Eur. J. Cell Biol. *81*, 77–85.

Béthune, J., Kol, M., Hoffmann, J., Reckmann, I., Brügger, B., and Wieland, F. (2006). Coatomer, the Coat Protein of COPI Transport Vesicles, Discriminates Endoplasmic Reticulum Residents from p24 Proteins. Mol. Cell. Biol. *26*, 8011–8021.

Bhandari, A., Zheng, C., Sindan, N., Sindan, N., Quan, R., Xia, E., Thapa, Y., Tamang, D., Wang, O., Ye, X., et al. (2019). COPB2 is up-regulated in breast cancer and plays a vital role in the metastasis via N-cadherin and Vimentin. J Cell Mol Med.

Bhave, M., Mino, R.E., Wang, X., Lee, J., Grossman, H.M., Lakoduk, A.M., Danuser, G., Schmid, S.L., and Mettlen, M. (2020). Functional characterization of 67 endocytic accessory proteins using multiparametric quantitative analysis of CCP dynamics. Proc. Natl. Acad. Sci. *117*, 31591–31602.

Bi, J., Tsai, N.-P., Lu, H.-Y., Loh, H.H., and Wei, L.-N. (2007). Copb1-facilitated axonal transport and translation of κ opioid-receptor mRNA. Proc. Natl. Acad. Sci. *104*, 13810–13815.

Bigay, J., Gounon, P., Robineau, S., and Antonny, B. (2003). Lipid packing sensed by ArfGAP1 couples COPI coat disassembly to membrane bilayer curvature. Nat. 2003 4266966 *426*, 563–566.

Bigay, J., Casella, J.-F., Drin, G., Mesmin, B., and Antonny, B. (2005). ArfGAP1 responds to membrane curvature through the folding of a lipid packing sensor motif. EMBO J. *24*, 2244–2253.

Bonifacino, J.S., and Glick, B.S. (2004). The Mechanisms of Vesicle Budding and Fusion. Cell *116*, 153–166.

Bonnon, C., Wendeler, M.W., Paccaud, J.-P., and Hauri, H.-P. (2010). Selective export of human GPI-anchored proteins from the endoplasmic reticulum. J. Cell Sci. *123*, 1705–1715.

Le Borgne, R., Griffiths, G., and Hoflack, B. (1996). Mannose 6-Phosphate Receptors and ADP-ribosylation Factors Cooperate for High Affinity Interaction of the AP-1 Golgi Assembly Proteins with Membranes. J. Biol. Chem. *271*, 2162–2170.

Bräuer, P., Parker, J.L., Gerondopoulos, A., Zimmermann, I., Seeger, M.A., Barr, F.A., and Newstead, S. (2019). Structural basis for pH-dependent retrieval of ER proteins from the Golgi by the KDEL receptor. Science (80-.). *363*, 1103–1107.

Bremser, M., Nickel, W., Schweikert, M., Ravazzola, M., Amherdt, M., Hughes, C. a, Söllner, T.H., Rothman, J.E., and Wieland, F.T. (1999). Coupling of Coat Assembly and Vesicle Budding to Packaging of Putative Cargo Receptors. Cell *96*, 495–506.

Bruno Mesmin, ‡, Guillaume Drin, ‡, Sharon Levi, §, Moran Rawet, §, Dan Cassel, §, Joëlle Bigay, ‡ and, and Bruno Antonny*, ‡ (2007). Two Lipid-Packing Sensor Motifs Contribute to the Sensitivity of ArfGAP1 to Membrane Curvature†. Biochemistry *46*, 1779–1790.

Buchan, D.W.A., and Jones, D.T. (2019). The PSIPRED Protein Analysis Workbench: 20 years on. Nucleic Acids Res. *47*, W402–W407.

Bykov, Y.S., Schaffer, M., Dodonova, S.O., Albert, S., Plitzko, M., Baumeister, W., Engel, B.D., and Briggs, J.A.G. (2017). The structure of the COPI coat determined within the cell. 1–18.

Cabrera, M., Muñiz, M., Hidalgo, J., Vega, L., Martín, M.E., and Velasco, A. (2003). The Retrieval Function of the KDEL Receptor Requires PKA Phosphorylation of Its C-Terminus. Https://Doi.Org/10.1091/Mbc.E03-04-0194 *14*, 4114–4125.

Cai, H., Reinisch, K., and Ferro-Novick, S. (2007). Coats, Tethers, Rabs, and SNAREs Work Together to Mediate the Intracellular Destination of a Transport Vesicle. Dev. Cell *12*, 671–682.

Chardin, P., Paris, S., Antonny, B., Robineau, S., Beraud-Dufour, S., Jackson, C.L., and Chabre, M. (1996).

A human exchange factor for ARF contains Sec7- and pleckstrin-homology domains. Nature *384*, 481–484.

Cherfils, J. (2014). Arf GTPases and their effectors: Assembling multivalent membrane-binding platforms. Curr. Opin. Struct. Biol. *29*, 67–76.

Cherfils, J., and Zeghouf, M. (2013). Regulation of Small GTPases by GEFs, GAPs, and GDIs. Https://Doi.Org/10.1152/Physrev.00003.2012 *93*, 269–309.

Collins, B.M., McCoy, A.J., Kent, H.M., Evans, P.R., and Owen, D.J. (2002). Molecular Architecture and Functional Model of the Endocytic AP2 Complex. Cell *109*, 523–535.

Cosson, P., and Letourneur, F. (1994). Coatomer interaction with di-lysine endoplasmic reticulum retention motifs. Science (80-.). *263*, 1629–1631.

Cosson, P., Lefkir, Y., Démollière, C., and Letourneur, F. (1998). New COP1-binding motifs involved in ER retrieval. EMBO J. *17*, 6863–6870.

Cukierman, E., Huber, I., Rotman, M., and Cassel, D. (1995). The ARF1 GTPase-Activating Protein: Zinc Finger Motif and Golgi Complex Localization. Science (80-.). *270*, 1999–2002.

Cureton, D.K., Burdeinick-Kerr, R., and Whelan, S.P.J. (2012). Genetic inactivation of COPI coatomer separately inhibits vesicular stomatitis virus entry and gene expression. J Virol *86*, 655–666.

Dacks, J.B., and Field, M.C. (2007). Evolution of the eukaryotic membrane-trafficking system: Origins, tempo and mode. J. Cell Sci. *120*, 2977–2985.

Dacks, J.B., and Robinson, M.S. (2017). Outerwear through the ages: evolutionary cell biology of vesicle coats. Curr. Opin. Cell Biol. *47*, 108–116.

Davies, A.K., Itzhak, D.N., Edgar, J.R., Archuleta, T.L., Hirst, J., Jackson, L.P., Robinson, M.S., and Borner, G.H.H. (2018). AP-4 vesicles contribute to spatial control of autophagy via RUSC-dependent peripheral delivery of ATG9A. Nat. Commun. 2018 91 *9*, 1–21.

Dell'angelica, E.C., and Bonifacino, J.S. (2019). Coatopathies: Genetic Disorders of Protein Coats. Annu. Rev. Cell Dev. Biol. Annu. Rev. Cell Dev. Biol *35*, 131–168.

Dell'Angelica, E.C., and Bonifacino, J.S. (2019). Coatopathies: Genetic disorders of protein coats. Annu. Rev. Cell Dev. Biol. *35*, 131–168.

Dell'Angelica, E.C., Klumperman, J., Stoorvogel, W., and Bonifacino, J.S. (1998). Association of the AP-3 Adaptor Complex with Clathrin. Science (80-.). *280*, 431–434.

Deng, Y., Golinelli-Cohen, M.-P., Smirnova, E., and Jackson, C.L. (2009). A COPI coat subunit interacts directly with an early-Golgi localized Arf exchange factor. EMBO Rep. *10*, 58–64.

Devos, D., Dokudovskaya, S., Alber, F., Williams, R., Chait, B.T., Sali, A., and Rout, M.P. (2004). Components of Coated Vesicles and Nuclear Pore Complexes Share a Common Molecular Architecture. PLOS Biol. *2*, e380.

DiStasio, A., Driver, A., Sund, K., Donlin, M., Muraleedharan, R.M., Pooya, S., Kline-Fath, B., Kaufman, K.M., Prows, C.A., Schorry, E., et al. (2017). Copb2 is essential for embryogenesis and hypomorphic mutations cause human microcephaly. Hum. Mol. Genet. *26*, 4836–4848.

Dodonova, S.O., Appen, A. Von, Hagen, W.J.H., Beck, R., Beck, M., Wieland, F., and Briggs, J.A.G. (2015). A structure of the COPI coat and the role of coat proteins in membrane vesicle assembly. Science (80-.). *349*, 195–198.

Dodonova, S.O., Aderhold, P., Kopp, J., Ganeva, I., Hagen, W.J.H., Sinning, I., Wieland, F., and Briggs, J.A.G. (2017). ˚ structure of the COPI coat reveals that the Arf1 GTPase occupies two contrasting molecular environments. 1–29.

Dominguez, M., Dejgaard, K., Füllekrug, J., Dahan, S., Fazel, A., Paccaud, J.-P., Thomas, D.Y., Bergeron, J.J.M., and Nilsson, T. (1998). gp25L/emp24/p24 Protein Family Members of the cis-Golgi Network Bind Both COP I and II Coatomer. J. Cell Biol. *140*, 751–765.

Donaldson, J.G., and Jackson, C.L. (2011). ARF family G proteins and their regulators: roles in membrane transport, development and disease. Nat. Rev. Mol. Cell Biol. 2011 126 *12*, 362–375.

Donaldson, J.G., Lippincott-Schwartz, J., Bloom, G.S., Kreis, T.E., and Klausner, R.D. (1990). Dissociation of a 110-kD peripheral membrane protein from the Golgi apparatus is an early event in brefeldin A action. J. Cell Biol. *111*, 2295–2306.

Drin, G., Mesmin, B., and Antonny, B. (2005). ArfGAP1 responds to membrane curvature through the folding of a lipid packing sensor motif. *24*, 2244–2253.

Duden, R. (2003). ER-to-Golgi transport: COP I and COP II function (Review). Mol. Membr. Biol. *20*, 197–207.

Duden, R., Kajikawa, L., Wuestehube, L., and Schekman, R. (1998). ϵ-COP is a structural component of coatomer that functions to stabilize α-COP. EMBO J. *17*, 985–995.

Dunlop, M.H., Ernst, A.M., Schroeder, L.K., Toomre, D.K., Lavieu, G., and Rothman, J.E. (2017). Land-locked mammalian Golgi reveals cargo transport between stable cisternae. Nat. Commun. 2017 81 *8*, 1–14.

E, C., I, H., M, R., and D, C. (1995). The ARF1 GTPase-activating protein: zinc finger motif and Golgi complex localization. Science *270*, 1999–2002.

Eckert, E.S.P., Reckmann, I., Hellwig, A., Röhling, S., El-Battari, A., Wieland, F.T., and Popoff, V. (2014). Golgi Phosphoprotein 3 Triggers Signal-mediated Incorporation of Glycosyltransferases into Coatomer-coated (COPI) Vesicles. J. Biol. Chem. *289*, 31319–31329.

Elkin, S.R., Lakoduk, A.M., and Schmid, S.L. (2016). Endocytic pathways and endosomal trafficking: a primer. Wiener Medizinische Wochenschrift *166*, 196–204.

Emsley, P., Lohkamp, B., Scott, W.G., and Cowtan, K. (2010). Features and development of Coot. Acta Crystallogr. D. Biol. Crystallogr. *66*, 486–501.

Eugster, A., Frigerio, G., Dale, M., and Duden, R. (2000). COP I domains required for coatomer integrity, and novel interactions with ARF and ARF-GAP. EMBO J. *19*, 3905–3917.

Evans, P.R., and Owen, D.J. (2002a). Endocytosis and vesicle trafficking. Curr. Opin. Struct. Biol. *12*, 814–821.

Evans, P.R., and Owen, D.J. (2002b). Endocytosis and vesicle trafficking. Curr. Opin. Struct. Biol. *12*, 814–821.

F, P., JA, M., R, F., R, M., TH, S., and JE, R. (2000). Topological restriction of SNARE-dependent membrane fusion. Nature *407*, 194–198.

Faini, M., Prinz, S., Beck, R., Schorb, M., Riches, J.D., Bacia, K., Brugger, B., Wieland, F.T., and Briggs, J. a. G. (2012). The Structures of COPI-Coated Vesicles Reveal Alternate Coatomer Conformations and Interactions. Science (80-.). *336*, 1451–1454.

Farías, G.G., Cuitino, L., Guo, X., Ren, X., Jarnik, M., Mattera, R., and Bonifacino, J.S. (2012). Signal-Mediated, AP-1/Clathrin-Dependent Sorting of Transmembrane Receptors to the Somatodendritic Domain of Hippocampal Neurons. Neuron *75*, 810–823.

Fernández-Ulibarri, I., Vilella, M., Lázaro-Diéguez, F., Sarri, E., Martínez, S.E., Jiménez, N., Claro, E., Mérida, I., Burger, K.N.J., and Egea, G. (2007). Diacylglycerol Is Required for the Formation of COPI Vesicles in the Golgi-to-ER Transport Pathway. Https://Doi.Org/10.1091/Mbc.E07-04-0334 *18*, 3250–3263.

Fiedler, K., Veit, M., Stamnes, M.A., and Rothman, J.E. (1996). Bimodal Interaction of Coatomer with the p24 Family of Putative Cargo Receptors. Science (80-.). *273*, 1396–1399.

Fölsch, H., Pypaert, M., Schu, P., and Mellman, I. (2001). Distribution and Function of Ap-1 Clathrin Adaptor Complexes in Polarized Epithelial Cells. J. Cell Biol. *152*, 595–606.

Fotin, A., Cheng, Y., Sliz, P., Grigorieff, N., Harrison, S.C., Kirchhausen, T., and Walz, T. (2004). Molecular model for a complete clathrin lattice from electron cryomicroscopy. Nat. 2004 4327017 *432*, 573–579.

Franco, M., Chardin, P., Chabre, M., and Paris, S. (1996). Myristoylation-facilitated Binding of the G Protein ARF1GDP to Membrane Phospholipids Is Required for Its Activation by a Soluble Nucleotide Exchange Factor (∗). J. Biol. Chem. *271*, 1573–1578.

Frigerio, G., Grimsey, N., Dale, M., Majoul, I., and Duden, R. (2007). Two human ARFGAPs associated with COP-I-coated vesicles. Traffic *8*, 1644–1655.

Gaidarov, I., and Keen, J.H. (1999). Phosphoinositide–Ap-2 Interactions Required for Targeting to Plasma Membrane Clathrin-Coated Pits. J. Cell Biol. *146*, 755–764.

Gaynor, E.C., te Heesen, S., Graham, T.R., Aebi, M., and Emr, S.D. (1994). Signal-mediated retrieval of a membrane protein from the Golgi to the ER in yeast. J. Cell Biol. *127*, 653–665.

Ge, X., Gong, H., Dumas, K., Litwin, J., Phillips, J.J., Waisfisz, Q., Weiss, M.M., Hendriks, Y., Stuurman, K.E., Nelson, S.F., et al. (2016). Missense-depleted regions in population exomes implicate ras

superfamily nucleotide-binding protein alteration in patients with brain malformation. Npj Genomic Med. 2016 11 *1*, 1–7.

Ghosh, P., and Kornfeld, S. (2003). Recommended Citation AP-1 binding to sorting signals and release from clathrin-coated vesicles is regulated by phosphorylation. J. Cell Biol. *160*, 699–708.

Gillingham, A.K., and Munro, S. (2007). The Small G Proteins of the Arf Family and Their Regulators. Http://Dx.Doi.Org/10.1146/Annurev.Cellbio.23.090506.123209 *23*, 579–611.

Goepfert, P. a, Shaw, K.L., Ritter, G.D., and Mulligan, M.J. (1997). A sorting motif localizes the foamy virus glycoprotein to the endoplasmic reticulum. J. Virol. *71*, 778–784.

Goldberg, J. (1998). Structural basis for activation of ARF GTPase. Cell *95*, 237–248.

Goldberg, J. (1999). Structural and functional analysis of the ARF1-aRFGAP complex reveals a role for coatomer in GTP hydrolysis. Cell *96*, 893–902.

Goldberg, J. (2000a). Decoding of Sorting Signals by Coatomer through a GTPase Switch in the COPI Coat Complex. Cell *100*, 671–679.

Goldberg, J. (2000b). Decoding of sorting signals by coatomer through a GTPase switch in the COPI coat complex. Cell *100*, 671–679.

Gommel, D.U., Memon, A.R., Heiss, A., Lottspeich, F., Pfannstiel, J., Lechner, J., Reinhard, C., Helms, J.B., Nickel, W., and Wieland, F.T. (2001). Recruitment to Golgi membranes of ADP-ribosylation factor 1 is mediated by the cytoplasmic domain of p23. EMBO J. *20*, 6751–6760.

Gravotta, D., Bay, A.P., Jonker, C.T.H., Zager, P.J., Benedicto, I., Schreiner, R., Caceres, P.S., and Rodriguez-Boulan, E. (2019). Clathrin and clathrin adaptor AP-1 control apical trafficking of megalin in the biosynthetic and recycling routes. Mol. Biol. Cell *30*.

Guo, Y., Walther, T.C., Rao, M., Stuurman, N., Goshima, G., Terayama, K., Wong, J.S., Vale, R.D., Walter, P., and Farese, R. V (2008). Functional genomic screen reveals genes involved in lipid-droplet formation and utilization. Nature *453*, 657–661.

Ter Haar, E., Harrison, S.C., and Kirchhausen, T. (2000). Peptide-in-groove interactions link target proteins to the β-propeller of clathrin. Proc. Natl. Acad. Sci. U. S. A. *97*, 1096–1100.

Hara-Kuge, S., Kuge, O., Orci, L., Amherdt, M., Ravazzola, M., Wieland, F.T., and Rothman, J.E. (1994). En Bloc incorporation of coatomer subunits during the assembly of COP-coated vesicles. J. Cell Biol. *124*, 883–892.

Hayashi, T., McMahon, H., Yamasaki, S., Binz, T., Hata, Y., Südhof, T.C., and Niemann, H. (1994). Synaptic vesicle membrane fusion complex: action of clostridial neurotoxins on assembly. EMBO J. *13*, 5051–5061.

Heldwein, E.E., Macia, E., Wang, J., Yin, H.L., Kirchhausen, T., and Harrison, S.C. (2004). Crystal structure of the clathrin adaptor protein 1 core. Proc. Natl. Acad. Sci. *101*, 14108–14113.

Hirst, J., Barlow, L.D., Francisco, G.C., Sahlender, D.A., Seaman, M.N.J., Dacks, J.B., and Robinson, M.S. (2011). The Fifth Adaptor Protein Complex. PLOS Biol. *9*, e1001170.

Hirst, J., Irving, C., and Borner, G.H.H. (2013). Adaptor Protein Complexes AP-4 and AP-5: New Players in Endosomal Trafficking and Progressive Spastic Paraplegia. Traffic *14*.

Hirst, J., Itzhak, D.N., Antrobus, R., Borner, G.H.H., and Robinson, M.S. (2018). Role of the AP-5 adaptor protein complex in late endosome-to-Golgi retrieval. PLOS Biol. *16*, e2004411.

Hutchings, J., Stancheva, V., Miller, E.A., and Zanetti, G. (2018). Subtomogram averaging of COPII assemblies reveals how coat organization dictates membrane shape. Nat. Commun. *9*.

Iannolo, G., Salcini, A.E., Gaidarov, I., Goodman, O.B., Baulida, J., Carpenter, G., Pelicci, P.G., Fiore, P.P. Di, and Keen, J.H. (1997). Mapping of the Molecular Determinants Involved in the Interaction between eps15 and AP-2. Cancer Res. *57*.

Inoue, H., and Randazzo, P.A. (2007). Arf GAPs and Their Interacting Proteins. Traffic *8*, 1465–1475.

Ishii, M., Suda, Y., Kurokawa, K., and Nakano, A. (2016). COPI is essential for Golgi cisternal maturation and dynamics.

Ismail, S.A., Vetter, I.R., Sot, B., and Wittinghofer, A. (2010). The structure of an Arf-arfgap complex reveals a Ca2+ regulatory mechanism. Cell *141*, 812–821.

Ivankovic, D., Drew, J., Lesept, F., White, I.J., Doménech, G.L., Tooze, S.A., and Kittler, J.T. (2019). Axonal autophagosome maturation defect through failure of ATG9A sorting underpins pathology in AP-4 deficiency syndrome. Https://Doi.Org/10.1080/15548627.2019.1615302 *16*, 391–407.

Izumi, K., Brett, M., Nishi, E., Drunat, S., Tan, E.S., Fujiki, K., Lebon, S., Cham, B., Masuda, K., Arakawa, M., et al. (2016). ARCN1 Mutations Cause a Recognizable Craniofacial Syndrome Due to COPI-Mediated Transport Defects. Am. J. Hum. Genet. *99*, 451–459.

Jackson, L.P. (2014). ScienceDirect Structure and mechanism of COPI vesicle biogenesis. Curr. Opin. Cell Biol. *29*, 67–73.

Jackson, C.L., and Bouvet, S. (2014). Arfs at a Glance. J. Cell Sci. *127*, 4103–4109.

Jackson, L.P., Kelly, B.T., McCoy, A.J., Gaffry, T., James, L.C., Collins, B.M., Höning, S., Evans, P.R., Owen, D.J., and Bonifacino, J.S. (2010). A large-scale conformational change couples membrane recruitment to cargo binding in the AP2 clathrin adaptor complex. Cell *141*, 1220–1229.

Jackson, L.P., Lewis, M., Kent, H.M., Edeling, M.A., Evans, P.R., Duden, R., and Owen, D.J. (2012). Molecular Basis for Recognition of Dilysine Trafficking Motifs by COPI. Dev. Cell *23*, 1255–1262.

Jackson, M.R., Nilsson, T., and Peterson, P.A. (1990a). Identification of a consensus motif for retention of transmembrane proteins in the endoplasmic reticulum. EMBO J. *9*, 3153–3162.

Jackson, M.R., Nilsson, T., and Peterson, P.A. (1990b). Identification of a consensus motif for retention of transmembrane proteins in the endoplasmic reticulum. EMBO J *9*, 3153–3162.

Jensson, B.O., Hansdottir, S., Arnadottir, G.A., Sulem, G., Kristjansson, R.P., Oddsson, A., Benonisdottir, S., Jonsson, H., Helgason, A., Saemundsdottir, J., et al. (2017). COPA syndrome in an Icelandic family caused by a recurrent missense mutation in COPA. BMC Med. Genet. 2017 181 *18*, 1–5.

Jia, X., Weber, E., Tokarev, A., Lewinski, M., Rizk, M., Suarez, M., Guatelli, J., and Xiong, Y. (2014). Structural basis of HIV-1 Vpu-mediated BST2 antagonism via hijacking of the clathrin adaptor protein complex 1. Elife *2014*.

Kadlecova, Z., Spielman, S.J., Loerke, D., Mohanakrishnan, A., Reed, D.K., and Schmid, S.L. (2017). Regulation of clathrin-mediated endocytosis by hierarchical allosteric activation of AP2. J. Cell Biol. *216*, 167–179.

Kahn, R.A., and Gilman, A.G. (1986). The protein cofactor necessary for ADP-ribosylation of Gs by cholera toxin is itself a GTP binding protein. J. Biol. Chem. *261*, 7906–7911.

Kahn, R.A., Bruford, E., Inoue, H., Logsdon, J.M., Nie, Z., Premont, R.T., Randazzo, P.A., Satake, M., Theibert, A.B., Zapp, M.L., et al. (2008). Consensus nomenclature for the human ArfGAP domain-containing proteins. J. Cell Biol. *182*, 1039–1044.

Kartberg, F., Asp, L., Dejgaard, S.Y., Smedh, M., Fernandez-rodriguez, J., Nilsson, T., and Presley, J.F. (2010). ARFGAP2 and ARFGAP3 Are Essential for COPI Coat Assembly on the Golgi Membrane of Living Cells * □. *285*, 36709–36720.

Kawada, D., Kobayashi, H., Tomita, T., Nakata, E., Nagano, M., Siekhaus, D.E., Toshima, J.Y., and Toshima, J. (2015). The yeast Arf-GAP Glo3p is required for the endocytic recycling of cell surface proteins. Biochim. Biophys. Acta - Mol. Cell Res. *1853*, 144–156.

Kelly, B.T., McCoy, A.J., Späte, K., Miller, S.E., Evans, P.R., Höning, S., and Owen, D.J. (2008). A structural explanation for the binding of endocytic dileucine motifs by the AP2 complex. Nat. 2008 4567224 *456*, 976–979.

Kelly, B.T., Graham, S.C., Liska, N., Dannhauser, P.N., Höning, S., Ungewickell, E.J., and Owen, D.J. (2014). AP2 controls clathrin polymerization with a membrane-activated switch. Science (80-.). *345*, 459–463.

Kilisch, M., Lytovchenko, O., Arakel, E.C., Bertinetti, D., and Schwappach, B. (2016). A dual phosphorylation switch controls 14-3-3-dependent cell surface expression of TASK-1. J. Cell Sci. *129*, 831–842.

Kirchhausen, T., Owen, D., and Harrison, S.C. (2014). Molecular Structure, Function, and Dynamics of Clathrin-Mediated Membrane Traffic. Cold Spring Harb. Perspect. Biol. *6*, a016725.

Kliouchnikov, L., Mesmin, B., Parnis, A., Rawet, M., Goldfeder, N., Antonny, B., and Cassel, D. (2009). Discrete Determinants in ArfGAP2 / 3 Conferring Golgi Localization and Regulation by the COPI Coat. *20*, 859–869.

Kloepper, T.H., Kienle, C.N., and Fasshauer, D. (2007). An Elaborate Classification of SNARE Proteins Sheds Light on the Conservation of the Eukaryotic Endomembrane System. Https://Doi.Org/10.1091/Mbc.E07-03-0193 *18*, 3463–3471.

Kovtun, O., Dickson, V.K., Kelly, B.T., Owen, D.J., and Briggs, J.A.G. (2020). Architecture of the AP2/clathrin coat on the membranes of clathrin-coated vesicles. Sci. Adv. *6*, eaba8381.

Krissinel, E., and Henrick, K. (2004). Secondary-structure matching (SSM), a new tool for fast protein structure alignment in three dimensions. Acta Cryst D *60*, 2256–2268.

Kumawat, A., Chakrabarty, S., and Kulkarni, K. (2017). Nucleotide Dependent Switching in Rho GTPase: Conformational Heterogeneity and Competing Molecular Interactions. Sci. Reports 2017 71 *7*, 1–11.

Langer, J.D., Roth, C.M., Béthune, J., Stoops, E.H., Brügger, B., Herten, D.-P., and Wieland, F.T. (2008). A Conformational Change in the α-subunit of Coatomer Induced by Ligand Binding to γ-COP Revealed by Single-pair FRET. Traffic *9*, 597–607.

Lanoix, J., Ouwendijk, J., Stark, A., Szafer, E., Cassel, D., Dejgaard, K., Weiss, M., and Nilsson, T. (2001a). Sorting of Golgi resident proteins into different subpopulations of COPI vesicles : a role for ArfGAP1. *155*, 1199–1212.

Lanoix, J., Ouwendijk, J., Stark, A., Szafer, E., Cassel, D., Dejgaard, K., Weiss, M., and Nilsson, T. (2001b). Sorting of Golgi resident proteins into different subpopulations of COPI vesicles: A role for ArfGAP1. J. Cell Biol. *155*, 1199–1212.

Lee, C., and Goldberg, J. (2010). Structure of Coatomer Cage Proteins and the Relationship among COPI, COPII, and Clathrin Vesicle Coats. Cell *142*, 123–132.

Lee, S.Y., Yang, J.-S., Hong, W., Premont, R.T., and Hsu, V.W. (2005). ARFGAP1 plays a central role in coupling COPI cargo sorting with vesicle formation. J. Cell Biol. *168*, 281–290.

Lemmon, S.K., and Traub, L.M. (2012). Getting in Touch with the Clathrin Terminal Domain. Traffic *13*, 511–519.

Letourneur, F., Gaynor, E.C., Hennecke, S., Démollière, C., Duden, R., Emr, S.D., Riezman, H., and Cosson, P. (1994). Coatomer is essential for retrieval of dilysine-tagged proteins to the endoplasmic reticulum. Cell *79*, 1199–1207.

Lewis, M.J., and Pelham, H.R.B. (1992). Ligand-induced redistribution of a human KDEL receptor from the Golgi complex to the endoplasmic reticulum. Cell *68*, 353–364.

Lewis, S.M., Poon, P.P., Singer, R.A., Johnston, G.C., and Spang, A. (2004). The ArfGAP Glo3 Is Required for the Generation of COPI Vesicles. Https://Doi.Org/10.1091/Mbc.E04-04-0316 *15*, 4064–4072.

Liebschner, D., Afonine, P. V, Baker, M.L., Bunkóczi, G., Chen, V.B., Croll, T.I., Hintze, B., Hung, L.W., Jain, S., McCoy, A.J., et al. (2019). Macromolecular structure determination using X-rays, neutrons and electrons: recent developments in Phenix. Acta Cryst D *75*, 861–877.

Liu, J., Prunuske, A.J., Fager, A.M., and Ullman, K.S. (2003). The COPI Complex Functions in Nuclear Envelope Breakdown and Is Recruited by the Nucleoporin Nup153. Dev. Cell *5*, 487–498.

Liu, L., Doray, B., and Kornfeld, S. (2018). Recycling of Golgi glycosyltransferases requires direct binding to coatomer. Proc. Natl. Acad. Sci. *115*, 8984–8989.

Liu, Y., Yerushalmi, G.M., Grigera, P.R., and Parsons, J.T. (2005). Mislocalization or Reduced Expression of Arf GTPase-activating Protein ASAP1 Inhibits Cell Spreading and Migration by Influencing Arf1 GTPase Cycling *. J. Biol. Chem. *280*, 8884–8892.

Liu, Y., Kahn, R.A., and Prestegard, J.H. (2009). Structure and Membrane Interaction of Myristoylated ARF1. Structure *17*, 79–87.

Lowe, M., and Kreis, T.E. (1996). In Vivo Assembly of Coatomer, the COP-I Coat Precursor *. J. Biol. Chem. *271*, 30725–30730.

Luo, R., and Randazzo, P.A. (2008). Kinetic Analysis of Arf GAP1 Indicates a Regulatory Role for Coatomer *.

Luo, R., Luan, V., Hayashi, R., and Randazzo, P.A. (2009a). Arf GAP2 is positively regulated by coatomer and cargo. Cell. Signal. *21*, 1169–1179.

Luo, R., Ha, V.L., Hayashi, R., and Randazzo, P.A. (2009b). Arf GAP2 is positively regulated by coatomer and cargo. Cell. Signal. *21*, 1169–1179.

Ma, W., and Goldberg, J. (2013). Rules for the recognition of dilysine retrieval motifs by coatomer. EMBO J. *32*, 926–937.

Ma, L., Umasankar, P.K., Wrobel, A.G., Lymar, A., McCoy, A.J., Holkar, S.S., Jha, A., Pradhan-Sundd, T., Watkins, S.C., Owen, D.J., et al. (2016). Transient Fcho1/2·Eps15/R·AP-2 Nanoclusters Prime the AP-2 Clathrin Adaptor for Cargo Binding. Dev. Cell *37*, 428–443.

Madeira, F., Park, Y. mi, Lee, J., Buso, N., Gur, T., Madhusoodanan, N., Basutkar, P., Tivey, A.R.N., Potter, S.C., Finn, R.D., et al. (2019). The EMBL-EBI search and sequence analysis tools APIs in 2019. Nucleic Acids Res. *47*, W636–W641.

Makowski, S.L., Kuna, R.S., and Field, S.J. (2020). Induction of membrane curvature by proteins involved in Golgi trafficking. Adv. Biol. Regul. *75*, 100661.

Manneville, J.-B., Casella, J.-F., Ambroggio, E., Gounon, P., Bertherat, J., Bassereau, P., Cartaud, J., Antonny, B., and Goud, B. (2008). COPI coat assembly occurs on liquid-disordered domains and the associated membrane deformations are limited by membrane tension. Proc. Natl. Acad. Sci. *105*, 16946–16951.

Martínez-Menárguez, J.A., Geuze, H.J., Slot, J.W., and Klumperman, J. (1999). Vesicular tubular clusters between the ER and Golgi mediate concentration of soluble secretory proteins by exclusion from COPI-coated vesicles. Cell *98*, 81–90.

Matsuda, S., Miura, E., Matsuda, K., Kakegawa, W., Kohda, K., Watanabe, M., and Yuzaki, M. (2008). Accumulation of AMPA Receptors in Autophagosomes in Neuronal Axons Lacking Adaptor Protein AP-4. Neuron *57*, 730–745.

Matsui, W., and Kirchhausen, T. (2002). Stabilization of clathrin coats by the core of the clathrin-associated protein complex AP-2. Biochemistry *29*, 10791–10798.

Mattera, R., Park, S.Y., Pace, R. De, Guardia, C.M., and Bonifacino, J.S. (2017). AP-4 mediates export of ATG9A from the trans-Golgi network to promote autophagosome formation. Proc. Natl. Acad. Sci. *114*, E10697–E10706.

McBride, C.E., Li, J., and Machamer, C.E. (2007). The Cytoplasmic Tail of the Severe Acute Respiratory Syndrome Coronavirus Spike Protein Contains a Novel Endoplasmic Reticulum Retrieval Signal That Binds COPI and Promotes Interaction with Membrane Protein. J. Virol. *81*, 2418–2428.

McCoy, A.J., Grosse-Kunstleve, R.W., Adams, P.D., Winn, M.D., Storoni, L.C., Read, R.J., and IUCr (2007). Phaser crystallographic software. Urn:Issn:0021-8898 *40*, 658–674.

McMahon, H.T., and Boucrot, E. (2011). Molecular mechanism and physiological functions of clathrin-mediated endocytosis. Nat. Rev. Mol. Cell Biol. 2011 128 *12*, 517–533.

McNicholas, S., Potterton, E., Wilson, K.S., Noble, M.E.M., and IUCr (2011). Presenting your structures: the CCP4mg molecular-graphics software. Urn:Issn:0907-4449 *67*, 386–394.

Michelsen, K., Schmid, V., Metz, J., Heusser, K., Liebel, U., Schwede, T., Spang, A., and Schwappach, B. (2007). Novel cargo-binding site in the β and δ subunits of coatomer. J. Cell Biol. *179*, 209–217.

Miele, A.E., Watson, P.J., Evans, P.R., Traub, L.M., and Owen, D.J. (2004). Two distinct interaction motifs in amphiphysin bind two independent sites on the clathrin terminal domain beta-propeller. Nat Struct Mol Biol *11*, 242–248.

Miller, K., and Moultrie, J. (2013). Understanding the Skills of Design Leaders. Des. Manag. J. *8*, 35–51.

Misselwitz, B., Dilling, S., Vonaesch, P., Sacher, R., Snijder, B., Schlumberger, M., Rout, S., Stark, M., von Mering, C., Pelkmans, L., et al. (2011). RNAi screen of Salmonella invasion shows role of COPI in membrane targeting of cholesterol and Cdc42. Mol. Syst. Biol. *7*, 474.

Mossessova, E., Gulbis, J.M., and Goldberg, J. (1998). Structure of the Guanine Nucleotide Exchange Factor Sec7 Domain of Human Arno and Analysis of the Interaction with ARF GTPase. Cell *92*, 415–423.

Muenzner, J., Traub, L.M., Kelly, B.T., and Graham, S.C. (2017). Cellular and viral peptides bind multiple sites on the N-terminal domain of clathrin. Traffic *18*, 44–57.

Munro, S., and Pelham, H.R.B. (1987). A C-terminal signal prevents secretion of luminal ER proteins. Cell *48*, 899–907.

Nicholls, R.A., Long, F., Murshudov, G.N., and IUCr (2012). Low-resolution refinement tools in REFMAC5. Urn:Issn:0907-4449 *68*, 404–417.

Nickel, W., Malsam, J., Gorgas, K., Ravazzola, M., Jenne, N., Helms, J.B., and Wieland, F.T. (1998). Uptake by COPI-coated vesicles of both anterograde and retrograde cargo is inhibited by GTPγS in vitro. J. Cell Sci. *111*, 3081–3090.

Nie, Z., and Randazzo, P.A. (2006). Arf GAPs and membrane traffic.

Nilsson, T., Jackson, M., and Peterson, P.A. (1989). Short cytoplasmic sequences serve as retention

signals for transmembrane proteins in the endoplasmic reticulum. Cell *58*, 707–718.

Noble, A.J., Zhang, Q., O'Donnell, J., Hariri, H., Bhattacharya, N., Marshall, A.G., and Stagg, S.M. (2012). A pseudoatomic model of the COPII cage obtained from cryo-electron microscopy and mass spectrometry. Nat. Struct. Mol. Biol. 2012 202 *20*, 167–173.

Noorelahi, R., Perez, G., and Otero, H.J. (2017). Imaging findings of Copa syndrome in a 12-year-old boy. Pediatr. Radiol. 2017 482 *48*, 279–282.

Ooi, C.E., Dell'Angelica, E.C., and Bonifacino, J.S. (1998). ADP-ribosylation factor 1 (ARF1) regulates recruitment of the AP-3 adaptor complex to membranes. J. Cell Biol. *142*, 391–402.

Ossipov, D., Schröder-Köhne, S., and Schmitt, H.D. (1999). Yeast ER-Golgi v-SNAREs Bos1p and Bet1p differ in steady-state localization and targeting. J Cell Sci *112*, 4135–4142.

Ostermann, J., Orci, L., Tani, K., Amherdt, M., Ravazzola, M., Elazar, Z., and Rothman, J.E. (1993). Stepwise assembly of functionally active transport vesicles. Cell *75*, 1015–1025.

Otwinowski, Z., and Minor, W. (1997). Processing of X-ray Diffraction Data Collected in Oscillation Mode. Methods Enzym. *276*, 307–326.

Owen, D.J., and Evans, P.R. (1998). A structural explanation for the recognition of tyrosine-based endocytotic signals. Science (80-.). *282*, 1327–1332.

Owen, D.J., Vallis, Y., Pearse, B.M.F., McMahon, H.T., and Evans, P.R. (2000). The structure and function of the β2-adaptin appendage domain. EMBO J. *19*, 4216.

Pääbo, S., Weber, F., Nilsson, T., Schaffner, W., and Peterson, P.A. (1986). Structural and functional dissection of an MHC class I antigen-binding adenovirus glycoprotein. EMBO J *5*, 1921–1927.

Pace, R. De, Skirzewski, M., Damme, M., Mattera, R., Mercurio, J., Foster, A.M., Cuitino, L., Jarnik, M., Hoffmann, V., Morris, H.D., et al. (2018). Altered distribution of ATG9A and accumulation of axonal aggregates in neurons from a mouse model of AP-4 deficiency syndrome. PLOS Genet. *14*, e1007363.

Park, J.S., Helble, J.D., Lazarus, J.E., Yang, G., Blondel, C.J., Doench, J.G., Starnbach, M.N., and Waldor, M.K. (2018). A FACS-Based Genome-wide CRISPR Screen Reveals a Requirement for COPI in Chlamydia trachomatis Invasion. IScience *11*, 71–84.

Park, J.S., Helble, J.D., Lazarus, J.E., Doench, J.G., Starnbach, M.N., and Waldor, M.K. (2019). A FACS-Based Genome-wide CRISPR Screen Reveals a Requirement for COPI in Chlamydia trachomatis Invasion.

Park, S.-Y., Yang, J.-S., Schmider, A.B., Soberman, R.J., and Hsu, V.W. (2015). Coordinated regulation of bidirectional COPI transport at the Golgi by CDC42. Nat. 2015 5217553 *521*, 529–532.

Pasqualato, S., Renault, L., and Cherfils, J. (2002). Arf, Arl, Arp and Sar proteins: A family of GTP-binding proteins with a structural device for "front-back" communication. EMBO Rep. *3*, 1035–1041.

Pavel, J., Harter, C., and Wieland, F.T. (1998). Reversible dissociation of coatomer: Functional characterization of a β/δ-coat protein subcomplex. Proc. Natl. Acad. Sci. *95*, 2140–2145.

Peden, A.A., Rudge, R.E., Lui, W.W.Y., and Robinson, M.S. (2002). Assembly and function of AP-3 complexes in cells expressing mutant subunits. J. Cell Biol. *156*, 327–336.

Peden, A.A., Oorschot, V., Hesser, B.A., Austin, C.D., Scheller, R.H., and Klumperman, J. (2004). Localization of the AP-3 adaptor complex defines a novel endosomal exit site for lysosomal membrane proteins. J. Cell Biol. *164*, 1065–1076.

Pelham, B.W. (1991). On Confidence and Consequence: The Certainty and Importance of Self-Knowledge. J. Pers. Soc. Psychol. *60*, 518–530.

Pepperkok, R., Whitney, J.A., Gomez, M., and Kreis, T.E. (2000). COPI vesicles accumulating in the presence of a GTP restricted Arf1 mutant are depleted of anterograde and retrograde cargo. *144*, 135–144.

Peyroche, A., Paris, S., and Jackson, C.L. (1996). Nucleotide exchange on ARF mediated by yeast Gea1 protein. Nature *384*, 479–481.

Poon, P.P., Cassel, D., Spang, A., Rotman, M., Pick, E., Singer, R.A., and Johnston, G.C. (1999). Retrograde transport from the yeast Golgi is mediated by two ARF GAP proteins with overlapping function. EMBO J. *18*, 555–564.

Poon, P.P., Nothwehr, S.F., Singer, R.A., and Johnston, G.C. (2001). The Gcs1 and Age2 ArfGAP proteins provide overlapping essential function for transport from the yeast trans-Golgi network. J. Cell Biol. *155*, 1239–1250.

Popoff, V., Adolf, F., Bru, B., and Wieland, F. (2011). COPI Budding within the Golgi Stack. 1–20.

Presley, J.F., Ward, T.H., Pfeifer, A.C., Siggia, E.D., Phair, R.D., and Lippincott-schwartz, J. (2002). Dissection of COPI and Arf1 dynamics in vivo and role in Golgi membrane transport. *788*, 784–788.

R, L.B., A, A., U, B., and B, H. (1998). The mammalian AP-3 adaptor-like complex mediates the intracellular transport of lysosomal membrane glycoproteins. J. Biol. Chem. *273*, 29451–29461.

Randazzo, P.A., and Hirsch, D.S. (2004). Arf GAPs: multifunctional proteins that regulate membrane traffic and actin remodelling. Cell. Signal. *16*, 401–413.

Rapoport, I., Miyazaki, M., Boll, W., Duckworth, B., Cantley, L.C., Shoelson, S., and Kirchhausen, T. (1997). Regulatory interactions in the recognition of endocytic sorting signals by AP-2 complexes. EMBO J. *16*, 2240–2250.

Rawet, M., Levi-Tal, S., Szafer-Glusman, E., Parnis, A., and Cassel, D. (2010). ArfGAP1 interacts with coat proteins through tryptophan-based motifs. Biochem. Biophys. Res. Commun. *394*, 553–557.

Reider, A., and Wendland, B. (2011). Endocytic adaptors - Social networking at the plasma membrane. J. Cell Sci. *124*, 1613–1622.

Rein, U., Andag, U., Duden, R., Schmitt, H.D., and Spang, A. (2002). ARF-GAP-mediated interaction between the ER-Golgi v-SNAREs and the COPI coat. J. Cell Biol. *157*, 395–404.

Reinhard, C., Harter, C., Bremser, M., Brügger, B., Sohn, K., Helms, J.B., and Wieland, F. (1999). Receptor-induced polymerization of coatomer. Proc. Natl. Acad. Sci. *96*, 1224–1228.

Reinhard, C., Schweikert, M., Wieland, F.T., and Nickel, W. (2003). Functional reconstitution of COPI coat assembly and disassembly using chemically defined components. Proc. Natl. Acad. Sci. U. S. A. *100*, 8253–8257.

Ren, X., Farías, G.G., Canagarajah, B.J., Bonifacino, J.S., and Hurley, J.H. (2013). Structural Basis for Recruitment and Activation of the AP-1 Clathrin Adaptor Complex by Arf1. Cell *152*, 755–767.

Ren, Y., Yip, C.K., Tripathi, A., Huie, D., Jeffrey, P.D., Walz, T., and Hughson, F.M. (2009). A Structure-Based Mechanism for Vesicle Capture by the Multisubunit Tethering Complex Dsl1. Cell *139*, 1119–1129.

Robinson, M.S. (2004). Adaptable adaptors for coated vesicles. Trends Cell Biol. *14*, 167–174.

Robinson, M.S. (2015). Forty Years of Clathrin-coated Vesicles. Traffic *16*, 1210–1238.

Robinson, M.S., and Bonifacino, J.S. (2001). Adaptor-related proteins. Curr. Opin. Cell Biol. *13*, 444–453.

Robinson, M., Poon, P.P., Schindler, C., Murray, L.E., Kama, R., Gabriely, G., Singer, R.A., Spang, A., Johnston, G.C., and Gerst, J.E. (2006). The Gcs1 Arf-GAP Mediates Snc1,2 v-SNARE Retrieval to the Golgi in Yeast. Https://Doi.Org/10.1091/Mbc.E05-09-0832 *17*, 1845–1858.

SA, Z., EJ, G., PV, R., G, S., AL, M., AA, P., and V, F. (2013). Chemical-genetic disruption of clathrin function spares adaptor complex 3-dependent endosome vesicle biogenesis. Mol. Biol. Cell *24*, 2378–2388.

Sato, K., Sato, M., and Nakano, A. (2001). Rer1p, a Retrieval Receptor for Endoplasmic Reticulum Membrane Proteins, Is Dynamically Localized to the Golgi Apparatus by Coatomer. J Cell Biol *152*, 935–944.

Scheffzek, K., Ahmadian, M.R., Kabsch, W., Wiesmüller, L., Lautwein, A., Schmitz, F., and Wittinghofer, A. (1997). The Ras-RasGAP complex: Structural basis for GTPase activation and its loss in oncogenic ras mutants. Science (80-.). *277*, 333–338.

Scheffzek, K., Ahmadian, M.R., and Wittinghofer, A. (1998). GTPase-activating proteins: helping hands to complement an active site. Trends Biochem. Sci. *23*, 257–262.

Schindler, C., and Spang, A. (2007). Interaction of SNAREs with ArfGAPs Precedes Recruitment of Sec18p/NSF. Https://Doi.Org/10.1091/Mbc.E06-08-0756 *18*, 2852–2863.

Schindler, C., Rodriguez, F., Poon, P.P., Singer, R.A., Johnston, G.C., and Spang, A. (2009). The GAP domain and the SNARE, coatomer and cargo interaction region of the ArfGAP2/3 Glo3 are sufficient for Glo3 function. Traffic *10*, 1362–1375.

Schledzewski, K., Brinkmann, H., and Mendel, R.R. (1999a). Phylogenetic Analysis of Components of the Eukaryotic Vesicle Transport System Reveals a Common Origin of Adaptor Protein Complexes 1, 2, and 3 and the F Subcomplex of the Coatomer COPI. J. Mol. Evol. 1999 486 *48*, 770–778.

Schledzewski, K., Brinkmann, H., and Mendel, R.R. (1999b). Phylogenetic Analysis of Components of the Eukaryotic Vesicle Transport System Reveals a Common Origin of Adaptor Protein Complexes 1, 2, and 3 and the F Subcomplex of the Coatomer COPI. J. Mol. Evol. *48*, 770–778.

Schmid, E.M., Ford, M.G.J., Burtey, A., Praefcke, G.J.K., Peak-Chew, S.-Y., Mills, I.G., Benmerah, A., and McMahon, H.T. (2006). Role of the AP2 β-Appendage Hub in Recruiting Partners for Clathrin-Coated Vesicle Assembly. PLOS Biol. *4*, e262.

Schwappach, B., Zerangue, N., Jan, Y.N., and Jan, L.Y. (2000). Molecular Basis for KATP Assembly: Transmembrane Interactions Mediate Association of a K+ Channel with an ABC Transporter. Neuron *26*, 155–167.

Seaman, M.J., Sowerby, P.J., and Robinson, M.S. (1996). Cytosolic and Membrane-associated Proteins Involved in the Recruitment of AP-1 Adaptors onto the Trans-Golgi Network *. J. Biol. Chem. *271*, 25446–25451.

Semenza, J.C., Hardwick, K.G., Dean, N., and Pelham, H.F.B. (1990). ERD2 , a Yeast Gene Required for the Receptor-Mediated Retrieval of Luminal ER Proteins from the Secretory Pathway. *61*, 1349–1357.

Serafini, T., Stenbeck, G., Brecht, A., Lottspeich, F., Orci, L., Rothman, J.E., and Wieland, F.T. (1991). A coat subunit of Golgi-derived non-clathrin-coated vesicles with homology to the clathrin-coated vesicle coat protein beta-adaptin. Nature *349*, 215–220.

Shibuya, A., Margulis, N., Christiano, R., Walther, T.C., and Barlowe, C. (2015). The Erv41–Erv46 complex serves as a retrograde receptor to retrieve escaped ER proteins. J. Cell Biol. *208*, 197–209.

Shikano, S., and Li, M. (2003). Membrane receptor trafficking: Evidence of proximal and distal zones conferred by two independent endoplasmic reticulum localization signals. Proc. Natl. Acad. Sci. *100*, 5783–5788.

Sicari, D., Chatziioannou, A., Koutsandreas, T., Sitia, R., and Chevet, E. (2020). Role of the early secretory pathway in SARS-CoV-2 Infection. J. Cell Biol. *219*.

Simossis, V.A., and Heringa, J. (2005a). PRALINE: a multiple sequence alignment toolbox that integrates homology-extended and secondary structure information. Nucleic Acids Res. *33*, W289–W294.

Simossis, V.A., and Heringa, J. (2005b). PRALINE: a multiple sequence alignment toolbox that integrates homology-extended and secondary structure information. Nucleic Acids Res. *33*, W289–W294.

Sohn, K., Orci, L., Ravazzola, M., Amherdt, M., Bremser, M., Lottspeich, F., Fiedler, K., Helms, J.B., and Wieland, F.T. (1996). A major transmembrane protein of Golgi-derived COPI-coated vesicles involved in coatomer binding. J. Cell Biol. *135*, 1239–1248.

Söllner, T., Whiteheart, S.W., Brunner, M., Erdjument-Bromage, H., Geromanos, S., Tempst, P., and Rothman, J.E. (1993). SNAP receptors implicated in vesicle targeting and fusion. Nat. 1993 3626418 *362*, 318–324.

Soni, K.G., Mardones, G.A., Sougrat, R., Smirnova, E., Jackson, C.L., and Bonifacino, J.S. (2009). Coatomer-dependent protein delivery to lipid droplets. J. Cell Sci. *122*, 1834–1841.

Spang, A. (2013). Retrograde Traffic from the Golgi to the Endoplasmic Reticulum. 1–10.

Spang, A., Matsuoka, K., Hamamoto, S., Schekman, R., and Orci, L. (1998). Coatomer, Arf1p, and nucleotide are required to bud coat protein complex I-coated vesicles from large synthetic liposomes. Proc. Natl. Acad. Sci. *95*, 11199–11204.

Spang, A., Shiba, Y., and Randazzo, P.A. (2010). Arf GAPs : Gatekeepers of vesicle generation. FEBS Lett. *584*, 2646–2651.

Stagg, S.M., LaPointe, P., Razvi, A., Gürkan, C., Potter, C.S., Carragher, B., and Balch, W.E. (2008). Structural Basis for Cargo Regulation of COPII Coat Assembly. Cell *134*, 474–484.

Stamnes, M.A., and Rothman, J.E. (1993). The binding of AP-1 clathrin adaptor particles to Golgi membranes requires ADP-ribosylation factor, a small GTP-binding protein. Cell *73*, 999–1005.

Suckling, R.J., Poon, P.P., Travis, S.M., Majoul, I. V, Hughson, F.M., Evans, P.R., Duden, R., and Owen, D.J. (2015). Structural basis for the binding of tryptophan-based motifs by δ-COP. Proc. Natl. Acad. Sci. U. S. A. *112*, 14242–14247.

Südhof, T.C., and Rothman, J.E. (2009). Membrane fusion: Grappling with SNARE and SM proteins. Science (80-.). *323*, 474–477.

Sun, Z., Anderl, F., Fröhlich, K., Zhao, L., Hanke, S., Brügger, B., Wieland, F., and Béthune, J. (2007). Multiple and Stepwise Interactions Between Coatomer and ADP-Ribosylation Factor-1 (Arf1)-GTP. Traffic *8*, 582–593.

Sutton, R.B., Fasshauer, D., Jahn, R., and Brunger, A.T. (1998). Crystal structure of a SNARE complex involved in synaptic exocytosis at 2.4 Å resolution. Nat. 1998 3956700 *395*, 347–353.

Swaney, D.L., Beltrao, P., Starita, L., Guo, A., Rush, J., Fields, S., Krogan, N.J., and Villén, J. (2013). Global analysis of phosphorylation and ubiquitylation cross-talk in protein degradation. Nat. Methods 2013 107 *10*, 676–682.

Szafer, E., Pick, E., Rotman, M., Zuck, S., Huber, I., and Cassel, D. (2000). Role of Coatomer and Phospholipids in GTPase-activating Protein-dependent Hydrolysis of GTP by ADP-ribosylation Factor-1 *. J. Biol. Chem. *275*, 23615–23619.

Tanigawa, G., Orci, L., Amherdt, M., Ravazzola, M., Helms, J.B., and Rothman, J.E. (1993). Hydrolysis of bound GTP by ARF protein triggers uncoating of golgi-derived COP-coated vesicles. J. Cell Biol. *123*, 1365–1371.

Taveira-Dasilva, A.M., Markello, T.C., Kleiner, D.E., Jones, A.M., Groden, C., Macnamara, E., Yokoyama, T., Gahl, W.A., Gochuico, B.R., and Moss, J. (2018). Expanding the phenotype of COPA syndrome: a kindred with typical and atypical features. J Med Genet *0*, 1–5.

Teal, S.B., Hsu, V.W., Peters, P.J., Klausner, R.D., and Donaldson, J.G. (1994). An activating mutation in ARF1 stabilizes coatomer binding to Golgi membranes. J. Biol. Chem. *269*, 3135–3138.

Terwilliger, T.C., Grosse-Kunstleve, R.W., Afonine, P. V., Moriarty, N.W., Zwart, P.H., Hung, L.-W., Read,

R.J., and Adams, P.D. (2008). Iterative model building, structure refinement and density modification with the PHENIX AutoBuild wizard. Acta Crystallogr. Sect. D Biol. Crystallogr. *64*, 61–69.

Theos, A.C., Tenza, D., Martina, J.A., Hurbain, I., Peden, A.A., Sviderskaya, E. V., Stewart, A., Robinson, M.S., Bennett, D.C., Cutler, D.F., et al. (2005). Functions of Adaptor Protein (AP)-3 and AP-1 in Tyrosinase Sorting from Endosomes to Melanosomes. Mol. Biol. Cell *16*, 5356.

Thiam, A.R., Antonny, B., Wang, J., Delacotte, J., Wilfling, F., Walther, T.C., Beck, R., Rothman, J.E., and Pincet, F. (2013). COPI buds 60-nm lipid droplets from reconstituted water–phospholipid–triacylglyceride interfaces, suggesting a tension clamp function. Proc. Natl. Acad. Sci. *110*, 13244–13249.

Townsley, F.M., and Pelham, H.R. (1994). The KKXX signal mediates retrieval of membrane proteins from the Golgi to the ER in yeast. Eur J Cell Biol *64*, 211–216.

Townsley, F.M., Wilson, D.W., and Pelham, H.R. (1993). Mutational analysis of the human KDEL receptor: distinct structural requirements for Golgi retention, ligand binding and retrograde transport. EMBO J. *12*, 2821–2829.

Traub, L.M., Ostrom, J.A., and Kornfeld, S. (1993). Biochemical dissection of AP-1 recruitment onto Golgi membranes. J. Cell Biol. *123*, 561–573.

Trautwein, M., Dengjel, J., Schirle, M., and Spang, A. (2004). Arf1p Provides an Unexpected Link between COPI Vesicles and mRNA in Saccharomyces cerevisiae. Https://Doi.Org/10.1091/Mbc.E04-05-0411 *15*, 5021–5037.

Travis, S.M., Kokona, B., Fairman, R., and Hughson, F.M. (2019). Roles of singleton tryptophan motifs in COPI coat stability and vesicle tethering. Proc. Natl. Acad. Sci. U. S. A. *116*, 24031–24040.

Tu, L., Tai, W.C.S., Chen, L., and Banfield, D.K. (2008). Signal-Mediated Dynamic Retention of Glycosyltransferases in the Golgi. Science (80-.). *321*, 404–407.

Tu, L., Chen, L., and Banfield, D.K. (2012). A Conserved N-terminal Arginine-Motif in GOLPH3-Family Proteins Mediates Binding to Coatomer. Traffic *13*, 1496–1507.

Vetter, I.R., and Wittinghofer, A. (2001). The Guanine Nucleotide-Binding Switch in Three Dimensions. Science (80-.). *294*, 1299–1304.

Volpi, S., Tsui, J., Mariani, M., Pastorino, C., Caorsi, R., Sacco, O., Ravelli, A., Shum, A.K., Gattorno, M., and Picco, P. (2018). Type I interferon pathway activation in COPA syndrome. Clin. Immunol. *187*, 33–36.

Wang, S., Zhai, Y., Pang, X., Niu, T., Ding, Y.H., Dong, M.Q., Hsu, V.W., Sun, Z., and Sun, F. (2016). Structural characterization of coatomer in its cytosolic state. Protein Cell *7*, 586–600.

Wang, Y.J., Wang, J., Sun, H.Q., Martinez, M., Sun, Y.X., Macia, E., Kirchhausen, T., Albanesi, J.P., Roth, M.G., and Yin, H.L. (2003). Phosphatidylinositol 4 Phosphate Regulates Targeting of Clathrin Adaptor AP-1 Complexes to the Golgi. Cell *114*, 299–310.

Watkin, L.B., Jessen, B., Wiszniewski, W., Vece, T.J., Jan, M., Sha, Y., Thamsen, M., Santos-Cortez, R.L.P., Lee, K., Gambin, T., et al. (2015). COPA mutations impair ER-Golgi transport and cause hereditary

autoimmune-mediated lung disease and arthritis. Nat. Genet. 2015 476 *47*, 654–660.

Watson, P.J., Frigerio, G., Collins, B.M., Duden, R., and Owen, D.J. (2004). Gamma-COP appendage domain - structure and function. Traffic *5*, 79–88.

Webb, B., and Sali, A. (2016). Comparative Protein Structure Modeling Using MODELLER. Curr. Protoc. Bioinforma. *54*, 5.6.1-5.6.37.

Weimer, C., Beck, R., Eckert, P., Reckmann, I., Moelleken, J., Br, B., and Wieland, F. (2008). Differential roles of ArfGAP1, ArfGAP2, and ArfGAP3 in COPI traffi cking. *183*, 725–735.

Weiss, M., and Nilsson, T. (2003). A Kinetic Proof-reading Mechanism for Protein Sorting. Traffic *4*, 65–73.

Whitney, J.A., Gomez, M., Sheff, D., Kreis, T.E., and Mellman, I. (1995). Cytoplasmic coat proteins involved in endosome function. Cell *83*, 703–713.

Wideman, J.G., Leung, K.F., Field, M.C., and Dacks, J.B. (2014). The cell biology of the endocytic system from an evolutionary perspective. Cold Spring Harb. Perspect. Biol. *6*.

Wilfling, F., Thiam, A.R., Olarte, M.J., Wang, J., Beck, R., Gould, T.J., Allgeyer, E.S., Pincet, F., Bewersdorf, J., Farese, R. V., et al. (2014). Arf1/COPI machinery acts directly on lipid droplets and enables their connection to the ER for protein targeting. Elife *2014*.

Willox, A.K., and Royle, S.J. (2012). Functional Analysis of Interaction Sites on the N-Terminal Domain of Clathrin Heavy Chain. Traffic *13*, 70–81.

Wilson$, D.W., Lewis, M.J., and Pelhams, H.R.B. (1993). THE JOURNAL pH-dependent Binding of KDEL to Its Receptor in Vitro*. *268*, 7465–7466.

Winn, M.D., Ballard, C.C., Cowtan, K.D., Dodson, E.J., Emsley, P., Evans, P.R., Keegan, R.M., Krissinel, E.B., Leslie, A.G.W., McCoy, A., et al. (2011). Overview of the CCP 4 suite and current developments. Acta Cryst D *67*, 235–242.

Xie, B., Jung, C., Chandra, M., Engel, A., Kendall, A.K., and Jackson, L.P. (2021). The Glo3 GAP crystal structure supports the molecular niche model for ArfGAPs in COPI coats. Adv. Biol. Regul. *79*, 100781.

Xu, P., Hankins, H.M., Macdonald, C., Erlinger, S.J., Frazier, M.N., Diab, N.S., Piper, R.C., Jackson, L.P., Macgurn, J.A., and Graham, T.R. (2017). COPI mediates recycling of an exocytic SNARE by recognition of a ubiquitin sorting signal. 1–22.

Yahara, N., Sato, K., and Nakano, A. (2006). The Arf1p GTPase-activating protein Glo3p executes its regulatory function through a conserved repeat motif at its C-terminus. J. Cell Sci. *119*, 2604–2612.

Yamasaki, A., Menon, S., Yu, S., Barrowman, J., Meerloo, T., Oorschot, V., Klumperman, J., Satoh, A., and Ferro-Novick, S. (2009). mTrs130 Is a Component of a Mammalian TRAPPII Complex, a Rab1 GEF That Binds to COPI-coated Vesicles. Https://Doi.Org/10.1091/Mbc.E09-05-0387 *20*, 4205–4215.

Yanagisawa, L.L., Marchena, J., Xie, Z., Li, X., Poon, P.P., Singer, R.A., Johnston, G.C., Randazzo, P.A., and

Bankaitis, V.A. (2002). Activity of Specific Lipid-regulated ADP Ribosylation Factor-GTPase–activating Proteins Is Required for Sec14p-dependent Golgi Secretory Function in Yeast. Mol. Biol. Cell *13*, 2193–2206.

Yang, J.-S., Lee, S.Y., Spanò, S., Gad, H., Zhang, L., Nie, Z., Bonazzi, M., Corda, D., Luini, A., and Hsu, V.W. (2005). A role for BARS at the fission step of COPI vesicle formation from Golgi membrane. EMBO J. *24*, 4133–4143.

Yang, J.-S., Gad, H., Lee, S.Y., Mironov, A., Zhang, L., Beznoussenko, G. V., Valente, C., Turacchio, G., Bonsra, A.N., Du, G., et al. (2008). A role for phosphatidic acid in COPI vesicle fission yields insights into Golgi maintenance. Nat. Cell Biol. 2008 1010 *10*, 1146–1153.

Yang, J.-S., Valente, C., Polishchuk, R.S., Turacchio, G., Layre, E., Moody, D.B., Leslie, C.C., Gelb, M.H., Brown, W.J., Corda, D., et al. (2011). COPI acts in both vesicular and tubular transport. Nat. Cell Biol. 2011 138 *13*, 996–1003.

Yang, J.S., Lee, S.Y., Gao, M., Bourgoin, S., Randazzo, P.A., Premont, R.T., and Hsu, V.W. (2002). ARFGAP1 promotes the formation of COPI vesicles, suggesting function as a component of the coat. J. Cell Biol. *159*, 69–78.

Yip, C.K., and Walz, T. (2011). Molecular Structure and Flexibility of the Yeast Coatomer as Revealed by Electron Microscopy. J. Mol. Biol. *408*, 825–831.

Yoon, T.Y., and Munson, M. (2018). SNARE complex assembly and disassembly. Curr. Biol. *28*, R397–R401.

Yu, X., Breitman, M., and Goldberg, J. (2012). A Structure-based mechanism for Arf1-dependent recruitment of coatomer to membranes. Cell *148*, 530–542.

Yuan, H., Michelsen, K., and Schwappach, B. (2003). 14-3-3 Dimers Probe the Assembly Status of Multimeric Membrane Proteins. Curr. Biol. *13*, 638–646.

Zabezhinsky, D., Slobodin, B., Rapaport, D., and Gerst, J.E. (2016). An Essential Role for COPI in mRNA Localization to Mitochondria and Mitochondrial Function. Cell Rep. *15*, 540–549.

Zanetti, G., Prinz, S., Daum, S., Meister, A., Schekman, R., Bacia, K., and Briggs, J.A.G. (2013). The structure of the COPII transport-vesicle coat assembled on membranes. Elife *2013*.

Zerangue, N., Schwappach, B., Jan, Y.N., and Jan, L.Y. (1999). A New ER Trafficking Signal Regulates the Subunit Stoichiometry of Plasma Membrane KATP Channels. Neuron *22*, 537–548.

Zerangue, N., Malan, M.J., Fried, S.R., Dazin, P.F., Jan, Y.N., Jan, L.Y., and Schwappach, B. (2001). Analysis of endoplasmic reticulum trafficking signals by combinatorial screening in mammalian cells. Proc. Natl. Acad. Sci. *98*, 2431–2436.

Zhang, C.-J., Bowzard, J.B., Anido, A., and Kahn, R.A. (2003). Four ARF GAPs in Saccharomyces cerevisiae have both overlapping and distinct functions. Yeast *20*, 315–330.

Zhang, C., Cavenagh, M.M., Kahn, R.A., Sci, U.S.A., and Gtpase-acti-, A. (1998). A Family of Arf Effectors

Defined as Suppressors of the Loss of Arf Function in the Yeast Saccharomyces cerevisiae *. *273*, 19792–19796.

Zhang, J., Wang, X., Li, G., He, J., Lu, Z., Yang, Y., Jiang, Y., Jiang, L., Li, F., and Liu, J. (2021). CoPB2: A novel prognostic biomarker that affects progression of HCC. Biomed Res. Int. *2021*.

Zivanov, J., Nakane, T., Forsberg, B.O., Kimanius, D., Hagen, W.J.H., Lindahl, E., and Scheres, S.H.W. (2018). New tools for automated high-resolution cryo-EM structure determination in RELION-3. Elife *7*.

APPENDIX I

Tables from Chapter II

Protein name	Protein accession numbers	Protein molecular weight (Da)	Exclusive unique peptide count	Exclusive unique spectrum count	Exclusive spectrum count	Percent total spectra	Sequence coverage
Pyruvate decarboxylase isozyme 1	sp|P06169|PDC1_YEAST	61,496.90	3	3	7	0.02%	9.77%
Uncharacterized protein YGR169C-A	sp|Q3E772|YG169_YEAST	10,495.30	0	0	0	0.00%	0.00%
Fructose-bisphosphate aldolase	sp|P14540|ALF_YEAST	39,621.50	2	2	3	0.01%	8.36%
Nuclear segregation protein BFR1	sp|P38934|BFR1_YEAST	54,641.70	0	0	0	0.00%	0.00%
ADP-ribosylation factor GTPase-activating protein GLO3	sp|P38682|GLO3_YEAST	55,095.20	1	1	1	0.00%	2.23%
Pyruvate kinase 1	sp|P00549|KPYK1_YEAST	54,545.40	30	40	184	0.41%	72.60%
Alcohol dehydrogenase 1	sp|P00330|ADH1_YEAST	36,848.70	13	15	124	0.28%	53.40%
Cystathionine beta-synthase	sp|P32582|CBS_YEAST	56,024.80	2	2	3	0.01%	4.73%
Peroxiredoxin DOT5	sp|P40553|DOT5_YEAST	24,120.40	0	0	0	0.00%	0.00%
Enolase 2	sp|P00925|ENO2_YEAST	46,915.10	2	2	2	0.00%	6.18%
Serine/threonine protein kinase KIN1	sp|P13185|KIN1_YEAST	120,072.90	0	0	0	0.00%	0.00%
T-complex protein 1 subunit beta	sp|P39076|TCPB_YEAST	57,205.70	2	2	3	0.01%	4.74%

Trehalose synthase complex regulatory subunit TSL1	sp|P38427|TSL1_YEAST	123,021.70	0	0	0	0.00%	0.00%
Obg-like ATPase 1	sp|P38219|OLA1_YEAST	44,175.90	0	0	0	0.00%	0.00%
T-complex protein 1 subunit gamma	sp|P39077|TCPG_YEAST	58,814.70	4	4	5	0.01%	7.49%
Actin	sp|P60010|ACT_YEAST	41,690.40	10	13	34	0.08%	36.50%
Serine--tRNA ligase, cytoplasmic	sp|P07284|SYSC_YEAST	53,311.00	8	8	26	0.06%	26.00%
Elongation factor 2	sp|P32324|EF2_YEAST	93,290.30	0	0	0	0.00%	0.00%
Tubulin beta chain	sp|P02557|TBB_YEAST	50,922.60	3	3	5	0.01%	9.19%
Heat shock protein SSA4	sp|P22202|HSP74_YEAST	69,652.70	1	1	1	0.00%	2.49%
Heat shock protein SSB2	sp|P40150|HSP76_YEAST	66,595.70	2	2	2	0.00%	4.40%
Tropomyosin-1	sp|P17536|TPM1_YEAST	23,541.30	7	7	9	0.02%	40.20%
ATP-dependent RNA helicase DBP5	sp|P20449|DBP5_YEAST	53,875.80	12	13	27	0.06%	32.60%
V-type proton ATPase subunit B	sp|P16140|VATB_YEAST	57,751.60	3	3	3	0.01%	8.12%
ADP-ribosylation factor 1	sp|P11076|ARF1_YEAST	20,530.10	3	3	5	0.01%	22.10%
Uncharacterized protein YER010C	sp|P40011|YEK0_YEAST	25,563.70	3	3	8	0.02%	20.50%
Nicotinamidase	sp|P53184|PNC1_YEAST	24,993.40	2	2	2	0.00%	9.72%

Glyceraldehyde-3-phosphate dehydrogenase 2	sp|P00358|G3P2_YEAST	35,846.90	3	4	9	0.02%	47.90%
Transposon Ty1-DR3 Gag-Pol polyprotein	sp|Q99231|YD12B_YEAST	198,846.80	0	0	0	0.00%	0.00%
Isocitrate dehydrogenase [NADP], mitochondrial	sp|P21954|IDHP_YEAST	48,192.80	2	2	2	0.00%	5.61%
Ribosome-associated complex subunit SSZ1	sp|P38788|SSZ1_YEAST	58,239.50	0	0	0	0.00%	0.00%
Coatomer subunit beta'	sp|P41811|COPB2_YEAST	99,446.40	31	55	538	1.20%	49.00%
Small COPII coat GTPase SAR1	sp|P20606|SAR1_YEAST	21,451.50	2	2	5	0.01%	13.70%
Alpha,alpha-trehalose-phosphate synthase [UDP-forming] 56 kDa subunit	sp|Q00764|TPS1_YEAST	56,148.30	1	1	2	0.00%	3.23%
ATP-dependent RNA helicase eIF4A	sp|P10081|IF4A_YEAST	44,698.30	3	3	4	0.01%	9.62%
Mannose-1-phosphate guanyltransferase	sp|P41940|MPG1_YEAST	39,566.60	8	8	23	0.05%	28.30%
Elongation factor 1-alpha	sp|P02994|EF1A_YEAST	50,032.60	5	5	13	0.03%	13.80%
Glyceraldehyde-3-phosphate dehydrogenase 1	sp|P00360|G3P1_YEAST	35,750.20	1	1	2	0.00%	24.70%
Glyceraldehyde-3-phosphate dehydrogenase 3	sp|P00359|G3P3_YEAST	35,746.60	15	25	107	0.24%	58.40%
Pyruvate decarboxylase isozyme 1	sp|P06169|PDC1_YEAST	61,496.90	5	5	9	0.02%	13.50%
Uncharacterized protein YGR169C-A	sp|Q3E772|YG169_YEAST	10,495.30	2	2	4	0.01%	28.30%

Nuclear segregation protein BFR1	sp|P38934|BFR1_YEAST	54,641.70	13	13	27	0.06%	26.00%
ADP-ribosylation factor GTPase-activating protein GLO3	sp|P38682|GLO3_YEAST	55,095.20	5	5	7	0.02%	13.80%
Pyruvate kinase 1	sp|P00549|KPYK1_YEAST	54,545.40	10	11	20	0.04%	25.60%
Phosphoglycerate kinase	sp|P00560|PGK_YEAST	44,739.60	2	2	3	0.01%	5.53%
Fructose-bisphosphate aldolase	sp|P14540|ALF_YEAST	39,621.50	1	1	1	0.00%	3.34%
Cell division control protein 12	sp|P32468|CDC12_YEAST	46,668.90	2	2	2	0.00%	7.62%
Alcohol dehydrogenase 1	sp|P00330|ADH1_YEAST	36,848.70	2	2	5	0.01%	6.03%
Cystathionine beta-synthase	sp|P32582|CBS_YEAST	56,024.80	0	0	0	0.00%	0.00%
Peroxiredoxin DOT5	sp|P40553|DOT5_YEAST	24,120.40	2	3	3	0.01%	13.50%
Serine/threonine protein kinase KIN1	sp|P13185|KIN1_YEAST	120,072.90	2	2	3	0.01%	2.44%
T-complex protein 1 subunit beta	sp|P39076|TCPB_YEAST	57,205.70	0	0	0	0.00%	0.00%
Trehalose synthase complex regulatory subunit TSL1	sp|P38427|TSL1_YEAST	123,021.70	2	3	3	0.01%	2.73%
Obg-like ATPase 1	sp|P38219|OLA1_YEAST	44,175.90	2	2	2	0.00%	5.33%
Very-long-chain 3-oxoacyl-CoA reductase	sp|P38286|MKAR_YEAST	38,709.70	2	2	2	0.00%	7.49%
Actin	sp|P60010|ACT_YEAST	41,690.40	2	2	2	0.00%	5.33%

Serine--tRNA ligase, cytoplasmic	sp|P07284|SYSC_YEAST	53,311.00	8	8	12	0.03%	26.00%
Mannose-1-phosphate guanyltransferase	sp|P41940|MPG1_YEAST	39,566.60	2	2	2	0.00%	8.03%
Elongation factor 2	sp|P32324|EF2_YEAST	93,290.30	6	6	8	0.02%	8.91%
Heat shock protein SSA4	sp|P22202|HSP74_YEAST	69,652.70	2	2	3	0.01%	4.36%
Heat shock protein SSB2	sp|P40150|HSP76_YEAST	66,595.70	10	11	19	0.04%	22.20%
ATP-dependent RNA helicase DBP5	sp|P20449|DBP5_YEAST	53,875.80	10	10	19	0.04%	24.90%
Elongation factor 1-gamma 2	sp|P36008|EF1G2_YEAST	46,521.90	4	4	7	0.02%	11.70%
ADP-ribosylation factor 1	sp|P11076|ARF1_YEAST	20,530.10	0	0	0	0.00%	0.00%
Nicotinamidase	sp|P53184|PNC1_YEAST	24,993.40	1	1	1	0.00%	5.56%
Glyceraldehyde-3-phosphate dehydrogenase 2	sp|P00358|G3P2_YEAST	35,846.90	3	3	6	0.01%	47.00%
NADPH-dependent 1-acyldihydroxyacetone phosphate reductase	sp|P40471|AYR1_YEAST	32,815.30	4	4	7	0.02%	16.50%
Transposon Ty1-DR3 Gag-Pol polyprotein	sp|Q99231|YD12B_YEAST	198,846.80	4	4	9	0.02%	4.50%
Plasma membrane ATPase 1	sp|P05030|PMA1_YEAST	99,621.60	4	4	6	0.01%	6.21%
Isocitrate dehydrogenase [NADP], mitochondrial	sp|P21954|IDHP_YEAST	48,192.80	15	16	25	0.05%	47.20%

Ribosome-associated complex subunit SSZ1	sp|P38788|SSZ1_YEAST	58,239.50	4	5	5	0.01%	10.20%
Suppressor protein STM1	sp|P39015|STM1_YEAST	29,995.40	8	8	22	0.05%	34.40%
Coatomer subunit beta'	sp|P41811|COPB2_YEAST	99,446.40	33	60	381	0.83%	55.10%
Serine hydroxymethyltransferase, cytosolic	sp|P37291|GLYC_YEAST	52,219.70	9	9	18	0.04%	21.50%
Alpha,alpha-trehalose-phosphate synthase [UDP-forming] 56 kDa subunit	sp|Q00764|TPS1_YEAST	56,148.30	7	8	13	0.03%	22.40%
Guanine nucleotide-binding protein subunit beta-like protein	sp|P38011|GBLP_YEAST	34,805.90	3	3	3	0.01%	11.90%
ATP-dependent RNA helicase eIF4A	sp|P10081|IF4A_YEAST	44,698.30	0	0	0	0.00%	0.00%
Elongation factor 1-alpha	sp|P02994|EF1A_YEAST	50,032.60	10	13	40	0.09%	32.80%
Glyceraldehyde-3-phosphate dehydrogenase 1	sp|P00360|G3P1_YEAST	35,750.20	3	3	3	0.01%	31.00%
Glyceraldehyde-3-phosphate dehydrogenase 3	sp|P00359|G3P3_YEAST	35,746.60	13	19	46	0.10%	57.50%
Heat shock protein 26	sp|P15992|HSP26_YEAST	23,880.20	2	2	3	0.01%	14.00%
RNA annealing protein YRA1	sp|Q12159|YRA1_YEAST	24,956.30	2	2	2	0.00%	9.73%

Table A2-1. Mass spectrometry data. This table summarizes the protein hits from the mass spectrometry experiment using purified β'-COP double propeller domains and yeast lysates. Human keratin and yeast ribosomal proteins are excluded.

β'-COP	Glo3	K_D	n	Dilysine peptide	Trace shown in
1-604 WT	230-260 WT	5.8	2.5	--	Figure 2
1-604 WT	230-270 WT	2.4	0.8	--	Figure 2
1-604 WT	230-280 WT	2.0	0.8	--	Figure 2
1-604 WT	230-290 WT	0.3	0.5	--	Figure 2, 3
1-604 WT	230-300 WT	0.8	0.8	--	Figure 2
1-304 WT	230-300 WT	n.b.	n.b.	--	Figure 2
300-604 WT	230-300 WT	n.b.	n.b.	--	Figure 2
1-604 WT	208-383 WT	0.8	0.8	--	Figure S3
1-604 WT	220-300 WT	0.8	0.7	--	Figure S3
1-604 WT	230-300 WT	0.8	0.8	--	Figure S3
1-604 WT	230-290 K233E	12	1.2	--	Figure 3
1-604 WT	230-290 K233E/K234E/K235E	n.b.	n.b.	--	Figure 3
1-604 WT	230-290 251E/K252E/K255E	12	0.9	--	Figure 3
1-604 D437A/D450A	230-290 WT	17.7	0.4	--	Figure 3
1-604 WT	230-290 WT	18.0	0.6	KTKLL	Figure S5
1-604 R15A/K17A/R59A	230-290 WT	5.3	0.8	--	Figure S5
1-604 D98A/D117A	230-290 WT	0.6	0.8	--	Figure S5

Table A2-2. ITC data summary. This table summarizes representative ITC experiments, including protein constructs with residue numbers and relevant point mutations; calculated K_D values; calculated stoichiometry (n) values; the addition of a dilysine peptide; and figure(s) showing relevant trace(s). "WT" denotes wild-type sequence.

β'-COP mutations	Position	K_D (M)	K_D (μM)	Construct
D437A D450A	C-term	1.77E-05	17.7	COP098
R15K K17A R59A	N-term	5.28E-06	5.3	COP064
D376A E378A	C-term	2.33E-06	2.3	COP072
D197A D327A E351A	N/C-term	2.30E-06	2.3	COP079
D303A E572A R590A E591A	C-term	2.26E-06	2.3	COP071
R36A E55A	N-term	2.15E-06	2.2	COP073
D327A E351A D356A	C-term	1.96E-06	2.0	COP075
D272A D291A	N-term	1.93E-06	1.9	COP080
D4 D327A E351A	N/C-term	1.51E-06	1.5	COP077
E411A E412A E424A	C-term	1.35E-06	1.4	COP076
D14A E38A E47A	N-term	9.25E-07	0.9	COP070
D98A D117A	N-term	6.77E-07	0.7	COP074

Table A2-3. ITC data summary for other β'-COP mutants. This table summarizes representative ITC experiments of the other β'-COP mutants we generated, including protein constructs with residue numbers and relevant point mutations; calculated K_D values; calculated stoichiometry (n) values; the addition of a dilysine peptide; and figure(s) showing relevant trace(s).

Yeast Strains
*gcs1*Δ::kan *glo3*Δ::kan pRS315-GLO3
*gcs1*Δ::kan *glo3*Δ::kan pRS315-*glo3 K233-235E*
*gcs1*Δ::kan *glo3*Δ::kan pRS315-*glo3 K251-252E, K255E*
*gcs1*Δ::kan *glo3*Δ::kan pRS315-GLO3 pRS416-mNG-Bet1
*gcs1*Δ::kan *glo3*Δ::kan pRS315-*glo3 K233-235E* pRS416-mNG-Bet1
*gcs1*Δ::kan *glo3*Δ::kan pRS315-*glo3 K251-252E, K255E* pRS426-mNG-Bet1
*gcs1*Δ::kan *glo3*Δ::kan pRS315-GLO3 pRS416-mNG-Gos1
*gcs1*Δ::kan *glo3*Δ::kan pRS315-*glo3 K233-235E* pRS416-mNG-Gos1
*gcs1*Δ::kan *glo3*Δ::kan pRS315-*glo3 K251-252E, K255E* pRS416-mNG-Gos1
*gcs1*Δ::kan *glo3*Δ::kan pRS315-GLO3 pRS416-GFP-Rer1
*gcs1*Δ::kan *glo3*Δ::kan pRS315-*glo3 K233-235E* pRS416-GFP-Rer1
*gcs1*Δ::kan *glo3*Δ::kan pRS315-*glo3 K251-252E, K255E* pRS416-GFP-Rer1
*gcs1*Δ::kan *glo3*Δ::kan pRS315-GLO3 pRS416-mNG-Snc1
*gcs1*Δ::kan *glo3*Δ::kan pRS315-*glo3 K233-235E* pRS416-mNG-Snc1
*gcs1*Δ::kan *glo3*Δ::kan pRS315-*glo3 K251-252E, K255E* pRS416-mNG-Snc1
*gcs1*Δ::kan *glo3*Δ::kan pRS315-GLO3 pRS426-GFP-Ste2
*gcs1*Δ::kan *glo3*Δ::kan pRS315-*glo3 K233-235E* pRS426-GFP-Ste2
*gcs1*Δ::kan *glo3*Δ::kan pRS315-*glo3 K251-252E, K255E* pRS426-GFP-Ste2

Table A2-4. Yeast strains used in this study.

APPENDIX II

Tables from Chapter III

Data Collection Statistics		
Beamline	LSCAT-21IDD	
Space group	$P2_1$	
Wavelength (Å)	1.77	
a, b, c (Å)	54.4, 74.0, 77.9	
α, β, γ (degrees)	90.0, 105.3, 90.0	
Resolution range (Å)	41.20 - 2.07	
R_{merge}	0.07785 (2.039)	
Mean *I/σI*	13.1 (0.80)	
Completeness (%)	92.6	
Multiplicity	2.0	
CC1/2	0.876 (0.00377)	
Total reflections	66787 (6852)	
Unique reflections	34077 (3495)	
Refinement		
Resolution Range (Å)	41.20 - 2.07	
No. reflections	34077	
R_{work}/ R_{free}	0.191/0.247	
Number of atoms	Protein	4458
	Ligands (glycerol, zinc)	16
	Solvent (water molecules)	51
	Wilson B-factor (Å^2)	37.47
R.M.S.D. from ideal values	Bond lengths (Å)	0.007
	Bond angles (°)	0.89
Ramachandran plot	Favored region (%)	99.3
	Allowed (%)	0.7
	Outliers (%)	0
	Rotamer outliers (%)	0.80
	Average B-factor (Å^2)	50.92
PDB ID	**7JTZ**	

Table A3-1. Glo3 GAP crystallographic data collection and refinements statistics. Values in parentheses refer to the highest resolution shell.

PDB ID	Protein(s)	Species	Overall r.m.s.d. (Å)	Zinc finger "core" r.m.s.d. (Å)
2P57	ArfGAP2	*Homo sapiens*	1.39	0.56
3SUB	ArfGAP	*Plasmodium falciparum*	1.4	0.52
3DWD	ArfGAP1	*Homo sapiens*	1.51	0.57
2CRR	SMAP1	*Homo sapiens*	1.74	0.76
2OLM	RIP/HRB	*Homo sapiens*	1.75	1.32
2B0O	ASAP3	*Homo sapiens*	1.77	0.53
3LVQ	ASAP3/Arf6	*homo sapiens*	1.77	0.62
2CRW	ArfGAP3	*Homo sapiens*	1.86	0.91
3O47	ArfGAP1/ Arf1	*Homo sapiens*	1.86	0.64
2OWA	ArfGAP	*Cryptosporidium parvum*	1.88	0.66
3JUE	ACAP1	*Homo sapiens*	2.16	0.58
2D9L	RIP/HRB	*Homo sapiens*	2.2	1.46
3T9K	ACAP1/ integrin □1	*Homo sapiens*	2.24	0.76

Table A3-2. Structural conservation among ArfGAP proteins. Glo3 GAP domain was compared with thirteen structures deposited in the PDB. The whole GAP domain and zinc finger core were compared using CCP4 Superpose. Root mean square deviation (r.m.s.d.) values are reported in angstroms.

Protein	Glo3 GAP
Beamline	LSCAT-21IDD
Distance to detector (mm)	100
Oscillation start angle (°)	0
Oscillation range (°)	360
Number of frames	1800
Frame width (°)	0.2
Rotation axis	Phi
Time/Frame (sec)	0.1
Time/Degree (sec)	0.5
Wavelength (Å)	1.77118

Table A3-3. Data Collection Settings.

Gene name	Gene ID	Accession #	ArfGAP family	Species	Isoform	Notes
ADP ribosylation factor GTPase activating protein 1	55738	XP_011527203	ArfGAP1	H_Sapiens	X1	
ADP-ribosylation factor GTPase activating protein 1	228998	XP_036017629	ArfGAP1	M_musculus	X2	
ADP ribosylation factor GTPase activating protein 1 S homeolog	447049	XP_018093019.1	ArfGAP1	X_laevis	X1	
ADP-ribosylation factor GTPase activating protein 1	100149572	NP_001007304	ArfGAP1	D_rerio		
ADP-ribosylation factor GTPase activating protein 1	39417	NP_524040	ArfGAP1	D_melanogaster		
Arf-GAP domain-containing protein	172643	NP_492310	ArfGAP1	C_elegans		BLAST identified only 1 homolog
ARF-GAP domain 7	818331	NP_001031503.1	ArfGAP1	A_thaliana		
Arf GTPase activating protein	8623152	XP_640542.1	ArfGAP1	D_discoideum		BLAST identified only 1 homolog
ARF GTPase activator-like protein [Chaetomium thermophilum var. thermophilum DSM 1495]	18257920	XP_006694297.1	ArfGAP1	C_thermophilum		
glo3 putative ARF GTPase-activating protein	2541825	NP_594843.2	ArfGAP1	S_pombe		
GCS1 GTPase-activating protein GCS1 [*Saccharomyces cerevisiae S288C*]	851372	GFP63814.1	ArfGAP1	S_cerevisiae		
ADP ribosylation factor GTPase activating protein 2	84364	Q8N6H7.1	ArfGAP2/3	H_Sapiens		
ADP ribosylation factor GTPase activating protein 3	26286	NP_055385.3	ArfGAP2/3	H_Sapiens		

ADP-ribosylation factor GTPase activating protein 2	77038	NP_076343.2	ArfGAP2/3	M_musculus	2	
ADP ribosylation factor GTPase activating protein 2 L homeolog	108713765	XP_018112824.1	ArfGAP2/3	X_laevis	X2	
ADP-ribosylation factor GTPase activating protein 2	641490	NP_001032507.1	ArfGAP2/3	D_rerio		
ArfGAP3 ADP-ribosylation factor GTPase activating protein 3	40487	NP_001262216.1	ArfGAP2/3	D_melanogaster	E	
Arf-GAP domain-containing protein	172643	NP_492310.1	ArfGAP2/3	C_elegans		Blast identified only 1 homolog
ARF-GAP domain 9	834718	NP_199487.1	ArfGAP2/3	A_thaliana		
Arf GTPase activating protein	8623152	XP_640542.1	ArfGAP2/3	D_discoideum		Blast identified only 1 homolog
ARF GTPase activator-like protein	8257920	XP_006694297.1	ArfGAP2/3	C_thermophilum		
Putative ARF GTPase-activating protein	2541825	NP_594843.2	ArfGAP2/3	S_pombe		
GLO3 ADP-ribosylation factor GTPase-activating protein	856859	NP_011048.1	ArfGAP2/3	S_cerevisiae		

Table A3-4. Sequences used in alignments.